Computational study of water mist for a tunnel fire application

Elizabeth Blanchard

CENTRE SCIENTIFIQUE ET TECHNIQUE DU BÂTIMENT
LABORATOIRE D'ÉNERGÉTIQUE ET DE MÉCANIQUE THÉORIQUE ET APPLIQUÉE – UMR 7563
ÉCOLE DOCTORALE EMMA – ED 409

THESIS

to be presented at

Université Henri Poincaré – Nancy Université

Computational study of water mist for a tunnel fire application

---

for the degree of

Doctor in Mechanics et Thermal engineering

by

Élizabeth BLANCHARD

on the 4th of November, 2011, with the PhD committee members

Sylvain	DESANGHERE	PhD	Sonovision Division Ligeron
Simo	HOSTIKKA	PhD	VTT Technical Research Centre of Finland
Michel	LANCE	Professor	Université Claude Bernard – Lyon I
Kevin	MCGRATTAN	PhD	National Institute of Standards and Technology
Bernard	PORTERIE	Professor	Université de Provence
Jean-Pierre	VANTELON	Professor	Université de Poitiers – Institut P′
Olivier	VAUQUELIN	Professor	Université de la Méditerranée
ADVISORS :			
Pascal	BOULET	Professor	Université Henri Poincaré – Nancy Université
Pierre	CARLOTTI	PhD	Centre Scientifique et Technique du Bâtiment

Summary

Introduction

Water spray during a fire test conducted in the midscale tunnel at CSTB

The present PhD study takes place in the domain of tunnel fire safety. In this domain, tunnel fires which have happened for one decade played a major role since they laid the emphasis on their potential consequences. In fact, human and financial consequences are often very important. The most tragically famous example could be the fire which occurred in the Mont Blanc tunnel in 1999 and which caused 39 dead people and very severe damages on the structure. In consequence, requirements for road tunnels have significantly evolved. For instance, we can cite France with the Inter-Ministry circular of August 2000 (replaced in March 2006 by the circular 2006-20) for national road tunnels and the European guideline of April 2004 for transborder road tunnels. In France, the strategy in case of fire aims at maintaining a free-smoke area near the roadway as long as possible. This strategy has two main objectives. At first, it promotes the self-evacuation of people. Then, it aims at making the operating conditions of fire-fighters easier. This fire safety management is ensured by a large sample of systems, among them the ventilation system.

In monitoring technological development, authorities and tunnel operators are still looking for new ways/systems for ensuring a higher safety level. In this context, mitigation systems are more and more cited and in particular water mist systems. These last systems are mainly characterized by the small size of droplets and the low sprayed water quantity. Their use in case of fire, in particular high HRR fire, could improve to operating conditions of fire-fighters and could also protect the tunnel structure [36].

Water mist systems are relatively recent. The first research studies dedicated to spray have been undertaken in the mid-fifties. After a break in sixties and seventies due the halogen-based fire suppressing agents, studies on water mist have grown at a very high rate. Research studies are now conducted by industrial firms, university laboratories and governmental agencies. For illustration, sixty of them are members of the International Water Mist Association in 2011. Since fifties, theoretical, experimental and computational studies have identified the involved phenomena when water is sprayed in a fire environment

- an amount of heat is transferred from the gases and surfaces to the water droplets. Droplets are also heated and evaporated. This "heat sink" results in a gas and surface temperature decrease,
- the phase change from liquid to vapor induces a high volumetric expansion rate consisting of water vapor gas. This phenomenon prevents the mixing between fresh air and combustible vapor, acting like an inert gas, thus being able to reduce the intensity of combustion reactions,
- water droplets interact with thermal radiation emitted by fire, tunnel surfaces and surrounding hot gases by absorption and scattering effects [29]. Water mist then acts as a radiative shield between the flames and the exposed objects,
- water droplets interact with smoke layer. Dynamic interaction and smoke cooling can induce a destratification.

The importance of each mechanism depends on the fire environment (fire heat release, ventilation, etc.) and on the water mist characteristics (droplet size, spray pattern, etc.). For instance, very small droplets have low initial momentum, so that they are rapidly decelerated after leaving the nozzle. Their residence time in the air is also longer promoting radiative attenuation and gas cooling but their ability to penetrate the flame zone is reduced [11], making it difficult to steer them toward a given target. For larger droplet spray, a more important fraction of the injected water falls to the ground or drips over the walls, promoting their cooling and also fire propagation. However, their inertia makes spray penetration in obstructed fire vicinity difficult.

The research studies, in particular the one conducted at the laboratory scale, have constituted data base for models. However, a bibliographic synthesis highlights that their sophistication degree is not the same for the four phenomena listed above. For instance, the interaction with the gaseous phase (cooling and radiative attenuation) is relatively well identified and many studies are devoted to its modeling. Concerning the interaction of droplets and liquid or solid surface, it seems that only the dynamic aspect has been widely studied. Predicting the fire activity when water droplets are sprayed remains difficult, even in an open area, due to the dilution effect which can occur locally in the flame and to heat absorbed by droplets in contact with the burning objects and the flame.

In tunnel, the current understanding and the complexity of the involved phenomena do not allow to design a water mist system on the only basis of its characteristics (droplet size, water flow rate, nozzle disposition, etc.) and the tunnel characteristics (tunnel size, traffic flow and type of vehicles, existing fire safety management, etc.). Before any installation, a water mist system must be assessed at real scale. Large-scale tests are very useful by involving real fire load and fluid flow. However, it could be difficult, and even impossible, to draw general conclusion concerning the influence and the efficiency of such system [20]. Moreover, such real-scale tests are very expensive since a large number of sensors is required to get a detailed measurement of velocity and temperature fields.

Objectives and approach

The present PhD study is based on an existing CFD model of fire-driven fluid flow which includes a water spray model. It aims at *estimating the capability of this model to predict the air flow and the thermal environment at the tunnel scale in order to determine which could be the contribution of computational codes in the assessment of water mist system*. This study has an additional objective. It aims at *analyzing and improving our understanding of the phenomena involved when water is sprayed in a tunnel fire environment*. A practical application of this study would be to define the use conditions of such code for understanding the interaction of water mist, fire and ventilation [1] in tunnel. *A priori*, models could help to define scenarii in a real scale tunnel test campaign and also limit the number of tests by assessing the expected phenomena and their orders of magnitude. *A posteriori*, models could help to understand the measurements.

It is important to mention that this study deals with the interaction of water mist and a fire situation and not the fire activity. In other words, we study the interaction of water droplets, gaseous phase, radiative source, solid surfaces and not the burning object and the flame (including pyrolysis).

The present study makes an extensive use of the CFD code Fire Dynamics Simulator (FDS) developed by the American National Institute of Standards and Technology (NIST) in cooperation with the Technical Research Centre of Finland VTT. This choice is motivated by many reasons [2], among them :

- the scientific literature mentions several validation cases in tunnel (see in particular Ref. [5, 9, 12, 23, 35]). Indeed, this code has shown good capabilities in such configuration,
- a water spray model had already been available at the beginning of this study.

The approach includes four stages. The first one is a bibliographic synthesis. In the second and third stages, the study consists in assessing the FDS code and then using it intensively. The assessment is conducted at two scales of increasing complexity, from the laboratory scale for assessing one

1. Longitudinal ventilation since that is the only case studied here
2. A couple of them are listed in the introduction of chapterII

particular part of the water spray model up to the tunnel scale for assessing the whole CFD code. Last, in the fourth stage, the study takes part in a preliminary study at the compartment scale.

The first stage (presented in Chapter I of the French dissertation and not presented here) aims at drawing the context of this research, in particular in tunnel fire safety and in research on water spray and tunnel fire. It has also for objectives to present physical phenomena of tunnel fire and water spray and to write few lines about the French regulation for road tunnel. Last, it aims at presenting a bibliographic synthesis of experimental and computational research studies on tunnel fire involving or not water spray.

The second stage consists in studying the FDS code for understanding some hypothesis underlying the model (this study is not presented in the English dissertation, the reader is sent to the technical guide [26]). Then, the code is verified and validated on the basis of comparisons with other computational codes and experimentations at the laboratory scale for attempting to assess one particular part of the water spray model. Two models are also evaluated, the model for heat and mass transfer (see Section II.1) and the model for radiative transfer through a two-phase participating media (see Section II.2). For the first model, experiments are extracted from the scientific literature. For the second model, experimentations and simulations conducted by Lechêne at LEMTA are used [17].

The third stage deals with tunnel fire with and without water mist (Chapter III). First, it aims at validating the code in that configuration. Then, it aims at improving our understanding of the involved phenomena and highlighting the key parameters influencing the environmental conditions. To accomplish it, we make use of the results of a reduced scale ($1/3^{rd}$) tunnel fire test campaign conducted between 2005 and 2008 at CSTB in cooperation with the French Tunnel Study Center (CETU), the French National Center for Scientific Research (CNRS, Institut P′) and the French Directorate for Civil Security (DSC) [4, 27]. This test campaign have two great assets for the present study :

- the instrumentation in the test tunnel is important and concern several variables, upstream and downstream the fire location,
- the campaign has tests involving a low number of nozzles and a low sprayed water quantity. Thus, in those tests, mist activation does not induce a HRR drop and allows also to study the thermal conditions during mist application which goes on several minutes.

The fourth and last stage is a part of a preliminary study before a test campaign which will be conducted at CSTB in 2012 (Chapter 4). This work is in fact an example of application of this research in a compartment. The experimental set-up is a room connected to a corridor. The corridor being ventilated mechanically, the objective is to understand the interaction of water mist, smoke layer and ventilation. The entire study is not presented here in the English dissertation, it is only summarized.

I Research background

AVAILABLE ONLY IN THE FRENCH DISSERTATION

The present chapter aims at drawing the context of this research, in particular in tunnel fire safety and in research. For that, it has also for objective to present physical phenomena of tunnel fire and water spray. Moreover, it aims at presenting a bibliographic synthesis of experimental and computational research studies on tunnel fire involving or not water spray.

The first section is to identify the main contributing factors to tunnel fire hazards and to explain the current strategy to minimize their impact. After detailing the specificities related to the tunnel geometry and the type of the involved fuel, the smoke movement is described first without any ventilation (natural or mechanical) and secondly when the tunnel is ventilated longitudinally. Then, the dangers faced by egressing people, firefighters, infrastructure and the environment are discussed. Finally, the strategy in case of fire in a tunnel current in France is broached. Last, the current French strategy in case of road tunnel fire is described briefly.

The second section deals with water mist system. This technology is first defined and several key dates are given. Then, the phenomena involved when water is sprayed in a fire environment are described. Last, an overview of their modeling is presented.

The third section consists in a literature review focusing on research dealing with tunnel fires, with and without water mist with an experimental and/or computational approach.

II Evaluation of the FDS code

The computational code on which this research is based on, is the CFD code Fire Dynamics Simulator (FDS) developed by NIST in cooperation with VTT. It presents three main advantages :

- it is widely used by scientists in the field of fire science. Thus, it profits of an important experience feedback for instance in tunnel (a bibliographic synthesis is available in the French dissertation),
- it has been free and open source since 2000. Current models can also be known precisely and modifications can be tested relatively easily. New outputs can also be implemented,
- it had already had a water spray model before this PhD study, it means models yielding water spraying at the injection point, droplet transport, heating and evaporation of liquid droplets.

Before using this code in a such complicated configuration as a tunnel fire, it appears essential to assess few submodels. This assessment consists in *verifications* and *validations*. *Verification* is a process to check the correctness of the solution of the governing equations [22]. Verification does not imply that the governing equations are appropriate ; only that the equations are being solved correctly. Verification is usually performed on simple physical problems by checking the principles of fluid mechanics (conservation of mass, momentum, energy, species), comparing the obtained solution to the analytical solution or by a numerical benchmark. *Validation* is a process to determine the appropriateness of the governing equations as a mathematical model of the physical phenomena of interest [22]. Typically, validation involves comparing model results with experimental measurement. This comparison can be performed at different scales, from the laboratory scale up to real scale. For this reason, tests conducted in the midscale tunnel at CSTB are validation cases.

Each new release of the FDS code undergoes wide testing both at NIST and VTT and beyond by its users. Several tests are provided on the FDS website – a verification suite and a validation suite. They are detailed in [22, 24]. This PhD study deals with water mist in a tunnel application. For this

reason, few submodels yielding the interaction of water spray, fire and gaseous phase are assessed. These cases fall into the two categories, validation and verification. In each case, it is indicated in table II.1.

The first verification, which is not presented here, concerns the free fall of a single droplet subject a transverse air flow. The verification is performed by comparing the computational trajectory to the analytical solution (by considering only gravity and air resistance).

The second assessment concerns the mass and heat transfer of water spray and is carried out in two steps. Firstly, the steady state predicted by FDS is verified by comparing the solution to an analytical solution given by the first law of thermodynamics. This steady state corresponds to the thermodynamic equilibrium of the two-phase system. Secondly, the rate of water evaporation is validated via comparisons with experimental measurements extracted from the scientific literature. Only the case of a single evaporating water droplet is studied since no data has been found for a sample of water droplets.

The third assessment deals with the propagation of thermal radiation through water curtain. This point is particularly important here since a water mist is characterized by the small size of its droplets. This assessment is proceeded in two steps. Firstly, radiative heat transfer is studied in a nonparticipating medium. An emitting surface is placed in front of a parallel panel receiving radiation. The also get heat flux is computed with the FDS code and compared to the analytical solution obtained with view factors [29]. Secondly, attenuation of thermal radiation through water curtain is validated and verified in two configurations, water is sprayed either in the downward direction or in the upward one.

Tab. II.1 — Type of assessment

	Verification	**Validation**	**Summarized in this English dissertation**
Spray evaporation			
Steady state	X		
Rate of evaporation		X	X
Attenuation of thermal radiation			
In a nonparticipating medium	X		
In a participating medium			
- Downward configuration	X	X	X
- Upward configuration	X	X	X

In the original dissertation, this chapter is divided into three sections. The first one starts with a brief presentation of the FDS code (version 5). Then, it lays the emphasis on the models yielding water spray (dynamics, mass and heat transfer, radiative properties) and radiative transfer. The two last sections concern the assessment of the code at the laboratory scale. The second section deals with the heat and mass transfer model, the third one with radiation propagation through water curtain.
In the English dissertation, only the two last sections are summarized.

II.1 Droplet evaporation

This sections is divided into two sub-sections. In the first one, few changes in the code which are now considered, are mentioned. In the second sub-section, validation cases allow to assess the evaporation model currently implemented in the FDS code.

II.1.1 Potential modifications

Modifications of the water spray model are now considered and few of them concern the heat and mass transfer, its structure and the model itself.

The current structure is presented on figure II.1. In short, these code sources are a loop over each droplet contained in the computational domain. For each droplet, the CC equation gives a humidity difference between droplet and gas phase. It participates in the calculation of droplet temperature. Heat is also transfered to or from the droplet and it is next traduced into gas/solid cooling/heating in the corresponding cell by updating its temperature. Last, the mass heat transfer model gives the droplet mass loss.

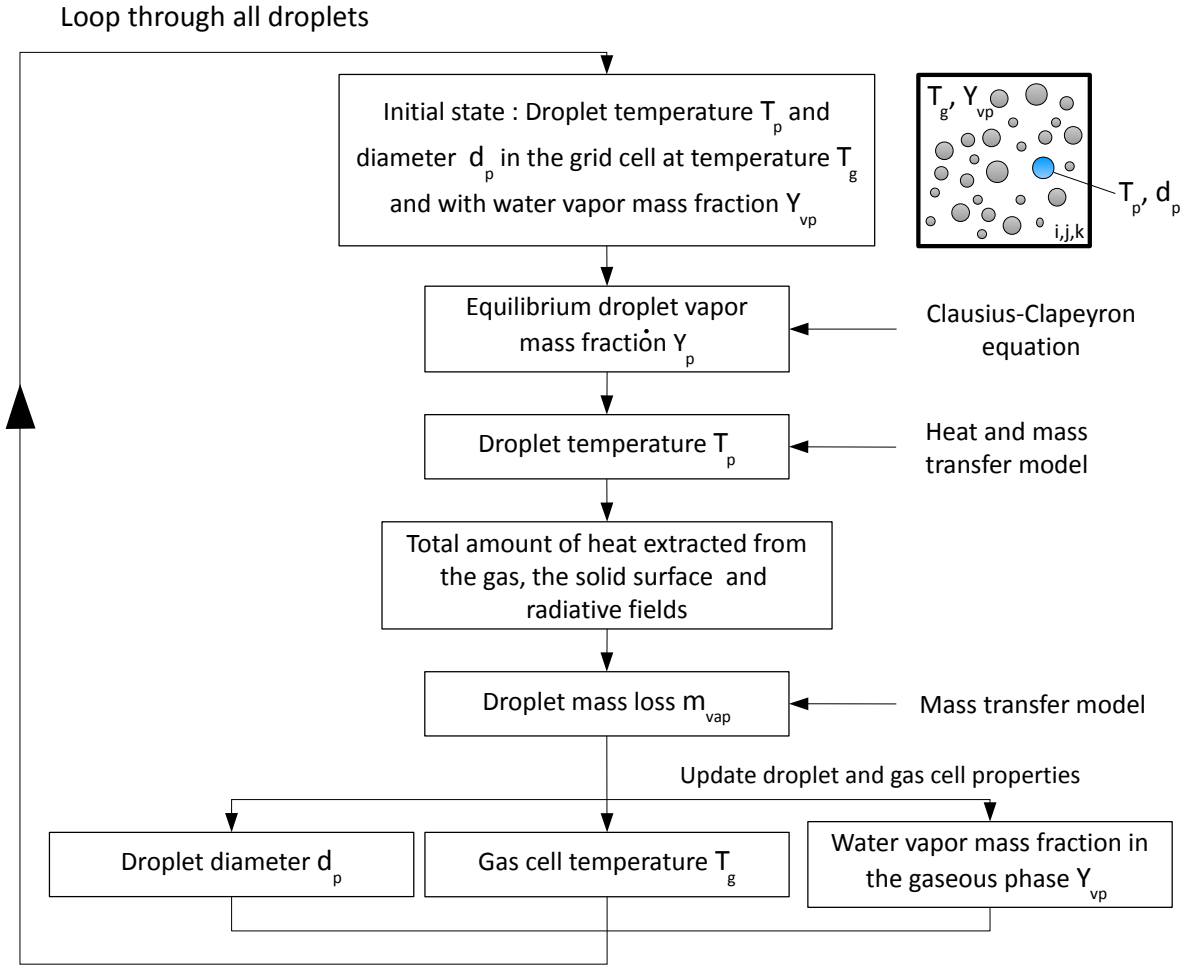

Fig. II.1 — Structure of the sources dealing with heat and mass transfer

The current code has two characteristics. Firstly, every droplet is processed independently without considering the droplets en mass present in the same gas cell. Secondly, gas temperature is updated inside the droplet loop. To understand the impact of these two characteristics, here are two examples.

Example 1 : An enclosure contains two identical water droplets (size and temperature). We suppose their temperatures lower than the gas one i.e. gas is cooled down due to their evaporation. In theory, since they are identical, their evaporation and their heating should be the same. In practice, with the current code structure, at the first round, the first droplet is (partially or totally) evaporated and its temperature increases. Consequently, at the end of the first round, gas temperature is lower and water vapor concentration is higher. Thus, mass loss and heating of the second droplet are less important than for the first droplet.

Example 2 : An enclosure contains two droplets. Their temperatures are lower than the gas one. At the initial time, the medium is unsaturated. We suppose that the medium is saturated after the evaporation of the first droplet. Thus, when the round for the second droplet begins, the gas relative humidity is equal to 1. The second droplet will not evaporate but will transfer heat if its temperature and gas temperature are different. Gas cooling will also conduct to a gas relative humidity higher than 1.

In practice, when a water spray is simulated with the FDS code, the influence of these two characteristics is reduced by the size of time step. However, the structure of the code will be likely modified in these two aspects. The objective would be to verify in a first time if the medium can be saturated at the grid cell scale. If yes, an algorithm would lead to the droplet temperature and its mass loss rate. An other modification would concern the variation of gas temperature due to heat transfer with liquid phase. It would be likely operated outside the loop over droplets. Moreover, this last modification would reduce the computational time.

An other modification is now considering. It concerns the choice of the evaporation model itself. This interest is explained by the fact that the model implemented in the current version does not take into account the Stefan diffusion. This transport phenomenon is the movement of water vapor away from the surface of the droplet by a flowing vapor/air mixture. Two models could also replace the current model, one has been developed by Abramzon and Sirignano [1] and the other by Taylor and Krishna [21, 33]. They consist of a coupled differential equations for the droplet mass loss and its temperature variation. They consider two film layers around the droplet, one for the mass transfer and one for the heat transfer. In the model of Abramzon and Sirignano, the radially outward directed flow transports the evaporating droplet mass and also gas. In the model of Taylor and Krishna, the molar diffusion flux in the film is only composed of water vapor.

II.1.2 Stationnay state

A simple configuration is used in order to verify the solution given by the CFD code for the stationary state. It consists in a cubic volume with a side length of 1 m containing 0.01 kg/m^3 of liquid water in the form of droplets at the initial time.The water vapor is equal to either 0 or to 0.005 kg/kg. At the initial time, gas temperature is comprised between 50 and 200 °C and liquid water temperature is comprised between 20 and 80 °C.

Analytical solution

The steady state predicted by FDS is verified by comparing the solution to an analytical solution given by the first law of thermodynamics. The domain being adiabatic and its volume being constant, composition and temperature of the gaseous phase at steady state conditions are related to the initial state as follows :

$$\textbf{Conservation of mass} \begin{cases} m_a^\infty = m_a^0 & \text{dry air} \\ m_{vp}^\infty = m_{vp}^0 + m_{p,\text{évap}} = m_{vp}^0 + m_p^0 & \text{water vapor} \\ m_p^\infty = m_p^0 - m_{p,\text{évap}} = 0 & \text{liquid water} \end{cases} \tag{II.1}$$

Conservation of energy

$$\begin{aligned} C_{v,a}\, m_a^\infty \cdot T_g^\infty + C_{v,vp}\, m_{vp}^\infty \cdot T_g^\infty + m_{vp}^\infty\, L_v - p^\infty\, V^\infty \approx \\ C_{v,a}\, m_a^0 \cdot T_g^0 + C_{v,vp}\, m_{vp}^0 \cdot T_g^0 + m_{vp}^0\, L_v + C_p\, m_p^0 \cdot T_p^0 - p^0\, V^0 \end{aligned} \tag{II.2}$$

where m refers to mass, T to temperature, C_v to specific heat at a constant volume, p to pressure and V to the domain volume.

Note : The gaseous phase (designated by the index g) is considered to be composed of two species, dry air (designated by the index a) and water vapor (designated by the index vp).

Numerical parameters

In input, the multiphase medium is caracterised by gas temperature, liquid water temperature and volumetric concentration in liquid water. The size and the number of the followed droplets do not influence the stationary state but only the duration the reach it. For that reason, all droplets have the same diameter at the inital state, equal to 200 µm and 10000 droplets are tracked.

Verification

Gas temperature at the steady state predicted by FDS is plotted on figure II.2 versus analytical solution. This figure indicates that the code predicts a steady state close to the thermodynamic equilibrium of the system and this, whatever the gas temperature, the initial liquid water temperature and the concentration of water vapor at the inital state.

Moreover, this figure illustrates the importance of water droplets evaporation in comparison with their variation in temperature (heating or cooling). Indeed, whatever the initial temperature of the liquid phase, even higher than the gas phase temperature, gas temperature at the steady state is almost the same.

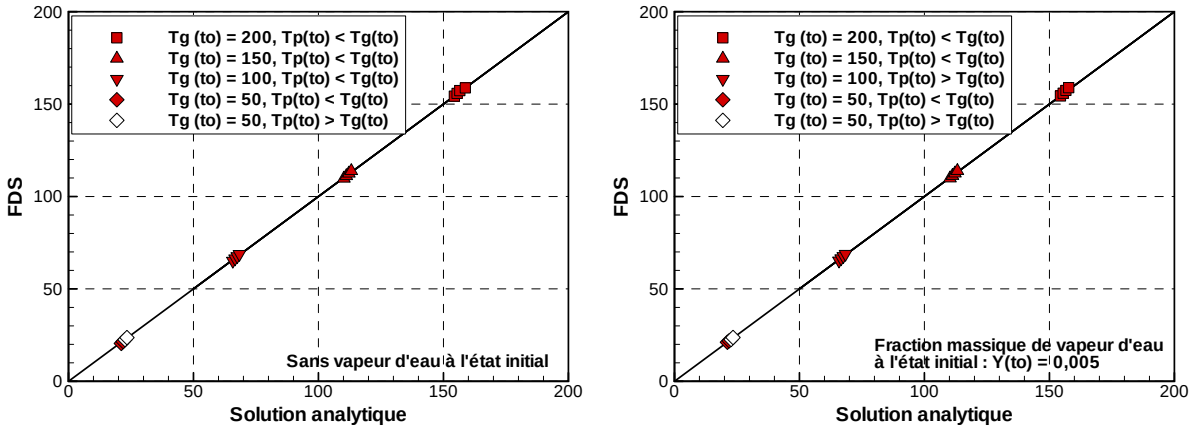

Fig. II.2 — Gas temperature at the steady state pedicted by FDS versus the analytical solution

II.1.3 Rate of evaporation

The previous sub-section dealing with the stationary state shows that the prediction of the steady state is consistent with the thermodynamic equilibrium of two-phase medium. The question concerns now the duration for reaching this equilibrium : is it correct ? Thus, we try to assess the rate of evaporation of water droplets by comparing to measurements which are all extracted from the scientific literature. Since we did not find any tests enough detailed for a sample of droplets or a single droplet in a hot gas, only one configuration is studied. It consists in one single evaporating motionless water droplet placed in gas at ambient temperature.

Since this configuration is simple, the model which is implemented in the current version of FDS is extracted and the configuration [1] is programmed with MATLAB. As it has been mentioned above, it is now considering to replace the evaporation model by the one developed by Taylor and Krishna (designated below by the term “model TK”) or by Abramzon and Sirignano (designated below by the term “model AS”). For this reason, these two models are assessed too.

The tests used for the validation are conducted by Ranz and Marshall [32] and by Kincaid and Longley [14, 15]. These tests are of double interest. Firstly, they involve a relatively wide range of test conditions (droplet size, droplet temperature, gas temperature, humidity and gas velocity). Secondly, they provide experimental values of different types. In the first case, this is the temporal evolution of the droplet size which allows to validate slope and magnitude predicted by the models.

1. Gas temperatures being almost ambient, thermal radiation is neglected

In the second case, this is the rate of evaporation. It means that data base can only validate the total amount of evaporated water quantity over a certain time period.

Note : The model implemented in the current version of FDS is coded with the same algorithm [26] in MATLAB. The models TK and AS are coded with a predictor-corrector scheme detailed in [21].

Test conducted by Ranz & Marshall

In the test conducted by Ranz and Marshall [32], one single water droplet is suspended in dry air at 24.9 °C. At the initial time, droplet diameter is 1050 µm and its temperature is 9.11 °C. The atmospheric pressure is equal to 98792 Pa.

The temporal evolution of the droplet size which is measured and predicted by the three models is plotted on figure II.3. First of all, we note the linear plot of the square diameter versus time in both experiment and computations. It also illustrates a fact which is frequently reported in scientific articles : the rate of vaporization increases for smallest droplets.

The rate of droplet vaporization illustrated by the slope is in turn different depending on the model. With the current model of FDS, the rate is overestimated, the relative difference between the measured and predicted slopes is equal to 22.7 %. Consequently, the drop is totally evaporated after 620 s. The two other models appear to better predict the rate. In fact, the relative difference between the measured and predicted slopes is lower, it is equal to 1.4 % for model AS and to 20.0 % for model TK. Note that model TK is the only model which underestimates the rate of droplet vaporization.

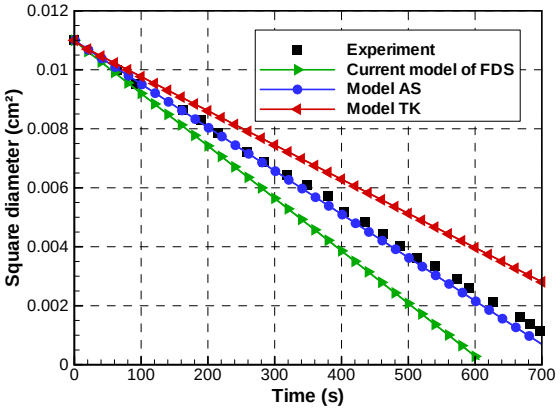

Fig. II.3 — Droplet size versus time in the test conducted by Ranz & Marshall [32]

Note : These computational results are very sensitive to the initial parameters and to the numerical algorithm.

Tests conducted by Kincaid & Longley

In the test campaign conducted by Kincaid and Longley [14, 15], the evaporation rate of individual droplet from 300 up to 1600 µm are measured when subjected to different temperature humidity and gas velocity condition over a certain time period (between 10 and 120 s). Gas temperature, relative humidity (RH) and air velocity are constant in each test, their range tested in the campaign are from 12.0 up to 19.9 °C, from 22 up to 81 % and from 0 up to 3 m/s. Table II.2 lists the test characteristics.

Tab. II.2 — Characteristics of the tests conducted by Kincaid & Longley [14, 15]

Liquid phase			Gas phase	
Relative humidity	**Temperature**	**Velocity**	**Temperature (°C)**	**Initial diameter**
22 %	31.0 °C	1 m/s	16,4 °C	between 0.3 and 0.9 mm
	31.2 °C	2.5 m/s	16.5 °C	between 0.3 and 0.7 mm
31 %	22.0 °C	0 m/s	12.0 °C	between 0.4 and 1.5 mm
81 %	22.4 °C	3 m/s	19.9 °C	between 0.7 and 1.6 mm

Figure II.4 shows measured and model predicted evaporation rates for different conditions. This loss rate has the same definition as in [14, 15]. It is computed as the ratio of the droplet mass variation $(m_p(t_0) - m_p(t_0 + \Delta t))$ over the time period Δt to its initial mass $m_p(t_0)$ times the period Δt :

$$\text{Loss rate} = \frac{m_p(t_0) - m_p(t_0 + \Delta t)}{m_p(t_0) \cdot \Delta t} \tag{II.3}$$

In most cases, the loss rates predicted by the model FDS are slightly higher than those predicted by the two other models. This tendency has indeed already been observed in the previous configuration of Ranz and Marshall. Relative to the measurements, there is a tendency for the three models to underpredict loss rates for HR lower or equal to 31 % and whatever the droplet size or the gas velocity. When HR is very high (80 %), there is not a global tendance for the three models. Computational results “are around” the measurement : model of FDS and model AS predict loss rates higher than measurements while model TK predicts lower values.

Model predictions are reasonably accurate in the 47 configurations. The mean relative discrepancy with measurements is equal to 17.6 % for the model of FDS, to 19.6 % for the model AS and to 21.4 % for the model TK. These values highlight that the model implemented in the current version of FDS gives the best estimation of loss rates during the test campaign. However, it seems difficult to select or even to discard one of these models on the only basis of this validation since agreement with the measurements depends at least on

- droplet size : agreement is better for the biggest drops,
- humidity conditions : figures II.4-a to c show that the three models tend to underpredict loss rates whereas on figure II.4-d for RH=81 % agreement is more disparate. In fact, when RH=81 %, model of FDS and model AS overestimate the loss rates rather than model TK tends to underestimate them. Moreover, we can draw a parallel with the previous test by Ranz and Marshall when RH is equal to 0. In that test, all the models overestimate the loss rate.

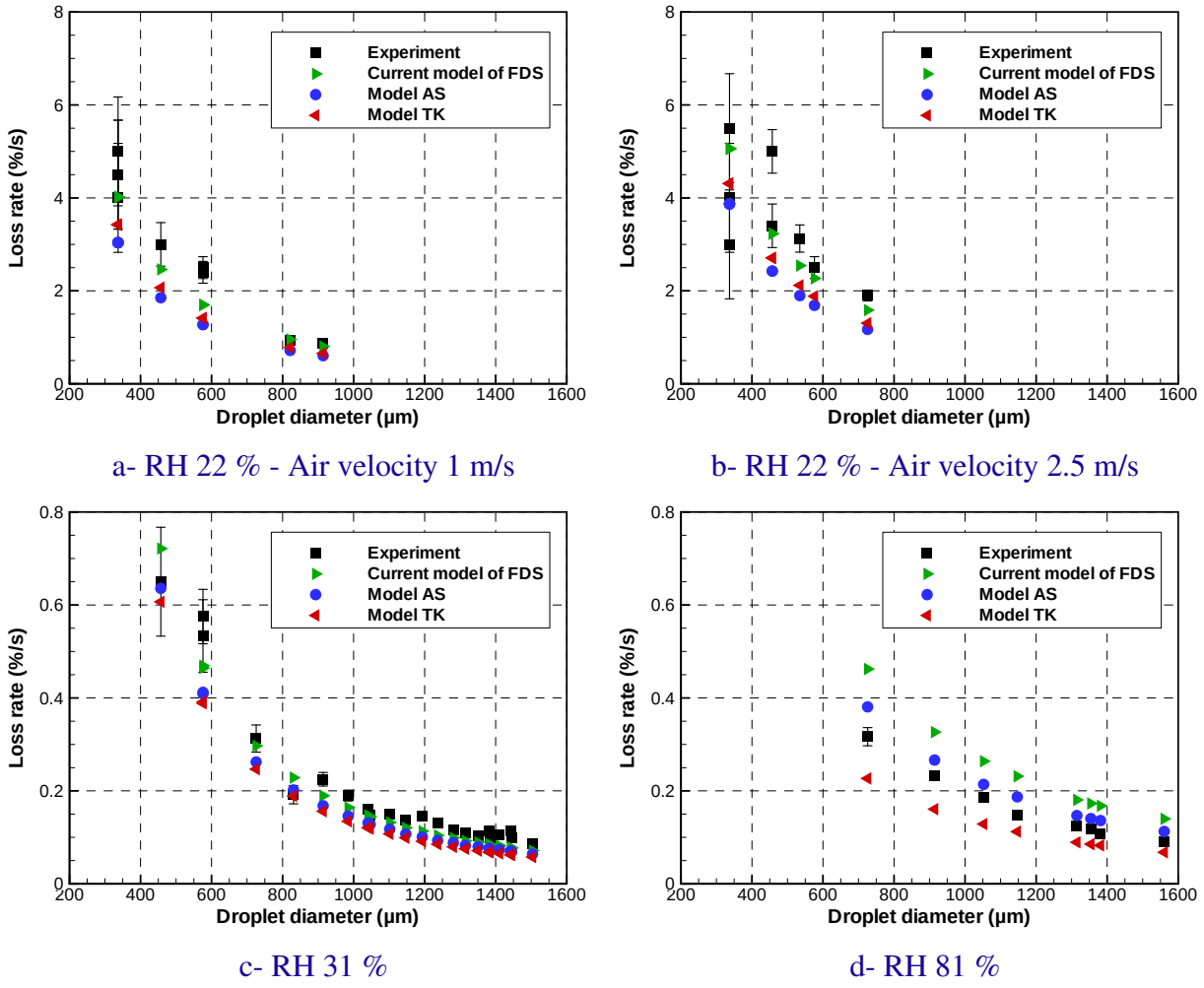

Fig. II.4 — Rate of evaporation versus droplet diameter at the initial time in the tests conducted by Kincaid & Longley [14, 15]

The cases presented in this section have been used to assess the capability of the FDS code to simulate the evaporation phenomenon. This evaluation consisted in first verifying the steady state (see French dissertation). It showed that the prediction is consistent with the thermodynamic equilibrium of two-phase medium. The second stage consisted in validating the rate of vaporization of droplets when subjected to different test conditions. By joining the 48 tests from [14, 32], the mean discrepancy between the loss rates measured and predicted by the model FDS is equal to 18.0 %. Moreover, validation has highlighted the difficulty for assessing a model yielding heat and mass transfer of water droplets. In fact, it is difficult to find useful data base in the scientific literature. Moreover, it appears that the database found and used can conduct to different, even opposite, tendency. For instance, there is a tendency for the model FDS to overpredict the loss rate in the test conducted by Ranz and Marshall and its predictions are further to the measurements in comparison to the two other models AS ans TK. A contrario, in the tests conducted by Kincaid and Longley, the model FDS predicts the best loss rate estimations even it tends to underpredict them.

The cases presented in this section have allowed to study a modification which is now considering but not decided. It concerns the way of modeling heat and mass transfer. The model implemented in the current version could also be modified by the one developed by Taylor and Krishna [21, 33] or the one by Abramzon and Sirignano [1]. Their validation on the basis of the 48 tests has not lead to an obvious improvement in predictions.

II.2 Radiative transfer through water mist

The evaluation of radiative transfer predicted by FDS (version 5.5) through a water curtain falls into the two categories, verification and validation. In fact, the computational results are compared to measurements and to other computational results predicted with the in-house code BERGAMOTE developed at the laboratory LEMTA. All these data which allow the comparison are extracted from [17]. BERGAMOTE code is of particular interest for this verification since its radiative model is strongly different. BERGAMOTE code is based on a two-way Eulerian-Lagrangian description of the dynamics of the spray (using a RANS model with a standard k-ε formulation for the turbulence modeling), combined with a Monte Carlo modeling of the radiation-spray interactions [6]. The radiative properties are evaluated based on the Mie theory involving the exact formulation of the scattering phase function with no simplification. The gas properties are given by a C-k model with a relatively fine spectral definition (based on 43 bands or 367 bands on the whole IR spectrum).

The two simulated configurations are the experiments conducted by Lechêne at the laboratory LEMTA [17]. Water mist is sprayed by seven nozzles (type TP400067, Spraying Systems & Co.) either in the upward direction or in the downward one. Nozzles are located on the same feed pipe and the space between neighboring nozzles is equal to 10 cm. Water mist is sprayed between a heat source (an extended blackbody surface 30 cmx35 cm at 773 K) and a target (IR spectrometer matrix by Bruker used as the detector). The measurement involves one acquisition with the spectrometer when the spray is on, then a second with the spray off. The ratio gives a characteristic transmissivity through the spray T_r or the attenuation A_t by the spray if the complementary part is considered :

$$A_t = 1 - T_r = 1 - \frac{\text{Transmission acquisition with the spray on}}{\text{Transmission acquisition with the spray off}} \tag{II.4}$$

Such measurements are repeated varying the vertical positions of the source and the measurement device between 20 and 100 cm from the injection point, allowing to draw a map of the attenuation ability of the curtain. The schematics on figure II.5 correspond to 40 cm.

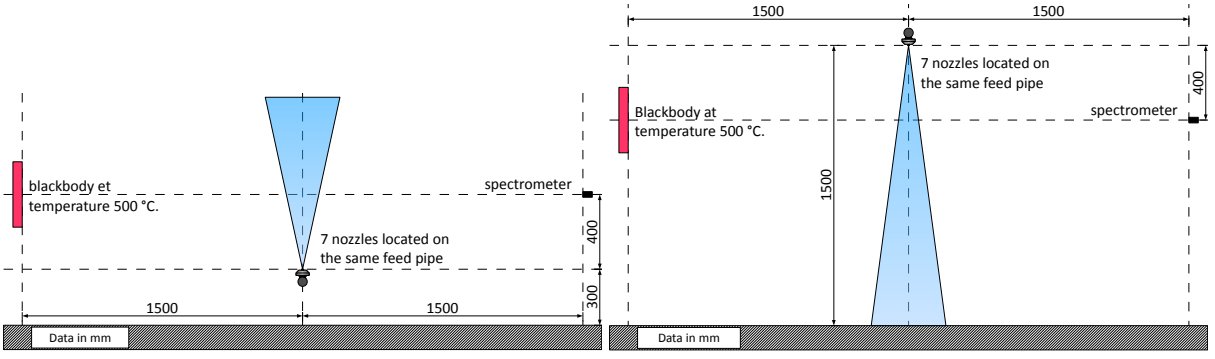

a- Upward configuration b- Downward configuration

Fig. II.5 — Test configurations for radiative model validation when blackbody and spectrometer are 40 cm distant from the nozzle pipe elevation

II.2.1 Modification in the FDS code

The following verification and validation have promoted a code modification (adopted for version 6). This modification allows first to reduce the initializing time in the beginning of the simulation when efficiencies are tabulated and secondly to improve the radiative modeling of a sample of droplets. The modification is strongly inspired of the two references [7, 19]. It concerns the method for computing the radiative properties (absorption and scattering) : the real particle size distribution inside a grid cell is modeled as a monodisperse suspension whose diameter corresponds to the Sauter mean diameter of the polydisperse spray. This simplification leads to a simplified expression of the radiative coefficients functions of the total cross sectional area per unit volume of the droplets A

$$\kappa_{\lambda,p}(s) = \frac{A(s)\, Q_a(r_{32},\lambda)}{\delta x\, \delta y\, \delta z} \qquad \text{et} \qquad \sigma_{\lambda,p}(s) = \frac{A(s)\, Q_s(r_{32},\lambda)}{\delta x\, \delta y\, \delta z} \tag{II.5}$$

As a reminder, in the version 5, local size distribution was supposed similar to that used at the injection point. Only the mean diameter for parameterizing this size distribution was local.

II.2.2 In a participating medium - Downward configuration

Modeling water spray

The nozzle TP400067 has been characterized in a preliminary study at LEMTA [17]. The measurements are summarized in table II.3. This nozzle produces an elliptic spray characterized by two angles equal to 9.25 and 24°. Under an operating pressure of 4 bars, flow rate at each nozzle is around 0.32 l/min, flow rate number [2] being $8.5.10^{-9}$ $m^3/s.Pa^{1/2}$. Considering the orifice diameter and the flow rate, the injection velocity is evaluated around 24 m/s. Mean droplet size in terms of Sauter diameter is 100 µm, 20 cm below the injection point.

Tab. II.3 — Measured spray characteristics

Orifice diameter	0.53 mm
Spray shape	elliptic
Angles of injection	9.25 and 24°
Operating pressure	4 bars
Water flow rate	0.32 l/min
Sauter diameter at 20 cm from the injection point on the spray central vertical centerline	100.8 µm

For modeling the spray produced by this type of nozzle, a spray is simulated at the center of an isothermal enclosure with the FDS code. Spray is defined with the characteristics listed in table II.3 (all these values are used except the orifice diameter and the Sauter diameter 20 cm from the injection point). The droplet size distribution is defined at the injection point in order to approach both the measurement at 20 cm from the injection point and the values computed with BERGAMOTE along the central vertical axis and along the major axis of the elliptic spray 20 and 40 cm below the nozzle.

2. The flow rate number is also called discharge coefficient or K-Factor

Measurement and predictions by the two codes are plotted on figure II.6. On this figure, the computational results for FDS are obtained for a spray defined with a log-normal size distribution parameterized by a dispersion parameter δ=0.4 and a mean diameter dm=150 µm. This definition corresponds to the best agreement we got.

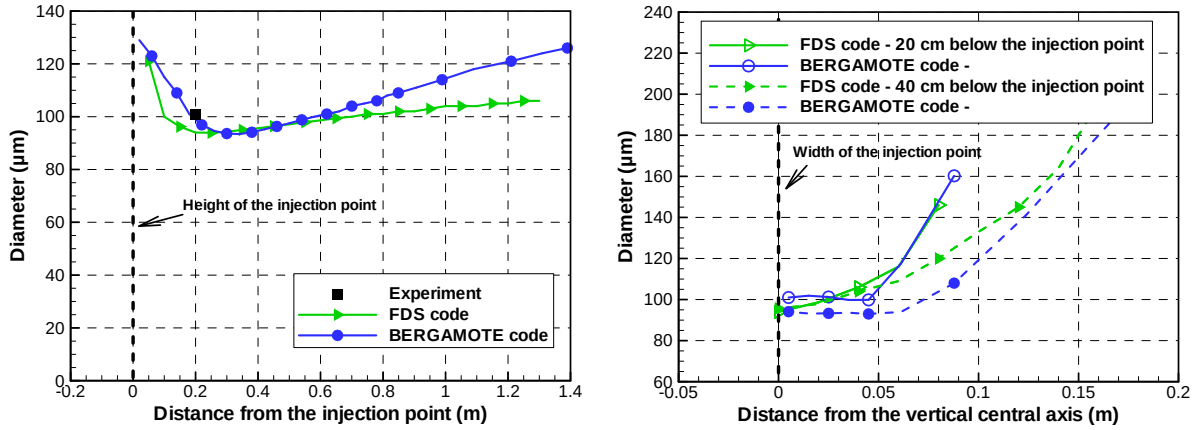

Fig. II.6 — Sauter diameter measured and predicted by the codes FDS and BERGAMOTE along the central vertical axis (on the left) and along the major axis of the elliptic spray at two distances from the nozzle (on the right)

Input data of the simulations

The computational domain in the downward configuration is 3 m long, 2 m wide and 3 m high. This height is set to limit the influence of boundary conditions on spray dynamics. Mesh grid is set for preserving the dimensions of the heat source and the target. The heat source is approached by a square 4 cm on a side. Concerning the angular discretization, the unit sphere is divided into 512 solid angles. The number by default (104) was not sufficient for simulating this configuration, the also obtained transmissivity being higher than 1.

Verification and validation of the code

Note : A first study consisted in verifying heat flux received by the target in a nonparticipating medium. In this verification presented briefly in the French dissertation, FDS predictions converge towards the analytical solution given by the view factors when spatial or angular resolution is increased. For a number of radiation angles equal to 512, the discrepancy is lower than 0.03 kW/m^2 or 7 %.

The measured and simulated attenuation results are compared on figure II.7 at five heights. All curves have the same evolution : attenuation increases almost linearly with distance from the injection point. This evolution results from the spray dynamics. Droplets are rapidly slowed down due to the drag force, their air residence time is also longer [17]. The good general agreement in curves allows to have some doubts about the data measured at 100 cm from the injection point.

The order of magnitude of attenuation is similar in the experiment and the computational simulations done by the codes BERGAMOTE and FDS (version 5.5.0 with the modification). The FDS code without any modification rather underestimates the attenuation. The discrepancy with the measured values is around 31 % with the default version and 11 % with the modified version, while discrepancy between the codes FDS and BERGAMOTE is around 42 % with the default version and 7 % with the modified version.

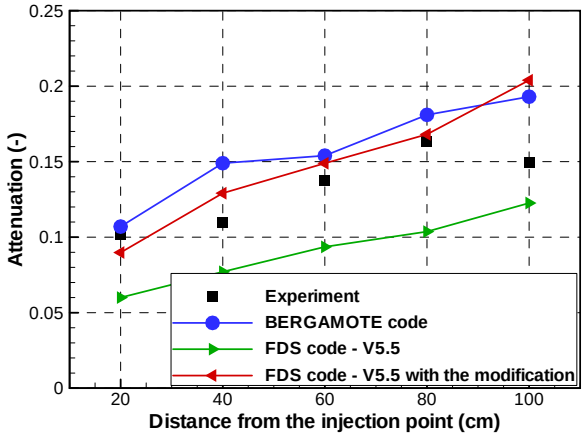

Fig. II.7 — Radiation attenuation through the water curtain measured and predicted with the CFD codes BERGAMOTE and FDS (version 5.5 with and without the modification)

In other words, with regard to these values, this configuration has highlighted a good capability of the CFD code FDS (with and without the modification) to give an estimation of the radiative attenuation through a water curtain. Moreover, the modification of the code presented above leads to an improvement. It means it conducts to a better description of the spatial evolution of the true size distribution through the use of the Sauter diameter.

II.2.3 In a participating medium - Upward configuration

Input data of the simulations

The computational domain in the downward configuration is 3 m long, 2 m wide and 4 m high. Its height is increased comparing to the previous configuration for limiting the influence of boundary conditions on spray dynamics and for conserving all the droplets inside the domain. The spatial and angular discretizations are the same as in the downward configuration, like all the other input data. Only the spray orientation is oriented in the upward direction.

Verification and validation of the code

The measured and simulated attenuation results are compared on figure II.8 at five heights. The upward configuration is particularly complex since gravity plays a stronger role and the residence time of water droplets is really longer (ten times as long [17]). Due to the higher water volumetric fraction, radiation attenuation is higher in the upward configuration compared to the downward one.

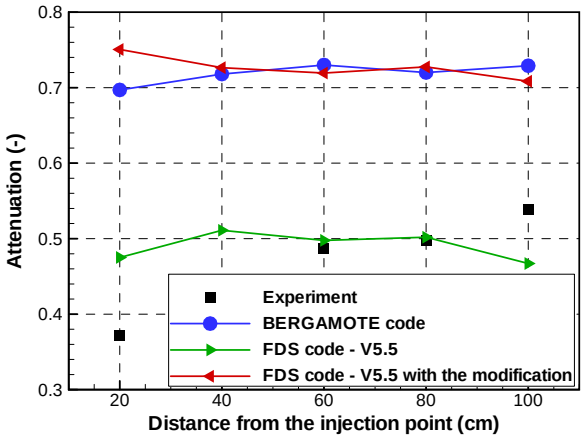

Fig. II.8 — Radiation attenuation through the water curtain measured and predicted with the CFD codes BERGAMOTE and FDS (version 5.5 with and without the modification)

Figure II.8 shows that measured attenuation increases linearly with distance from the injection point. *A contrario*, all predicted attenuations have the same evolution : they are almost constant. Also, the measurements vary between 35 and 55 %, the predictions with BERGAMOTE and FDS (with the modification) are in the order of 70 % and the predictions with the default version of FDS are in the order of 50 %. Consequently, the discrepancy between measurements and computational results is quite high.

The good agreement between the two codes BERGAMOTE and FDS (with the modification) supports Lechêne's idea : the spraying seems to depend on the orientation of the injection [17, 18]. In other words, the droplet size distribution which has been determined on the basis of downward measurements must not be true anymore for this upward configuration. Droplets would be likely biggest inducing lowest attenuation through the spray.

Magnitude of attenuation through water curtain is similar in the simulations with BERGAMOTE and the modified FDS, the agreement is around 2 %. The default FDS code tends to underestimate attenuations, the agreement is also around 31 %. Finally, based on the absolute and relative discrepancies, the FDS code is able to give an estimation of the radiation attenuation through the curtain along the vertical axis and this estimation appears better with the modified radiative model.

The cases presented in this section have been used to assess the capability of the FDS code to simulate the radiative transfer. In the French dissertation, this work is executed by verifying first of all the propagation in a nonparticipating medium thanks to view factors. Only the validation/verification in a participating medium is presented here in the English dissertation. This assessment has shown the tendency of the FDS code (version 5.5.0) to underestimate the radiative attenuation through the spray in the tests conducted by LEMTA. In the downward configuration, the relative difference with measurements is around 31 % and the values are in the same order of magnitude : the measu-

red attenuation are comprised between 10 and 17 % whereas the predicted values vary between 6 and 12 %. In the upward configuration, the relative difference with BERGAMOTE is again around 30 % but the values are not in the same order of magnitude anymore : the attenuations predicted with the default FDS is around 50 % whereas the one predicted with BERGAMOTE are around 70 %.

Moreover, these validation/verification cases have allowed to assess one modification of the FDS code which concerns the way of computing the radiative properties of a sample of droplets located in the grid cell (see Sub-section II.2.1). In the two configurations, this modification has lead to an improvement in predictions of attenuations. This modification is now integrated in the new version 6.

II.3 Conclusion

This chapter in the French dissertation aims first at presenting the FDS code (version 5) by laying the emphasis on the water spray model and the radiative model. Its second objective is to evaluate the capability of some models. Only this second task is presented here in the English dissertation. This evaluation is conducted at the laboratory scale for focusing on one particular part of the FDS code. The topic of this PhD study motivates us to look at the models yielding the interaction of water spray, fire source and environment. Note that the interaction with solid surface has not been studied. Overall, the evaluation has shown a good capability of the FDS code to simulate the studied phenomena. The evaporation model extracted from FDS has predicted loss rates of a single motionless water droplet in 48 tests with a mean discrepancy with measurements of 18.0 %. Concerning radiative attenuation, the evaluation has highlighted a tendency of the FDS code to underestimate attenuations through water curtain with a discrepancy [3] close to 30 % for upward and downward configurations.

The evaluation has also highlighted few weaknesses of the FDS code. For this reason, few modifications have been considered. Among them one in the radiative model has been integrated to the new version 6. In the case of tests conducted at LEMTA, this modification has allowed to improve the numerical representation of a sample of droplets for radiative considerations. The other modifications concern the vaporization model and more precisely its structure and the model of heat and mass transfer itself. Concerning the structure, this modification would allow to simulate saturation cases and also reduce the computational time. Concerning the choice of the model, validation of two models, even sophisticated, has not conducted to an obvious improvement in prediction than the one implemented in the current version. These modifications are still under discussion.

After this chapter, it can likely be considered that the FDS code (version 5) is able to be used in the computational study dealing with tunnel fire involving or not water mist, at least if water spray is conveniently simulated (droplet size, water flow rate, etc.).

3. In the downward configuration, the discrepancy is computed by comparing with measurements. In the upward configuration, it is computed relative to data predicted with the other CFD code BERGAMOTE

III At the tunnel scale

The present chapter deals with tunnel fire with and without any mitigation system. It allows to assess the FDS code in this configuration. Moreover, it aims at improving our understanding of the phenomena involved, at quantifying them and at highlighting key parameters influencing the tunnel environment. To do that, the study uses a tunnel test campaign conducted between 2005 and 2008 within a framework of a research project involving the French organizations CSTB, CETU, PPRIME Institute and DSC [4, 27]. This campaign was carried out in a one third scale tunnel. The varied parameters were the fire load (two types of wood crib, heptane pool), the longitudinal ventilation rate, the activation or not of the mitigation system and the number and the arrangement of the nozzles. The all tests are deeply described and studied in [4, 27]. In the context of the present PhD study, only a few of them is used.

The approach consists first in evaluating the measurement uncertainty in order to estimate the level of confidence associated to experimental data. This evaluation is not presented here in the English dissertation, a detailed presentation is available in annex I of the French dissertation. Then, the computational code is validated first without any mitigation system (cf. Section III.2) and secondly when a water mist is sprayed (cf. Section III.3). In other words, the ability of the FDS code for simulating the tunnel fire environment (thermal conditions and smoke flow) is estimated based on comparisons with experimental data. The extensive use of the numerical reconstructions allows last to highlight the tunnel configuration characteristics and to measure the impact of water mist on the tunnel environment, especially thermal and toxic conditions.

III.1 Description of the tests

Four tests are used in the present study, two of them involve water mist. These tests have been selected because they involve a liquid fuel (heptane). This choice aims at limiting the uncertainty concerning the fire activity. In fact, this fuel type is of great interest to have a quasi-constant surface area.

These two tests without water mist (tests 2 and 9) have been conducted with two different longitudinal ventilation rates. The two tested velocities allow to study the two different ventilation regimes : the sub-critical one with an expected backlayering effect, and the over-critical one with a simple smoke flow downstream. The two tests with water mist (tests 27 and 28) have been conducted with a ventilation velocity above the critical backlayering value. The difference between tests 27 and 28 concern the mitigation system and more particularly the number of nozzles.

III.1.1 Set-up

The model tunnel dimensions are such that the scale ratio with a real tunnel is in the order of 0.3. The use of a midscale experimental gallery has several assets, among them, the possibility to conduct tests in a easier way with reasonable costs. Moreover, it allows studying phenomena in a more realistic way than with laboratory scale ($1/20^{th}$).

The tunnel is horizontal and completely belowground. It is 43 m long, with a partial circle cross section around 4 m^2 in surface and with a 2.16 m hydraulic diameter. Figure III.1 presents a cross-sectional view of the tunnel.

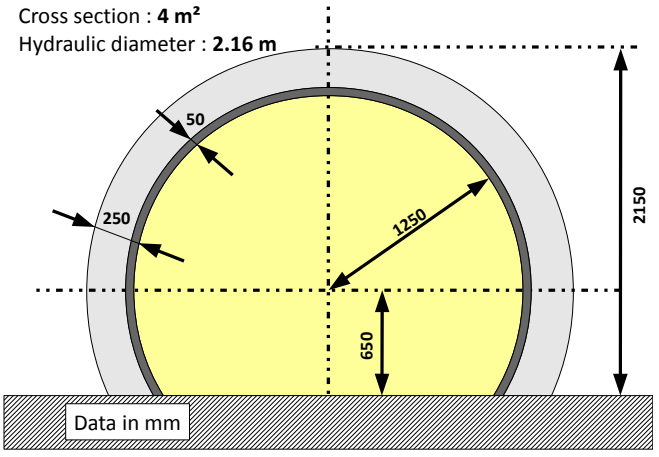

Fig. III.1 — Cross-sectional view of the model tunnel

The tunnel walls and the floor are made in concrete. The lateral walls are covered by 5 cm of a fire resistant mortar cement. Its thermal properties are well-known, they have been measured in a preliminary study, for temperature range from 27 to 608 ˚C. Their values are listed in table III.1. In the same table, thermal characteristics used in the computational study for concrete are given too.

Tab. III.1 — Thermal characteristics of tunnel materials

Temperature	Density	Thermal conductivity	Specific heat
Mortar			
27 °C	969 kg/m^3	0,357 W/m · K	1100 J/(kg · K)
207 °C	931 kg/m^3	0,272 W/m · K	1192 J/(kg · K)
409 °C	921 kg/m^3	0,264 W/m · K	1308 J/(kg · K)
608 °C	919 kg/m^3	0,245 W/m · K	1319 J/(kg · K)
Concrete			
-	2100 kg/m^3	1,2 W/m · K	1400 J/(kg · K)

III.1.2 Fire load

The fire load is provided by a heptane pool at a central location on the transverse section. The steel pool is 1 m long, 0.5 m wide and 0.1 m high. The pool surface area A is also equal to 0.5 m^2. This value can be considered high enough to be in the radiative mode : radiative transfer dominates burning [2]. In such case, the heat release rate (HRR) can be approximated for an open space by Zabetakis and Burgess model [2] :

$$\dot{Q} = \Delta H_c \cdot \dot{m}''_\infty A \left(1 - \exp^{-k \cdot D}\right) \tag{III.1}$$

where D is the pool diameter ans ΔH_c is the heat of combustion of heptane. The two empirical factors k and $\dot{m}''_\infty$ vary widely with the type of fuel considered. For heptane, Babrauskas advises the following values [2] :

$$\Delta H_c = 44,8 \text{ MJ/kg}, \qquad \dot{m}''_\infty = 0,101 \text{ kg/m}^2\text{/s}, \qquad k = 1,1 \text{ /m} \tag{III.2}$$

Considering the pool dimensions, HRR would be equal to 1.32 MW in an open space. It should be noted that the confined situation of tunnel fires is not taken into account rather than the influence of the ceiling and the walls is substantial (see Chapter I in the French dissertation).

HRR is deduced from fuel weight loss monitoring by supposing that its mass loss $\dot{m}''$ is equal to its burning rate such as :

$$\dot{Q} = \Delta H_c \cdot \dot{m} \tag{III.3}$$

In the tests involving water mist, gas composition monitoring allows to estimate HRR based on oxygen consumption. Moreover, this approach is in theory more accurate because the heat released per oxygen consumed does depend on neither the type of fuel considered, nor the combustion reaction. This approach consists in measuring the oxygen consumed in a combustion system in order to determine the neat heat released. It is detailed in [10]. This approach is not used in the two tests without water mist because of a malfunction in the measuring chain.

III.1.3 Tunnel ventilation

The ventilation system is located at the downstream side of the tunnel. It allows to extract a roughly constant volumetric gas volume flux. One of the aim of the test campaign is to study the two different ventilation regimes : the sub-critical one with an expected backlayering effect where some combustion gases are transported upstream the fire, and the over-critical one with a simple smoke flow downstream. The critical velocity allows to prevent backlayering. Many theoretical or empirical models gives an estimation of this critical velocity from the tunnel geometrical characteristics (slope, height, hydraulic diameter) and HRR. The values predicted by five models for a 1.4 MW fire are listed in table III.2. They are comprised between 1.1 and 1.8 m/s.

Tab. III.2 — Critical velocity estimated with five models for a 1.4 MW fire

Model	**Danziger and Kennedy [8]**	**Oka and Atkinson (*) [30]**	**Wu and Bakar [37]**	**Kunsch [16]**	**Mégret [28]**
Type	theoretical	empirical	empirical	theoretical	semi-empirical
Velocity	1,4 m/s	1,5 m/s	1,8 m/s	1,8 m/s	1,1 m/s

(*) In Oka and Atkinson's model, the coefficient is set to 0,35 in order to be closer to the CSTB campaign (location and rectangular shape of the fir load)

Without water mist, the two studied tests have been performed with exhausted volumetric rates of 5.2 m^3/s (test 9) and 8.8 m^3/s (test 2) at the initial time. These values correspond to longitudinal velocities equal to respectively 1.3 m/s and 2.2 m/s without fire. These two velocities would also be below and above the critical backlayering velocity, leading consequently to the two different ventilation regimes. The two tests involving a mitigation system are conducted with longitudinal velocities around 3.0 m/s corresponding to an over-critical regime.

III.1.4 Water mist system

The water mist system is composed of a high-pressure pump connected to several nozzles located on the same row on the center line of the tunnel, close to the roof. The number of nozzles varies : there are three nozzles in test 28 and six nozzles in test 27. All the nozzles are the same. In test 27, nozzles are located upstream and downstream the fire location : between 4 m upstream and 3.5 m downstream the fire location, 1.5 m apart one other. In test 28, nozzles are only located upstream the fire location : at 4 m, 2.5 m and 1 m from the fire location.

The operating pressure is set around 90 bars. The flow rate number provided by the manufacturer is equal to 0.58 $l/min/bar^{1/2}$. The water flow rate injected at each nozzle is also close to 5.5 L/min, corresponding to a total mist discharge rate around 16.5 l/min in test 28 and 33 L/min in test 27. The water mist system is a deluge one. It means all the nozzles are manually activated at the same time. The activation time is 300 s after ignition, which allows to reach the stationary state for the fire activity.

Each nozzle installed in the midscale tunnel consists of four side injectors and one central injector (see Figure III.2). Each solid spray pattern is conic and the ejection angle has been evaluated [1] as 20°. The geometrical dimensions are indicated on figure III.2. The orifice diameter of all injectors is around 0.5 mm. According to the above mentioned water flow rate, an initial velocity of 60 m/s is assumed.

One nozzle used in the test campaign has been characterized by the French tunnel study center (CETU) in collaboration with the laboratory LMFA of École Centrale de Lyon [31]. The spray characterization was done by Phase Doppler Analysis (PDA). A description of the PDA technique is given in [11]. Droplet size has been determined at five positions along the central axis between 4 and 50 cm from the injection point (see figure III.3). The measurement will be next used for calibrating the Lagrangian particle submodels of the FDS code. It is also assumed in the present study that sprays produced by the side injectors are similar to the central one.

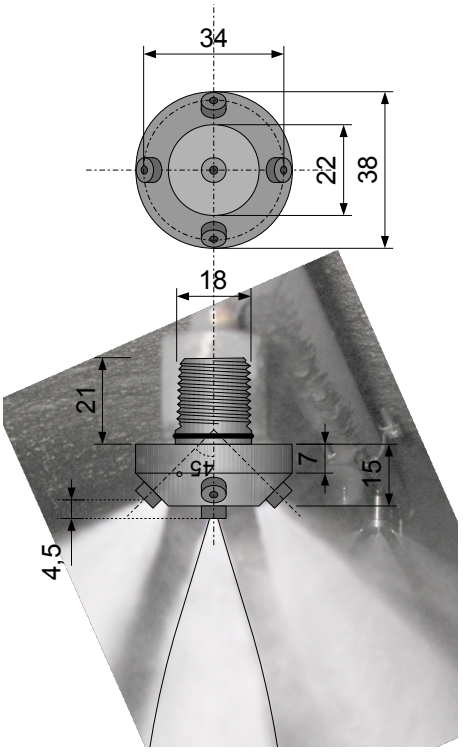

Fig. III.2 — Nozzle geometrical characteristics

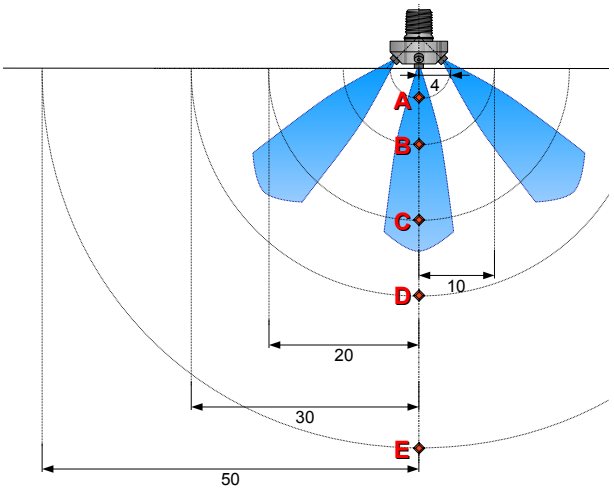

Fig. III.3 — Location of droplet size measurement in PDA

1. This value is estimated with the PDA technique with measurements over a circle, its center being at the central injector and the radius being 30 cm [31]

III.1.5 Measurement characteristics

In addition to the fuel mass, several parameters are measured : gas temperature, gas velocity, heat flux and in the tests involving water mist, gas composition. The corresponding sensors are located on 10 sections (6 downstream the fire location and 4 upstream) at various heights. The output signals of these sensors are fed to a data acquisition system. The key longitudinal sections are indicated in figure III.4 according to the measured quantity : "T" for gas temperature, "V" for gas velocity, "FM" for heat flux measurement, "Compo" for gas composition. The values and the signs indicate the location in meter with reference to the fire location at section 0.

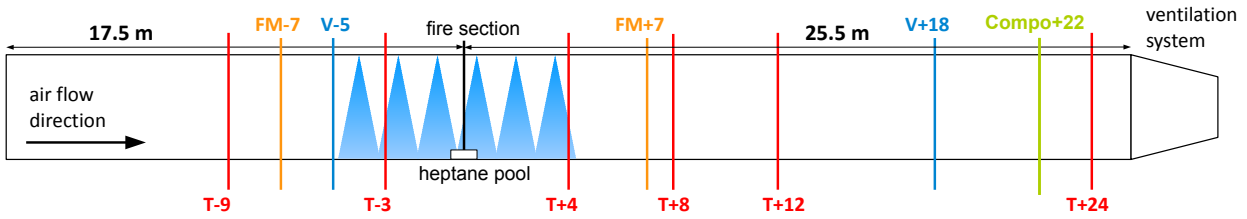

Fig. III.4 — Longitudinal view. Position of measurement sections. The location of the nozzles of the water mist system are represented by blue triangles

In order to get complete thermal distributions in the tunnel, a set of thermocouples is used upstream and downstream the fire section (see Ref. [3]). Upstream the fire, thermocouples are mainly located in the upper part in order to characterize the smoke layer that could counter-flow out of the tunnel due to the backlayering phenomenon. Downstream the fire, thermocouples are placed more uniformly on the sections in order to get the temperature field over the whole section.

Longitudinal ventilation rate is measured with Recknagel bi-directional pressure probes. This type of probes is particularly suitable in that context to detect the smoke counter-flowing since it works in both flow directions. The sensors are located at each measurement section so as to obtain a velocity vertical profile.

Heat fluxes are measured by radiometers oriented toward the fire located at 7 m upstream and downstream at several heights on a vertical central line.

Gas composition (oxygen, carbon monoxide and carbon dioxide) is measured 22 m downstream the fire by sampling gases in nine points. The sampled gases are mixed and cooled before being analyzed.

III.2 Tests without water mist

Two tests without water mist are simulated. In the test campaign, they correspond to tests 2 and 9. They are conducted under two different ventilation regimes, a sub-critical one in test 9 and an over-critical one in test 2. HRR reached during the stationary period in these tests is close to the estimation mentioned before in subsection III.1.2. However, this tendency can not be generalised to all tests in the campaign. In fact, for instance, in test 1 conducted with the same fire load than in tests 2 and 9 but with a lower ventilation velocity (around 1 m/s), the maximal HRR is in the order of 3 MW. This difference between the measured rate and the estimation around 1.4 MW has been attributed to the influence of the tunnel characteristics on the fire activity i.e. the continuous supply in oxygen due to the tunnel ventilation and the additional heat to the burning object emitted by the tunnel walls and the hot smoke [3]. So, as figures III.6-a and III.6-b illustrate, increase the tunnel ventilation velocity in the range between 1.4 et 2.2 m/s has reduced the influence of the tunnel configuration on the fire activity. This tendency is very interesting here since it allows to study the influence of the ventilation on the thermal conditions and on the tunnel heat distribution (see Section III.2.4 in particular).

The present section deals with input data in the test simulation (boundary conditions, initial conditions, etc.), the comparison between the measurements and the numerical results and the study of the heat distribution.

III.2.1 Input data definition

Simulate the tests consists in numerically describing them to be able of predicting the thermal conditions and the air flow in the tunnel. Within the framework of this thesis, the modelling concerns essentially the tunnel structure, the fire (fuel, HRR) and the longitudinal ventilation of the tunnel. Except the tunnel ventilation velocity and HRR which are specific to each test, all the input data are identical in both tests such as the geometrical and thermal characteristics of the tunnel and the combustion reaction.

Computational domain and discretization

The computational domain includes a free area at the upstream side, the whole tunnel (ramp at the upstream side and tube) and the ventilation system at the downstream side. The gas grid cells located outside the tunnel are defined as obstruction to reduce the computational time (see Figure III.5). The free area at the upstream side is simulated in order to better promote the flow turbulence in the tunnel [9].

The grid is made of a structured mesh with cubic cells 10 cm in size, providing a total grid with 440 000 cells. The angular discretization regarding the radiation involves 512 control angles and the grey gas model is used, as in the verification and the validation cases presented in chapter II.

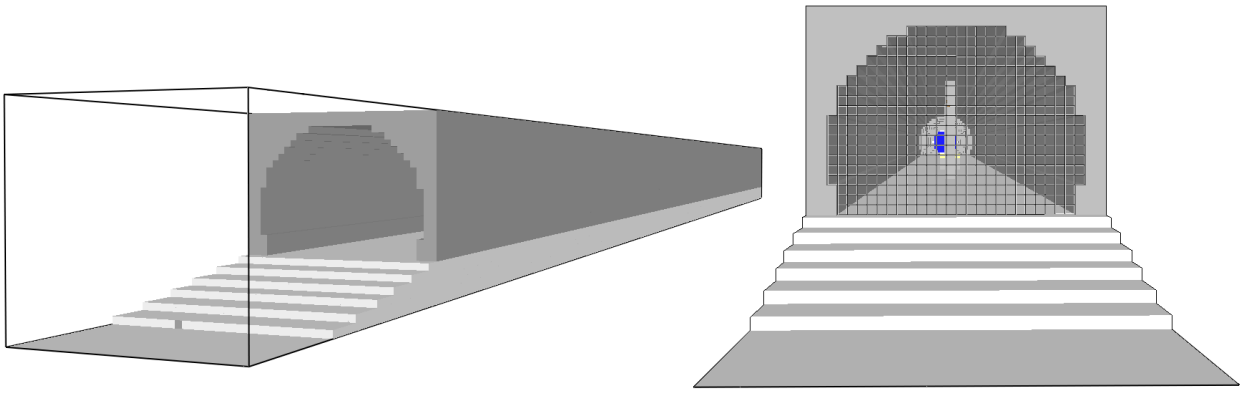

Fig. III.5 — Computational domain, discretization and representation of the simulated tunnel structure

Tunnel walls

The bend of the tunnel and the ventilation system is approached by a succession of cubic obstructions, the space step corresponding to the spatial discretization (see Figure III.5).

The 1-D model of thermal transfer is used for the obstructions. The thickness and the thermal properties of the tunnel structure are defined as input. Concerning the mortar protecting the side walls of the tunnel, its thickness is equal to 5 cm and its thermal properties correspond to those measured in the preliminary study (see Table III.1). To obtain the characteristics at a given temperature, the CFD code does a linear interpolation from the input data. Concerning the floor made in concrete, a thickness equal to 8 cm is considered. Its thermal characteristics are defined so as to be representative of this material, they are listed in table III.1.

Fire load

The studied tests have been conducted with the same fire load produced by a heptane pool. This pool is represented by an obstruction (1 m long, 50 cm wide and 0.1 m high) located 30 cm high from the floor (dimensions et locations are similar to the experiment). The used combustion model is the default one in the version 5.4. Upon mixing, the reaction of fuel and oxygen occurs rapidly and completely, the combustion process is also referred to as “mixing-controlled” [26]. The products yields are directly function of the fuel consummation, they are defined as input. In all simulations, the fraction of fuel mass converted into smoke particulate and carbon monoxide is set based on the values indicated in [34] which refer to a well ventilated fire : the soot yield is set to 3.7 % and the CO yield is set to 1.0 %. The corresponding combustion reaction is as follows :

$$C_7H_{16} + 10,668\,(O_2 + 3,76\,N_2) = 7,983\,H_2O + 6,659\,CO_2 + 0,036\,CO + 0,339\,\text{Suie} + 40,117\,N_2 \quad \text{(III.4)}$$

Fuel consummation is deduced from HRR defined as input. This input data is a piecewise linear function approximating HRR deduced during the experiment from fuel weight loss monitoring. Figure III.6 presents the temporal evolution of input data and measured HRR in tests 2 and 9, uncertainty to this variable is also plotted.

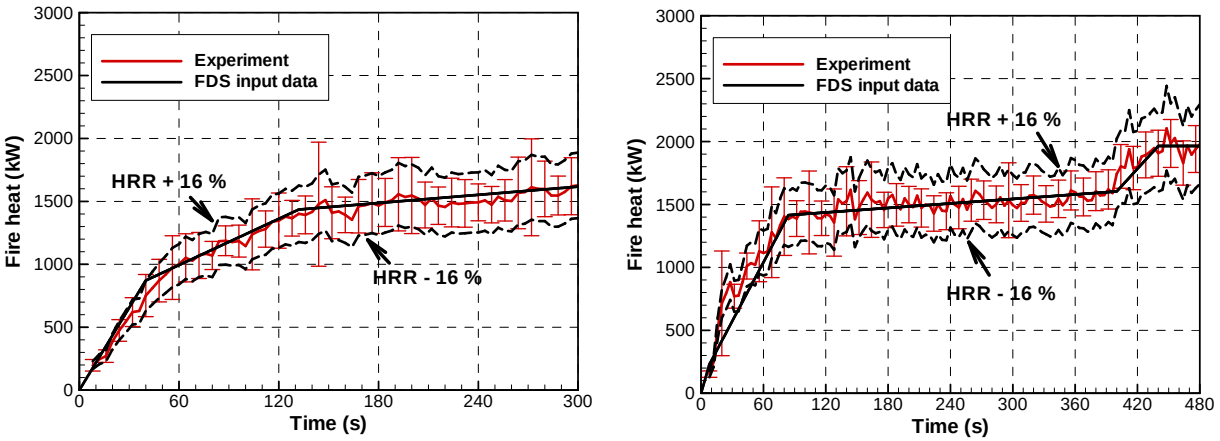

a- Test 9 b- Test 2

Fig. III.6 — HRR versus time, with uncertainty data and smoothing function entered as the source term in the simulation.

As illustrated in figure III.6, the HRR evolution is composed of two stages in test 9 and three stages in test 2. During the first hundred seconds, HRR increases strongly. Then, there is a level-off period : HRR is almost equal to 1.5 MW in the two tests. Last, in test 2, the test duration of which is longer, there is a sharp peak up to 2 MW at 420 s. This peak results from an increasing volume temperature of the fuel (all the substrate reaches the boiling point).

Ventilation

A constant volumetric flow rate is extracted at the downstream tunnel extremity. It is equal to 5.4 m^3/s in test 9 and to 8.8 m^3/s in test 2. The corresponding longitudinal velocity in the tube at the initial time is equal to 1.35 m/s in test 9 and 2.2 m/s in test 2.

III.2.2 In the sub-critical case

The longitudinal velocity induces a sub-critical ventilation regime. In other words, a counterflow is observed upstream with smoke exiting the tunnel at its entrance ; smoke is also flowing downstream toward the ventilation system. Consequently, the environment is thermally stratified upstream and downstream the fire location (see Figures III.7 and III.8). For illustration, after 240 s, 12 m upstream the fire, predicted and measured temperature close to the roof is comprised between 270 and 300 °C. In comparison, at the time and at the same distance from the fire, predicted and measured temperature is around 130 °C at mid-height and around 30 °C close to the floor.

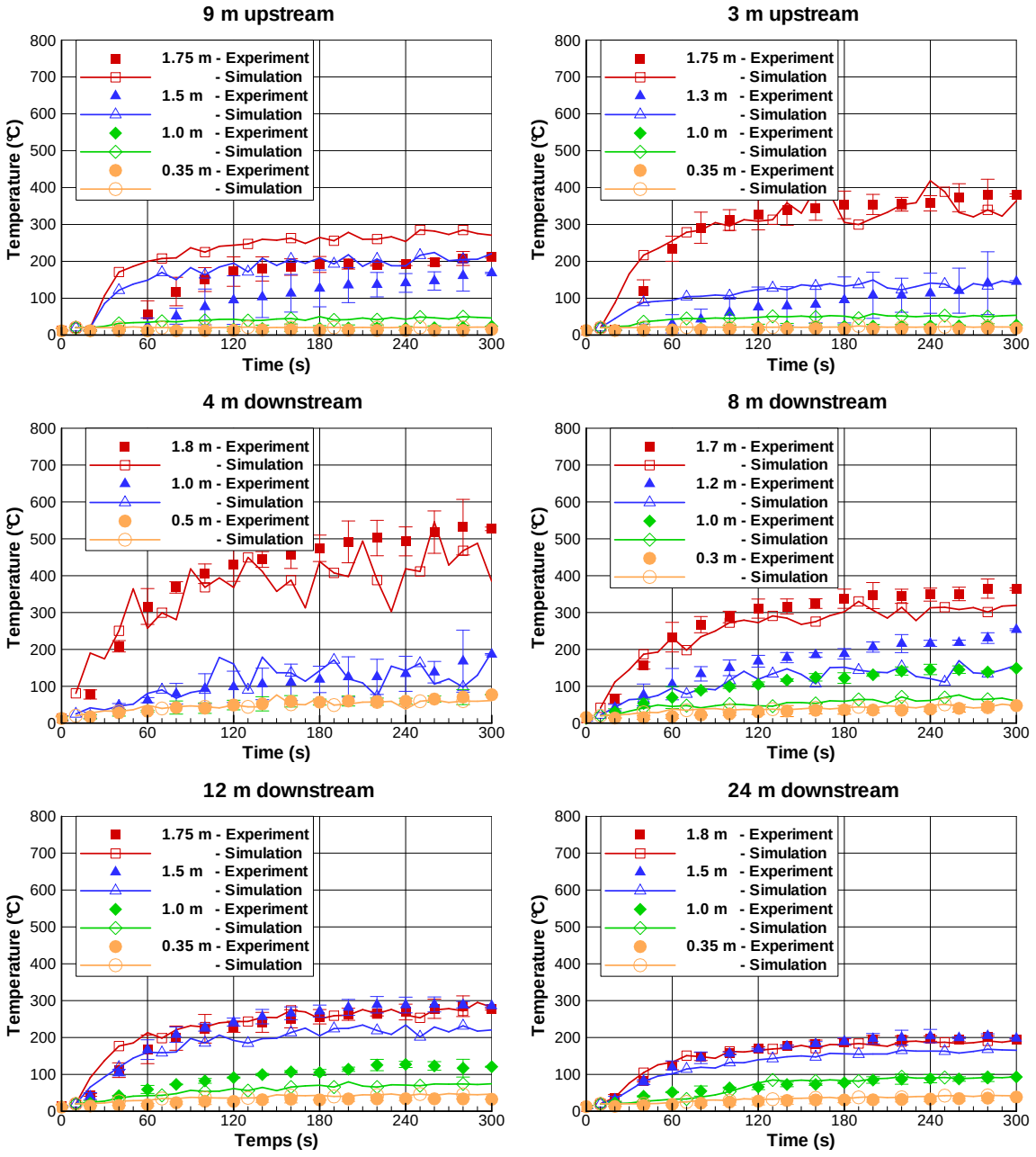

Fig. III.7 — Predicted and measured temperatures on the vertical centerline of six measurement sections (point for experimental data and solid line for simulation)

As smoke is flowing toward both tunnel extremities, heat is transfered to walls and smoke is mixing with the incoming fresh air. Consecutively, air temperature decreases in the upper part of the tunnel and increases in the lower part, the further the measurement section is.

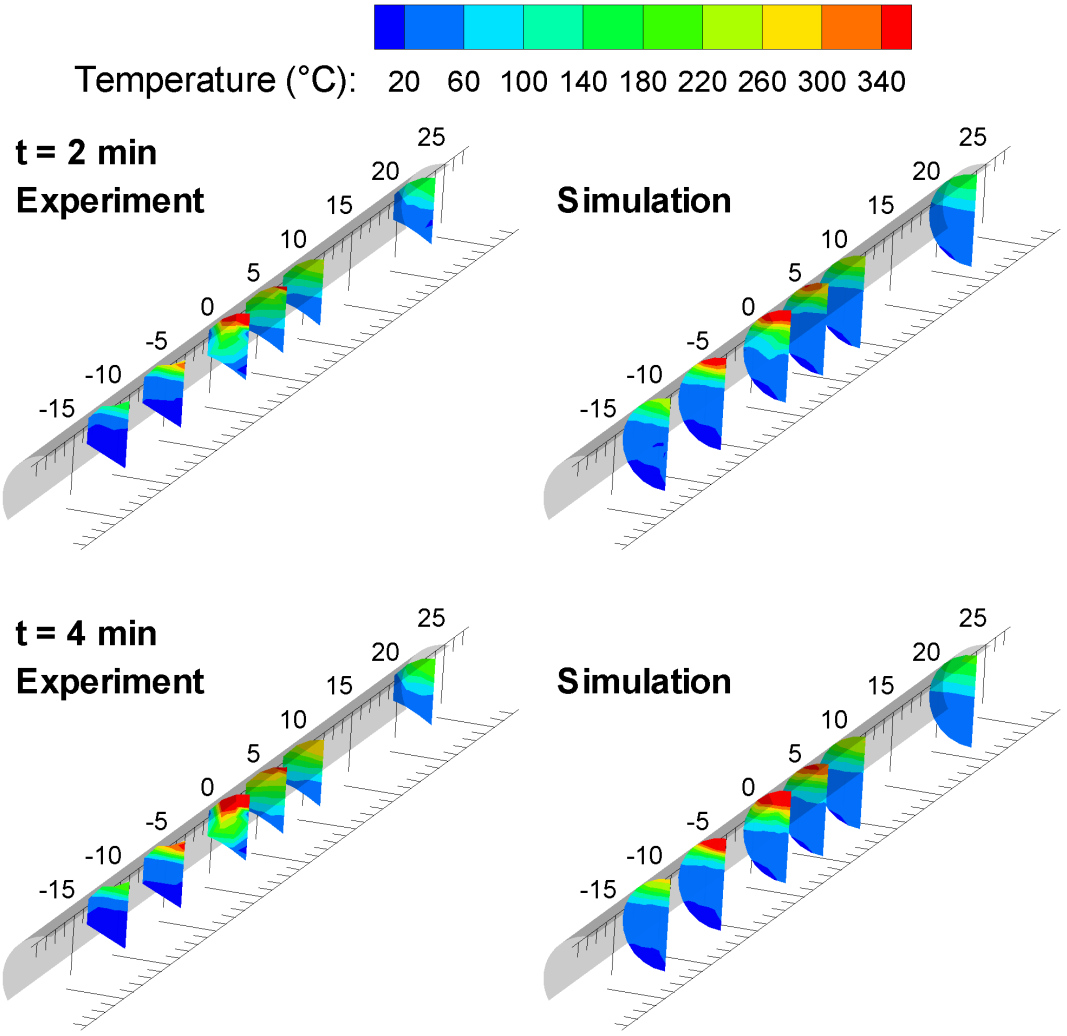

Fig. III.8 — Temperature contour at six measurement sections (2 and 4 minutes after ignition)

Air temperature

In general, the temporal evolution of temperature is well predicted by the CFD code (see Figure III.7). Like the measurements, predicted temperatures have the same evolution than HRR : a growth phase followed by a quasi-stationary phase.

Moreover, predicted data are in the confidence interval given by the error bars (except 9 m upstream and at mid-height downstream). The agreement defines as the mean square relative difference between predicted and measured temperatures is comprised between 15 % and 26 %, except 9 m upstream (60 %) where the thermal vertical gradient is overpredicted by the code (see Figure III.7).

The agreement appears to depend on the locations of the measurement sections (distance and position from the fire). Figure III.9 shows the longitudinal temperature profile at two heights for two moments. It confirms the observations made by Trelles et Mawhinney in [35] and Demouge in [9]. Firstly, the CFD code tends to under-estimate the temperatures in the flame region. Secondly, the difference between experiment and simulation is much smaller when the measurement section is away from fire. This could be attributed to a poor representation of the zone releasing heat by the CFD tool. The flame tilt is likely tricky to reproduce due to the longitudinal ventilation.

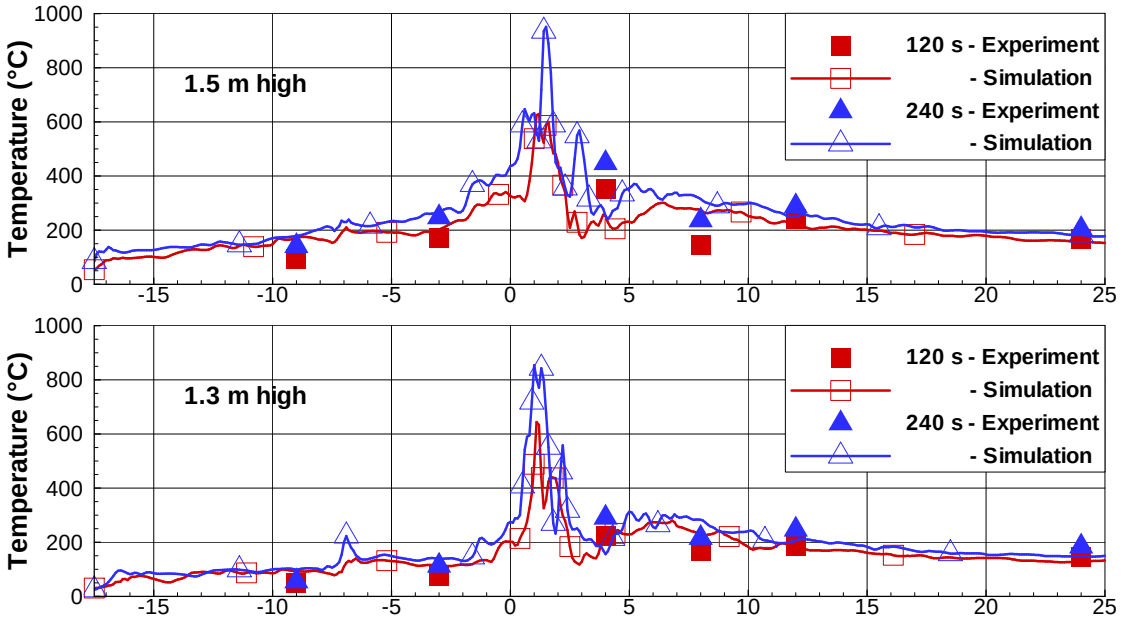

Fig. III.9 — Longitudinal profiles of temperature at 1.3 and 1.5 m high after 120 and 240 s

However, upstream the fire location, this tendency is reversed : agreement is better at 3 m from the fire than at 9 m (see Figure III.7). In fact, temperature and thickness of the smoke layer appear to be better predicted over the test duration at 3 m whereas at 9 m smoke layer is hotter and less thick than the measured one. The first chapter in the French dissertation details the tunnel air flow upstream and downstream the fire location. It consists in two parallel motions with different velocities and densities. The unstable tangential discontinuity manifests itself in the form of waves being generated at the interface. The tangential discontinuity is more important upstream the fire where smoke and incoming fresh air are flowing in opposite directions. When longitudinal air velocity is below the critical backlayering value, mixing between the two motions upstream the fire location is also important. It appears on figure III.7 that the FDS code does not well reproduce the interface between the two motions upstream the fire location : it underestimates the mixing between the smoke layer in the upper part and the fresh air in the lower part. This underestimation induce a discrepancy which is bigger and bigger when the measurement section is going further toward the upstream tunnel extremity.

The impact of this underestimation of mixing between the two motions is also observed downstream the fire. Indeed, the difference between predicted and measured gas temperatures vary with the location of the measurement point within the section. This difference is generally small near the roof and the floor but higher in an intermediate zone at mid-height. This can be partly solved by using 5 cm grid cell size in this area ((instead 10 cm). Indeed, this zone is particularly difficult to model due to the high shear rates occurring at smaller scales than the numerical grid size ; dividing the grid cell size by two has induced a better estimation of the hot layer temperature and thickness. However, the 5 cm grid cell size can be used only for sensitivity study because it requires a pretty longer computational time (362 h with 2 processors for the 5 cm grid cell size compared to 36 h with 1 processor for the 10 cm grid cell size of a 3 GHz Xeon with 8 Go of RAM). The underestimation of the mixing of the hot smoke layer with the incoming fresh air can also be solved by setting a periodic exhaust volumetric rate condition at the downstream boundary which artificially promotes a turbulent flow.

Air velocity

Air velocity versus time measured in six points (three located 5 m upstream and three located 18 m downstream the fire) is plotted on figure III.10. These points belong to the vertical centerline between 40 cm and 1.85 m high. The measured and predicted velocities have the same evolution and the agreement between the experimental and numerical curves is within the overlapping uncertainty limits. It also shows that the air flow is well captured by the CFD code. Note the significant back-layering effect in the upstream section where the gases are flowing in a counter current in the upper part as compared to the lower part of the tunnel.

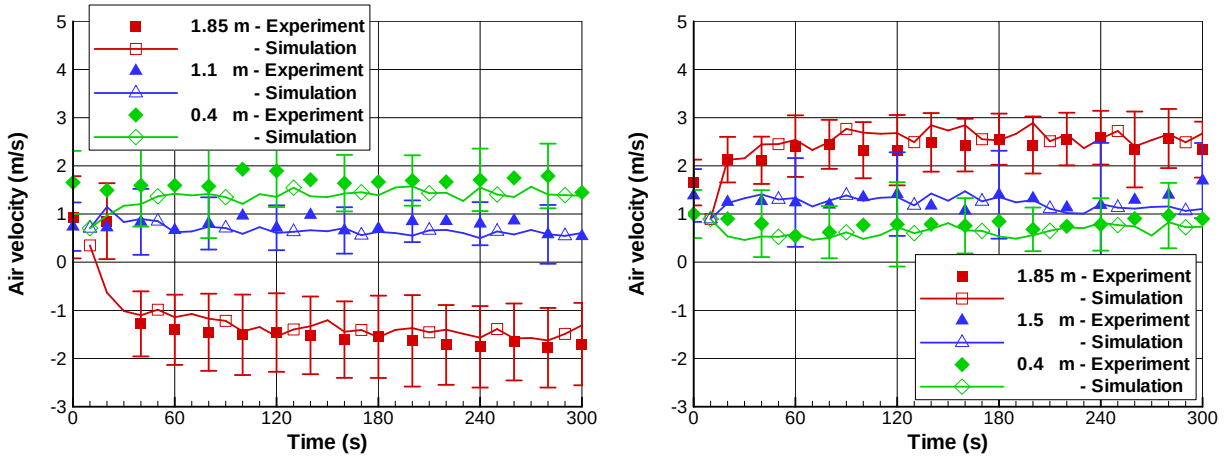

a- 5 m upstream

b- 18 m downstream

Fig. III.10 — Local velocity acquisition versus time on the vertical centerline of two measurement sections (point for experimental data and solid line for simulation)

Heat flux

Radiative fluxes have been measured at equal distances from the fire, 7 m upstream and downstream the fire location. Data are reported on figure III.11. This figure shows a correct agreement between measured and predicted values when the measurement point is located below 1.1 m upstream the fire and below 1.3 m downstream the fire whereas an overestimated flux is observed in the upper part. This is attributed to first the poor quality of heat flux measurement in hot smoke that is partly constituted of water vapor and soot and secondly, to the extreme measurement conditions for the radiometers, the air temperature exceeding 200 °C.

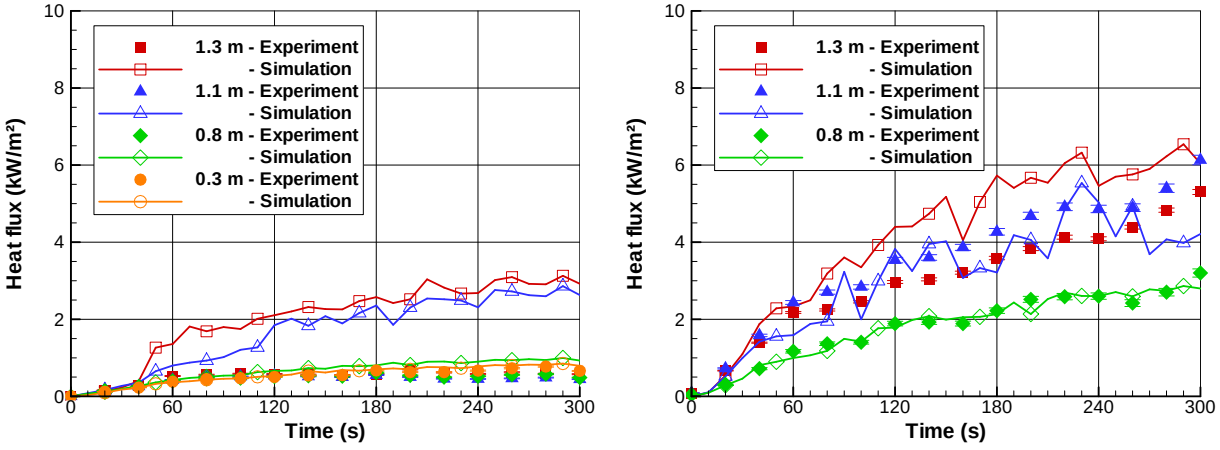

a- 7 m upstream b- 7 m downstream

Fig. III.11 — Radiative fluxes versus time on the vertical centerline of two measurement sections (point for experimental data and solid line for simulation)

III.2.3 In the supercritical case

For a better comparison between the sub-critical and supercritical cases, temperature data are first given versus time (see Figure III.12) and second as contours (see Figure III.13), to be compared respectively with figures III.7 and III.8 of the previous subsection.

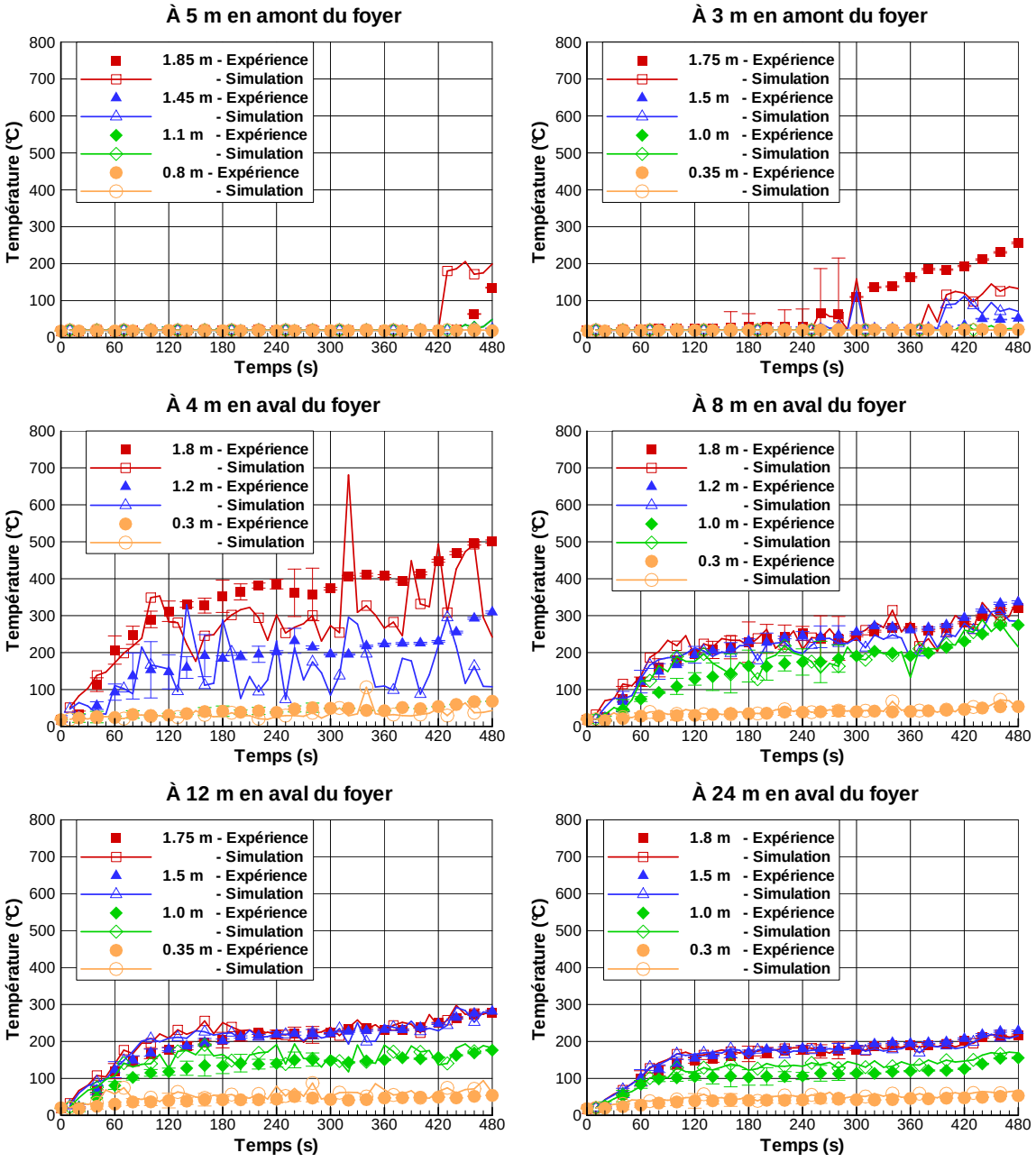

Fig. III.12 — Predicted and measured temperatures on the vertical centerline of six measurement sections (point for experimental data and solid line for simulation)

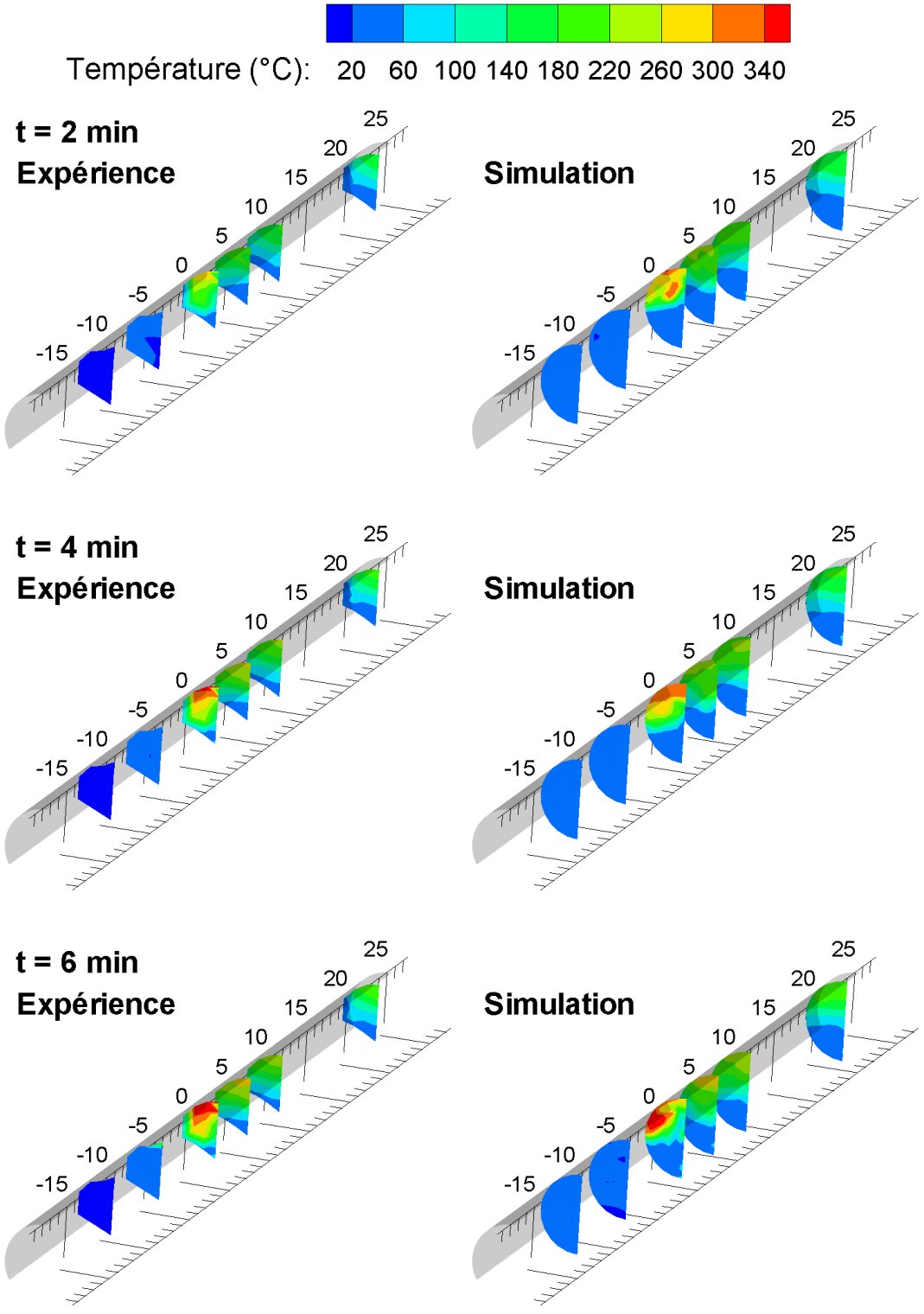

Fig. III.13 — Temperature contour at six measurement sections (2, 4 and 6 minutes after ignition)

The main difference with the previous case is related to the thermal stratification in the upstream part of the tunnel where no smoke counterflow is observed, at least during the first stages of the test. In fact, temperature in the main upstream part is roughly equal to the ambient value. This is confirmed by the experimental velocity profile since the velocity is now clearly forward oriented whatever the vertical position of the sensor (see Figure III.14). However, when HRR exceeds 1.6 MW, a thin hot layer is observed along few meters despite a higher velocity, which was expected above the critical one. Figure III.14 shows that in the experiment, the back-layering length does not exceed 5 m since local temperatures are there equal to the ambient value. The CFD code predicts this counterflow (its length is short but exceeds 5 m) with delay of about a hundred seconds (see Figure III.12).

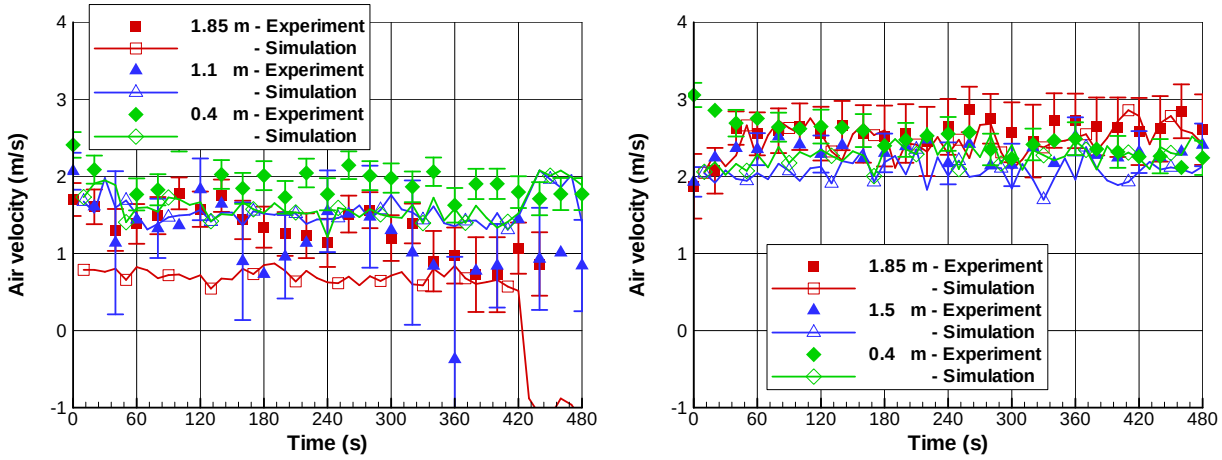

a- 5 m upstream

b- 18 m downstream

Fig. III.14 — Local velocity acquisition versus time on the vertical centerline of two measurement sections (point for experimental data and solid line for simulation)

This backlayering may be related to the way of inducing the longitudinal air flow in the tunnel : a device at the downstream side extracts a roughly constant gas volume flux. This means that when the fire grows, the temperature of the smoke/air increases downstream the fire location and also the longitudinal ventilation velocity in the tunnel decreases. As a consequence, the instantaneous velocity at the fire location is not as high as at the initial time and may induce a backlayering phenomenon. Indeed, about a hundred seconds after ignition, the instantaneous velocity at the fire location is lower than 1.8 m/s, the upper bound of the estimated backlayering value range for a 1.4 MW fire (see Figure III.15).

A supplementary possible explanation of this backlayering is that the preliminary analysis of the fire power and the related critical velocity have been done applying relationships by Zabetakis and Burgess for fires in open space (see Sub-section III.1.2), whereas the confined configuration of the tunnel affects the heat release rate. Actually, the HRR has been finally measured over the value of 1400 kW predicted considering the heptane pool size (see Figure III.6-b). As a consequence the present velocity is probably close or slightly above to the critical one, explaining the small backlayering effect.

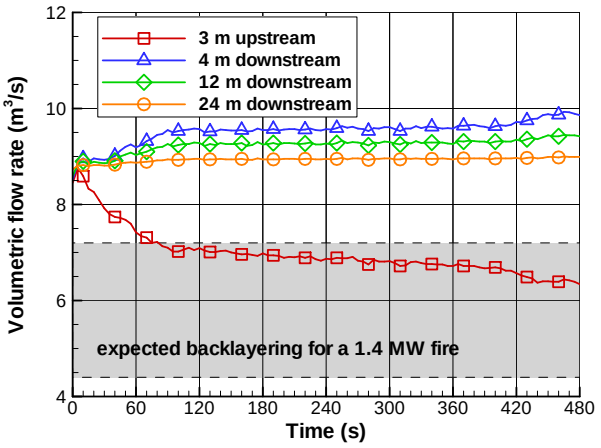

Fig. III.15 — Temporal evolution of the air volumetric rate at four transversal sections (one upstream and three downstream). The grey zone corresponds to the critical backlayering value predicted for a 1.4 MW fire with several models (see Sub-section III.1.3). Note that a constant volumetric rate of 8.8 m^3/s is extracted at the downstream side

As previously in the sub-critical case, temporal evolution is well predicted by the CFD code and both predicted and measured temperature have the same evolution than HRR : a first growth phase followed by a level-off period and then a peak. This peak resultinf from an increasing volume temperature of the fuel (all the substrate reaches the boiling point) is more marked in the test and the simulation when the measurement section is close to the fire (cf. Figure III.12).

Moreover, predicted data are in the confidence interval given by the error bars. The agreement is comprised between 11 and 19 % wherever except at 3 m upstream where the difference is much higher (57 %). At this location, the backlayering phenomenon is predicted by the computational code but with a delay time when compared to the experiment (see Figure III.12-a). Thus, air temperature in the upper part increases in less than 60 s from 20 °C to a value higher than 100 °C. Moreover, the backlayering length is then overpredicted since it is observed after 420 s on the measurement section located 5 m upstream the fire location (see Figure III.14).

The comparison between predicted and measured temperatures on figure III.16 confirms the previous observations for the sub-critical case. Agreement is better when the measurement section is away from fire. However, this tendency is less obvious than in the sub-critical case. Relative difference integrated on the whole duration of the test is equal to 19 % and 18 % on the measurement sections located respectively at 8 and 24 m downstream the fire. Temperatures are underestimated by the code at 4 m downstream the fire, the discrepancy is equal to 32 %. However, the signal is very noisy, and it can also be supposed that the thermocouples are greatly affected by the fire flame (see Figure III.12). Experimental signals are not as noisy as the computational one but it must be filtered due to the acquisition period (20 s).

Last, the mixing zone between hot smoke layer and fresh air in the lower part seems to be better predicted by the computational code in that case in comparison with the sub-critical case.

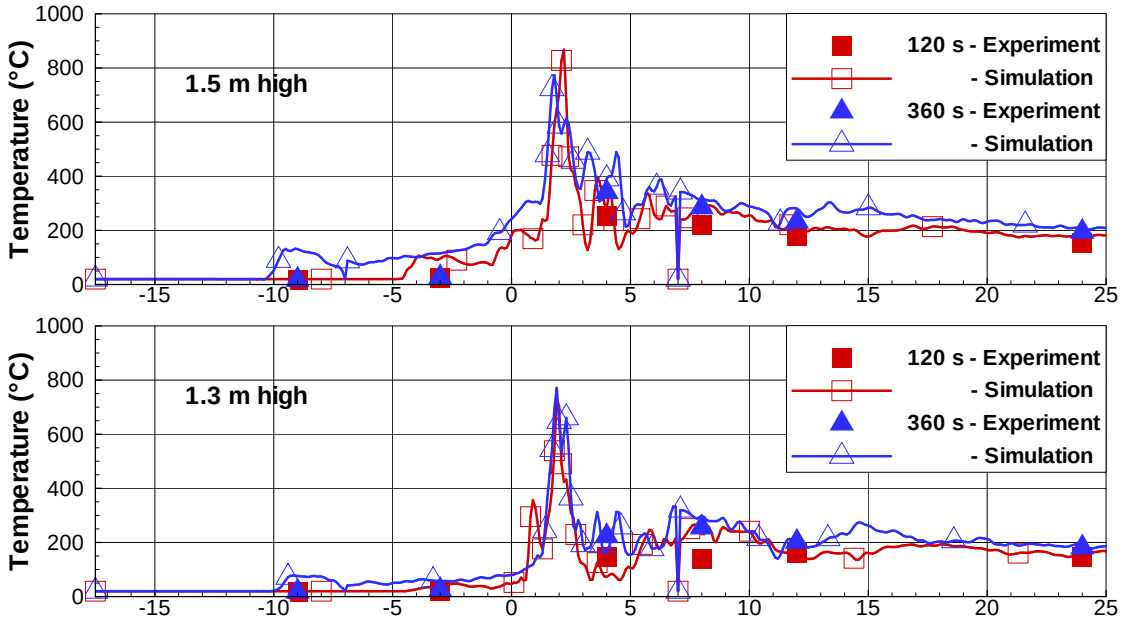

Fig. III.16 — Longitudinal profiles of temperature at 1.3 and 1.5 m high after 120 and 360 s

Radiative fluxes have been measured at equal distances from the fire, 7 m upstream and downstream the fire location. Data are reported on figure III.17. These points belong to the vertical centerline between 30 cm and 1.30 m high. Difference between values measured upstream and downstream highlights the flame tilt due the longitudinal ventilation : heat fluxes are almost constant and very low upstream the fire (lower than 1 kW/m^2) rather than downstream the fire, they are higher and their evolution are the same as HRR. The FDS code captures well these tendencies in most locations. Only in the two measurement points located downstream the fire at 1.1 and 1.3 m high, heat fluxes are greatly overestimated. The discrepancy even reaches 5 kW/m^2 under the roof. However, temperatures plotted on Figure III.12 for 4 and 8 m downstream seem to indicate extreme measurement conditions for the radiometers (higher than 200 °C).

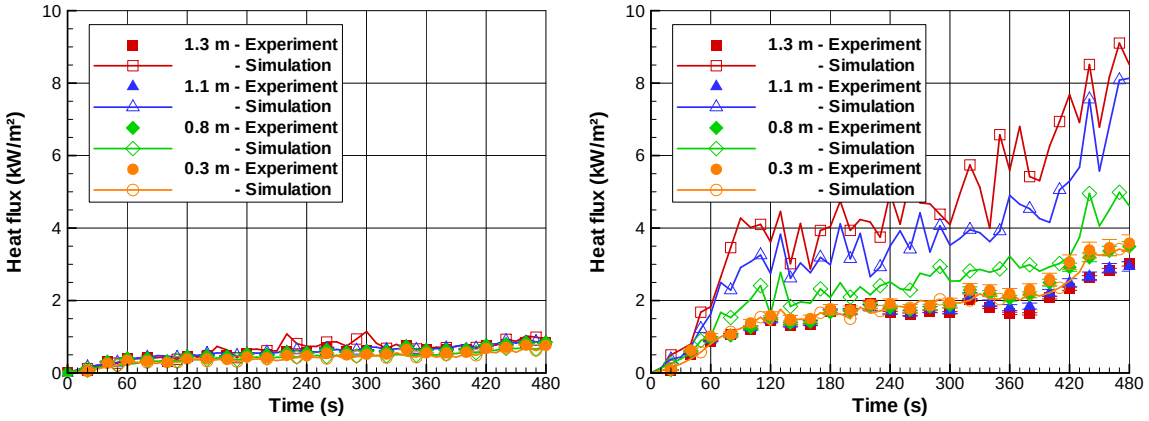

a- 7 m upstream

b- 7 m downstream

Fig. III.17 — Radiative fluxes versus time on the vertical centerline of two measurement sections (point for experimental data and solid line for simulation)

III.2.4 Quantification of heat transfer

In both tests, as smoke is flowing toward both tunnel extremities, smoke in contact with walls is cooled down. Sections III.2.2 and III.2.3 also highlight heat transfer to walls. The following section allows us to study in a more general way the heat distribution within the tunnel.

Global energy balance can be computed for the whole tunnel by extracting and collecting information from FDS calculation by adding a subroutine in the dump file. This subroutine does not touch the physical sub-models, it allows to extract additional outputs that are not a part of the official FDS version. Conservation of energy holds that the fire heat release Q_{fire} :

– goes to heat the gases within the domain, noted Q_g,
– is transferred to boundaries by radiation and convection, noted Q_w,
– is transported through the openings, noted Q_d.

Figure III.18 illustrates this global energy balance in our tunnel test as a function of time for each ventilation regime. For a better comparison, the fire heat is also plotted. Firstly, energy can be considered as conserved in the control volume because the sum of wall loss, opening loss and energy matches the HRR plot. This point is particularly interesting in the FDS case since the energy equation is never explicitly solved but its source terms are included in the expression for the flow divergence [26].

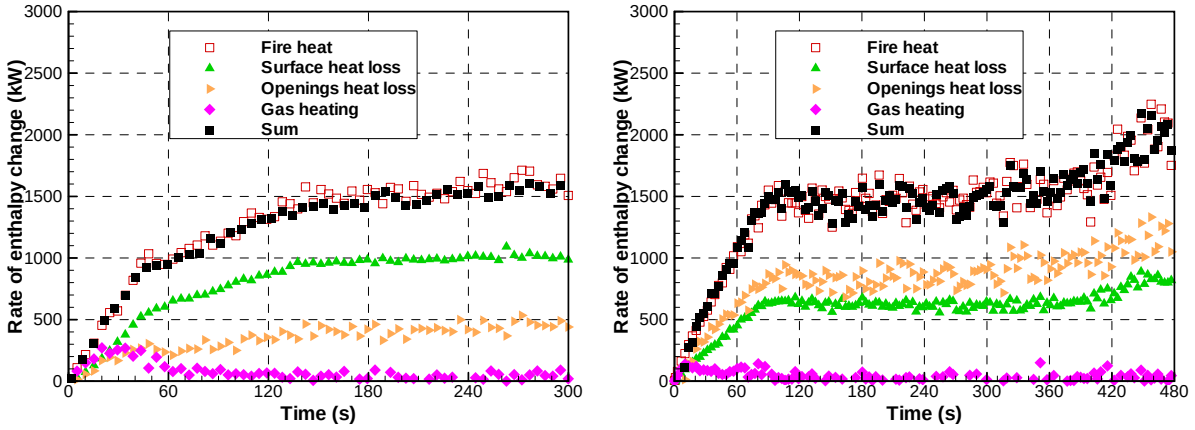

a- In the sub-critical case (test 9)

b- In the supercritical case (test 2)

Fig. III.18 — Energy balance and contribution of the different heat exchanges

Figure III.18 shows that the main part of heat released is transfered to the wall, but this tendency is less obvious for the larger flow velocity as a larger mass flow of gases is flowing in the tunnel. In both cases, such important part of energy exchanged with the walls illustrates also the confined situation of tunnel fires and not especially for this tunnel structure which is protected by a fire resistant mortar cement. In fact, other simulations have been run by defining the lateral sides and the floor made of concrete, roughly the same distribution has been obtained. Moreover, heat is mainly transfered to wall by radiation, it represents 46 % in test 9 and 37 % in test 2 of fire heat rather than the convective heat transfer represents 19 % in test 9 and 5 % in test 2 (see Figure III.19).

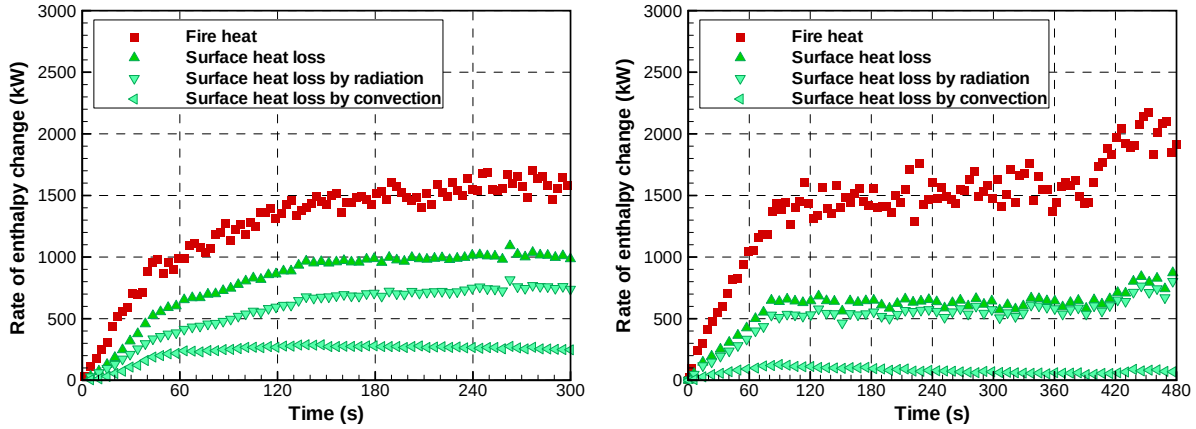

a- In the sub-critical case (test 9)

b- In the supercritical case (test 2)

Fig. III.19 — Rate of heat loss to surfaces by radiation and convection in tests 2 and 9. For comparison, the global heat loss is also shown

In all cases, the rate of change of energy within the domain is very low in both cases relative to other contributions. This low proportion results from the quasi-steady state of the flow. In fact, temperature variation is not sufficient to induce a high rate of change of enthalpy within the domain.

Even though HRR is similar in tests 2 and 9 in terms of evolution and amplitude (see Figure III.20), figure III.18 illustrates also that the energy balance is strongly different in the two tests. In fact, whereas the main part of the heat released (65 %) is dissipated through exchanges with the wall for the sub-critical regime, the fire heat is half-distributed through exchanges with the wall (41 %) and in the gas phase (59 %) for the supercritical regime. This tendency has also been observed for other tests of the midscale campaign where HRR is higher and longitudinal velocity quite different. For instance, test 1 (not detailed in the present document, see Ref. [3] for more details) involves the same fire load whith a HRR peak reaching 3 MW and a velocity around 1 m/s. In that test, nearly 67 % of the fire energy goes to heat tunnel surfaces. The remaining heat is transported by the has phase and goes mainly out through the outlet.

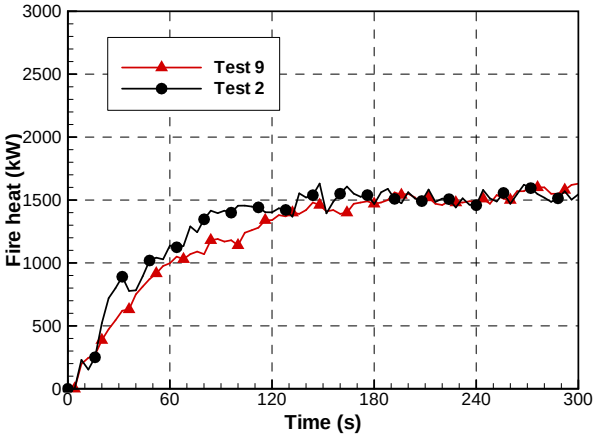

Fig. III.20 — HRR in tests 2 and 9

The difference in heat distribution between tests 2 and 9 could be attributed to :

– the contribution of backlayering in the energy balance. In fact, smoke layer that goes counter-flow, increases the surface area in contact with hot gazes in tunnel and also heat transfers between tunnel walls and gaseous phase, by radiation and convection,
– the influence of longitudinal ventilation on the zone releasing heat. Ventilation affect the flame tilt, the heat released to tunnel walls and gas can also be changed in the fire region,
– and/or the influence of longitudinal ventilation on the heat transfer downstream the fire location. In fact, heat transfer coefficient between gaseous phase and walls depends on the air flow velocity and air temperature can possibly be modified with ventilation by mixing (see Figures III.7 et III.12).

To understand this difference, tunnel is divided into three zones in the longitudinal direction, the upstream and downstream parts separated by the fire region. The fire region is defined as the zone where the released heat is higher than 0 kW. Heat loss to walls can also be attributed to each zone by summing. It is plotted on figure III.21 in tests 2 and 9.

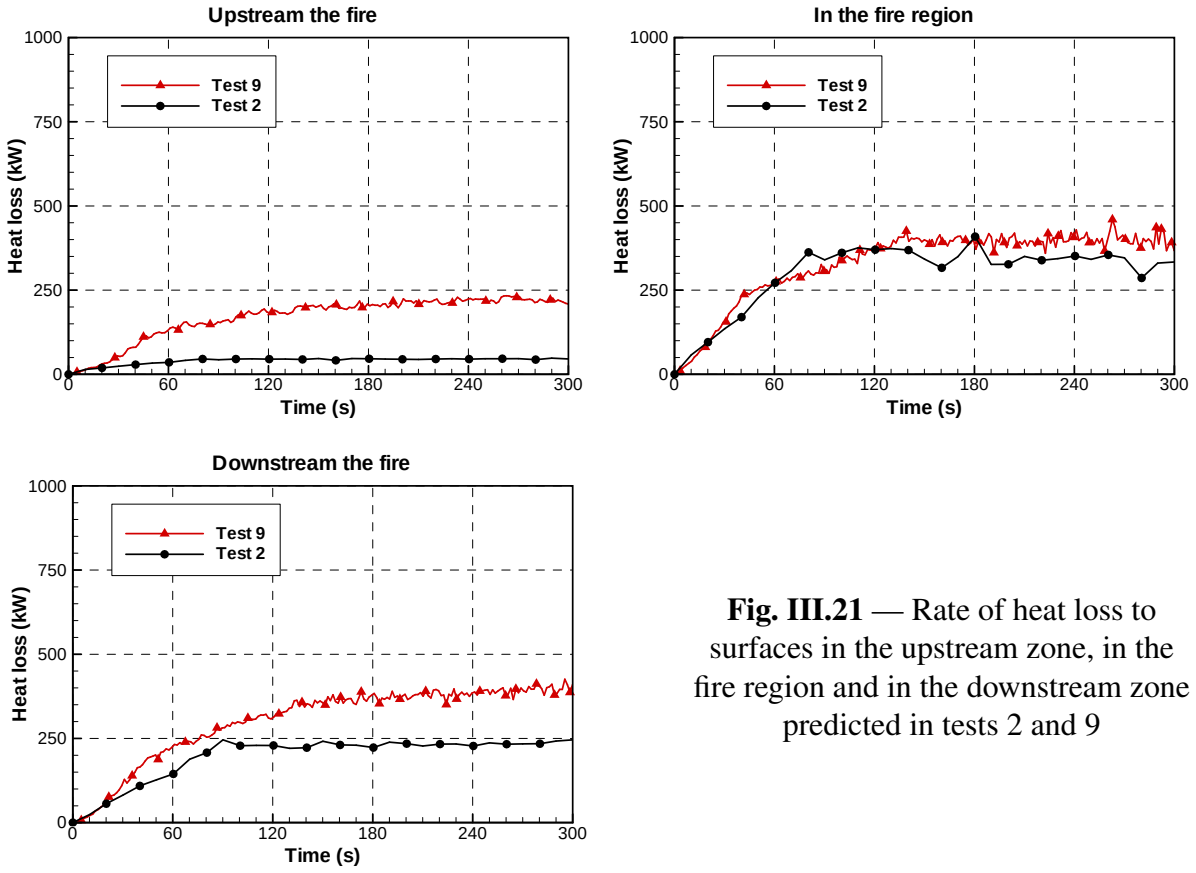

Fig. III.21 — Rate of heat loss to surfaces in the upstream zone, in the fire region and in the downstream zone predicted in tests 2 and 9

Figure III.21 shows that almost the same quantity of energy is lost in the fire region even if this zone length differs : it is longer for a higher longitudinal ventilation. For instance, in the supercritical case, its mean length is equal to 3.8 m over [0 ; 300 s] whereas in the sub-critical case, it is 2.5 m long over the same period.

Unlike the fire region, heat loss to surface in the upstream and downstream parts varies with ventilation (see Figure III.21). The mean ratio of heat loss to surfaces to global fire heat over [0 ; 300 s] is given in table III.3.

Tab. III.3 — Mean ratio of heat loss to surfaces to global fire heat over [0 ; 300 s] in the upstream and downstream zones

	Upstream zone	**Downstream zone**
Test 9	13 %	23 %
Test 2	3 %	15 %

Upstream the fire, the backlayering phenomenon induces 10 % of supplementary heat loss to surfaces compared to the supercritical case. Downstream the fire location, increasing the longitudinal ventilation velocity induces a decrease of heat loss to surfaces of 8 %. This decrease is not induced equally by the convective and radiative heat transfers. In fact, that is the consequence of a radiative transfer reduction (by a factor of 2.5) which is induced by a decrease of gas temperature due the gas mixing (see Figures III.7 et III.12).

In practice, it means that for reducing heat loss to surfaces and also protecting tunnel structure in case of fire, it is necessary to blow air at the maximal longitudinal velocity.

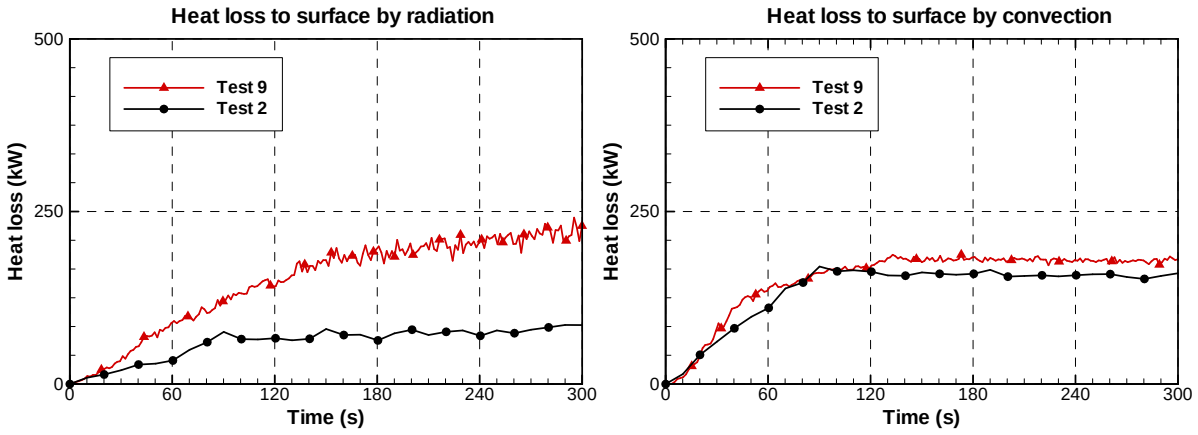

Fig. III.22 — Heat transfered to surface by convection and radiation in the downstream zone

III.3 Tests with water mist

Two tests involving water mist are simulated. In the test campaign, they correspond to tests 27 and 28. They are conducted with an initial longitudinal ventilation velocity around 3.0 m/s. This velocity being higher than the critical backlayering value, an supercritical ventilation regime is expected without smoke backlayering upstream the fire (see Sub-section III.1.3). The water mist system differs in these two tests :

- six nozzles are activated in test 27. They are located between 4 m upstream and 3.5 m downstream the fire location, 1.5 m apart one other,
- only the three nozzles located upstream the fire are activated in test 28.

Because of the nozzle locations, few sensors can be affected by water mist either by deposit or by obstruction and measurement can also be skewed. Thus, during the water mist application, the following measurements are not interpreted : air velocity measured downstream the fire location and air temperature at the mist system location.

No repeatability test has been conducted with water mist. Thus, measurement uncertainty is only evaluated by “Type B” evaluation. In other words, it does not take “Type A” components evaluated from the statistical distribution of the quantity values from series of measurements. “Type B” components being very small for air temperature, the associated uncertainty is also not represented for tests 27 and 28.

Tests 27 and 28 have been selected for the present study because they are characterized by a low injected water quantity and distant nozzles. Consequently, mitigation does not induce a drop for HRR and an associated important gas cooling. It also allows to study the fire environment when the mitigation system is activated. For information, during the campaign in the midscale tunnel, one test was performed in similar conditions (same fire load and supercritical ventilation regime) except that a higher number of nozzles (14 nozzles) was involved. Fire was also suppressed in less than 1 min which does not allow studying surrounding conditions during mitigation [27].

III.3.1 Input data definition

Concerning fire and ventilation, these tests are simulated in a similar way as the two tests without water mist (see Sub-section III.2.1). The following section deals firstly with the difference in fire definition in comparison to the previous tests and secondly with input data defining water spray.

Fire load

Unlike tests without water mist, HRR is deduced from fuel weight loss monitoring and by oxygen consumption monitoring. As Figure III.23 shows HRR deduced with the two methods are almost the same before mist system activation. After that, deduced HRR are clearly different because fuel weight is altered by droplets accumulated in the pool. Moreover, the effect of water mist application on the heptane burning rate is represented by the experimental HRR curve. For this reason, FDS fire suppression model is not activated. HRR defined as input is plotted on figure III.23.

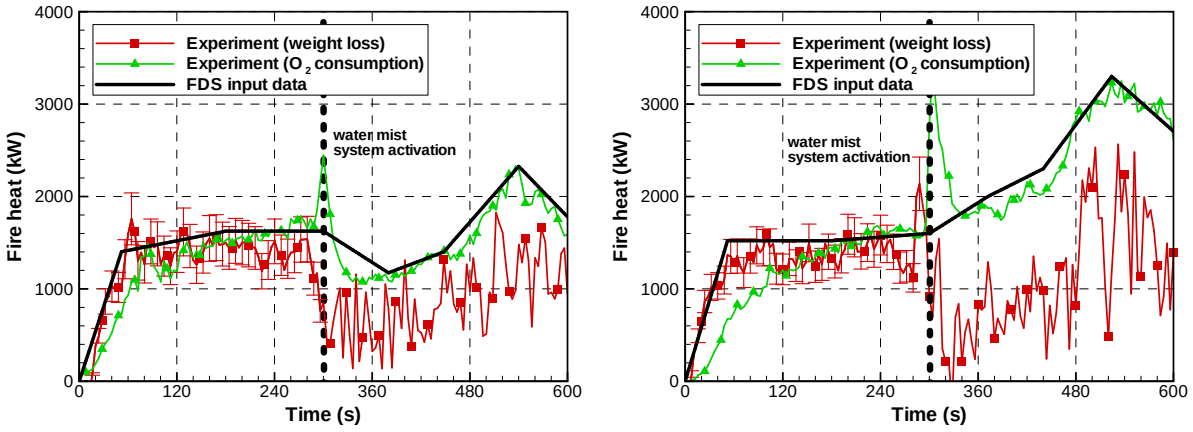

a- Test 27 b- Test 28

Fig. III.23 — HRR deduced from fuel weight loss and oxygen consumption in tests 27 and 28. The piecewise linear function used as input in the simulation are also presented

Water mist system

In FDS, the spray characteristics are defined at the injection point by a considerable number of parameters such as fluid thermal properties, droplet size distribution and injection features (spray pattern, volumetric flow rate, etc.). In particular, the droplet size distribution is represented by a probability function that describes the fraction of the water volume transported by droplets whose dimension is less than a given diameter. The default probability function is a combination of log-normal and Rosin-Rammler distribution. To calibrate this probability function, PDA analysis has been simulated, by varying mean diameter at the injection point from 20 to 60 µm. The spray is injected in a closed room and the nozzle is located at a central position of the room, represented by five injection points. FDS prediction and experimental measurement are then compared. At each location, the spray is characterized by the mean Sauter diameter which is by definition the ratio of the volume of a sample of droplets to the surface area of the same sample. Figure III.24 presents the comparison between simulations and measurements.

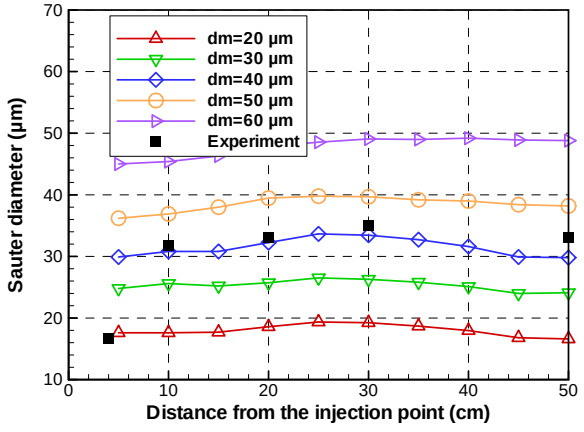

Fig. III.24 — Predicted (solid line) and measured (point) droplets size along the central vertical axis

The best agreement appears to be obtained with the spray defined at the injection point with a hybrid law defined by a mean diameter and a Rosin-Rammler dispersion parameter equal to 40 μm and 2.85 respectively. The measurement at 4 cm is not taken into account because the authors consider that the atomization may not yet be completed.

III.3.2 Mist sprayed upstream and downstream the fire location

The longitudinal velocity induces a sub-critical ventilation regime. Before mist activation, configuration is expected to be comparable to the one in test 2, without water mist : there would be no smoke counterflow and the whole smoke would be pushed away to the downstream side. Downstream the fire, environment would be consequently thermally stratified (see Figure III.25). However, as previously in test 2, whereas ventilation velocity is higher at the initial time than the expected backlayering value, a short smoke counterflow is observed during the experiment after 100 s. As figures III.25 and III.27 illustrate, its thickness does not exceed 40 cm 3 m upstream the fire and its length is comprised between 5 et 9 m.

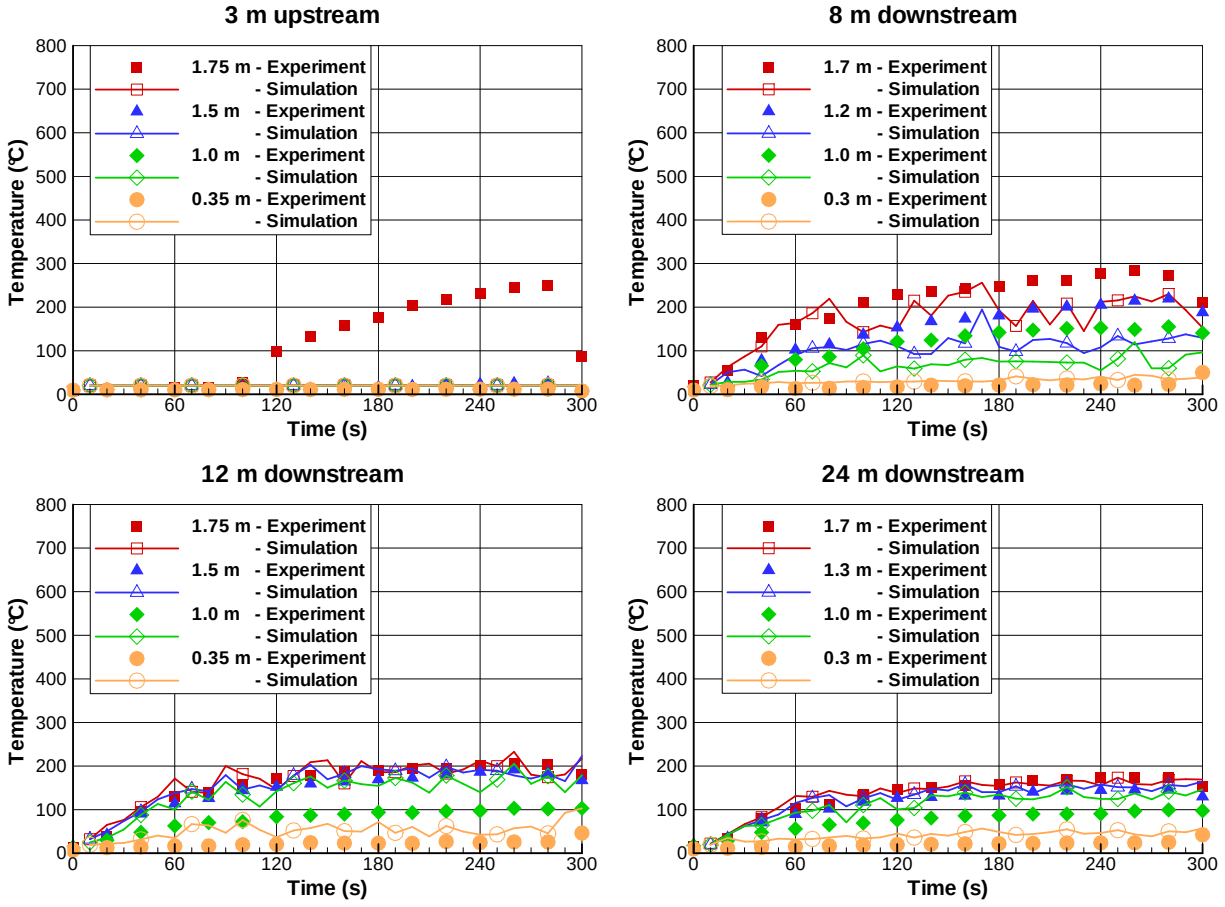

Fig. III.25 — Before mitigation system activation, predicted and measured temperature versus time on the vertical centerline of four measurement sections (point for experimental data and solid line for simulation)

The CFD code does not predict the counter-flow upstream the fire location. Downstream, comparison of predicted temperatures to measurements shows a good general agreement at most of the locations : the slope and the magnitudes are similar (see Figure III.25). Like in test 2, farther the measurement section from the fire is, better the numerical accuracy is. In fact, temperature tends to be under-predicted in the flame region. Moreover, the bigger discrepancy is measured at mid-height in the mixing zone between the hot smoke layer in the upper part and the fresh air in the lower part.

Mist system activation induces the disappearance of counter-flow upstream the fire (see Figure III.27) and gaseous phase is cooled down downstream the fire. Air temperatures go also down and become more uniform over each measurement section located downstream. For instance, temperatures are around 60 °C at 8 m from the fire between 360 and 400 s. This homogeneity in air temperature over each measurement section seem to highlight a thermal destratification. Then, two minutes after mist system activation, the environment tends to be stratified again. Temperature are indeed higher in the upper part than in the lower part. For instance, at 8 m from the fire and at 540 s, temperature is around 160 °C close to the roof, 120 °C at mid-height and 80 °C below 30 cm high.

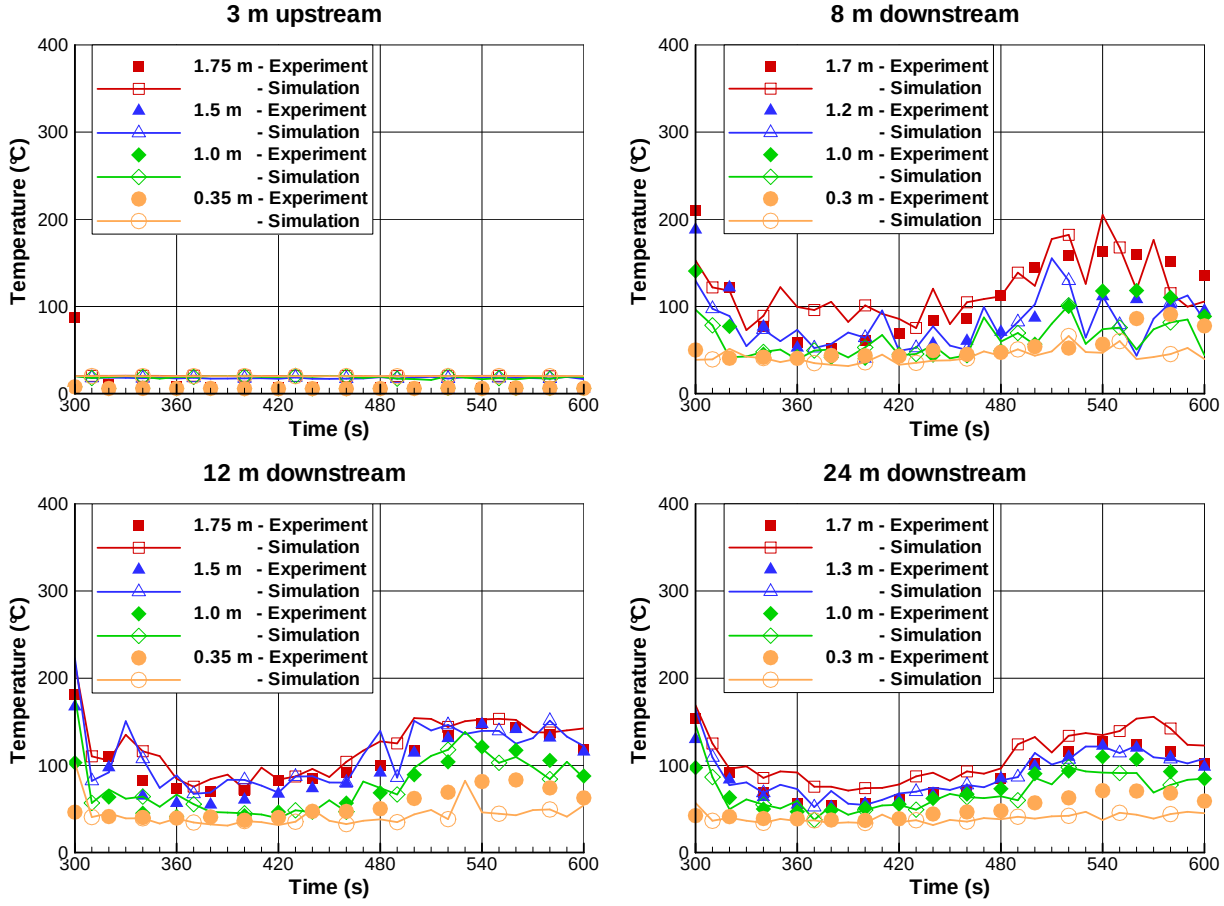

Fig. III.26 — After mitigation system activation, predicted and measured temperature versus time on the vertical centerline of four measurement sections (point for experimental data and solid line for simulation)

At all locations, temperature decreases and its evolution after mist activation is closely reproduced in the simulation, even when between 340 and 480 s when air temperature is almost constant while fire heat value changes or when HRR increases again around 540 s.

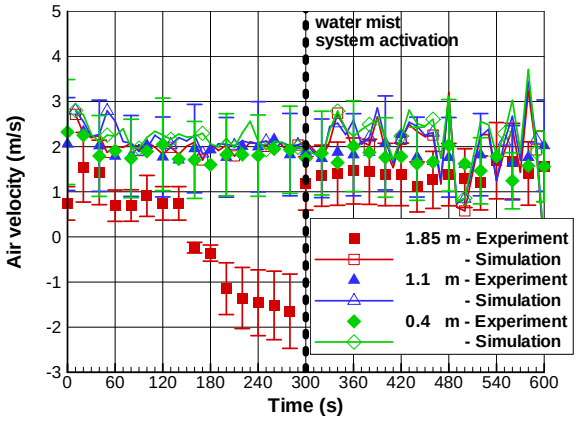

Fig. III.27 — Local velocity acquisition versus time on the vertical centerline 5 m upstream the fire (point for experimental data and solid line for simulation)

Radiative fluxes have been measured at equal distances from the fire, 7 m upstream and downstream the fire location. Data are reported on figure III.28. Like in test 2, before mist system activation, difference between values measured upstream and downstream highlights the flame tilt due to the longitudinal ventilation. On the one hand, heat fluxes are very low (lower than 0.5 kW/m^2) and almost constant upstream. Heat fluxes are there very well captured by the CFD code. On the other hand, heat fluxes are higher downstream the fire and their evolution follows fire heat changes. Heat fluxes are there hardly overpredicted by the code. After mist activation, heat fluxes decrease and agreement is better : the mean discrepancy over [300 ; 600 s] at all measurement points is lower than 0.25 kW/m^2.

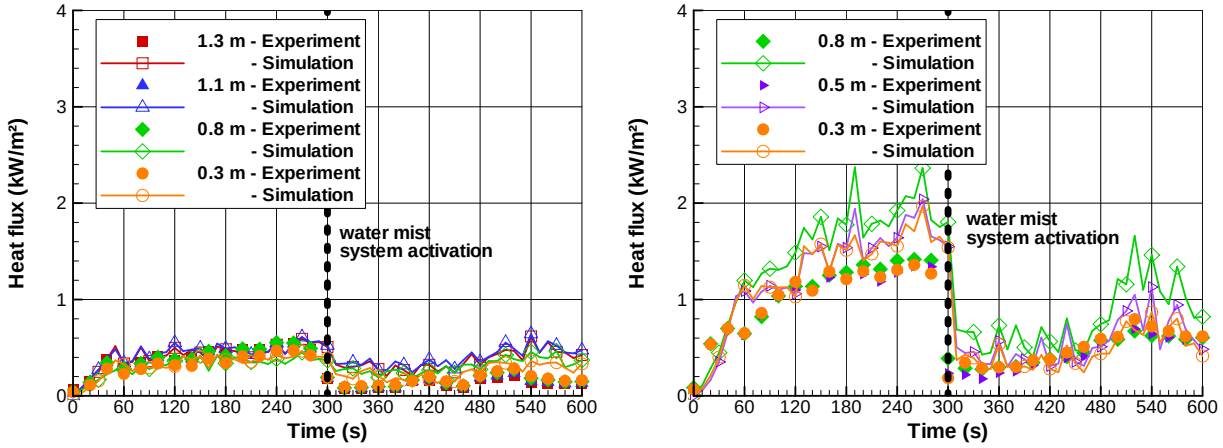

a- 7 m upstream

b- 7 m downstream

Fig. III.28 — Radiative fluxes versus time on the vertical centerline of two measurement sections (point for experimental data and solid line for simulation)

III.3.3 Mist sprayed upstream the fire location

Before mist activation, the situation is very close to the one in test 27 since extracted volumetric rate and HRR (value and evolution) are almost similar (see Figure III.23). Thus, the corresponding ventilation regime is supercritical without any counterflow upstream. As previously, the CFD code predicts well the thermally stratified environment downstream the fire location even if the agreement is better close to the fire or when the measurement point is not located at mid-height in the mixing zone.

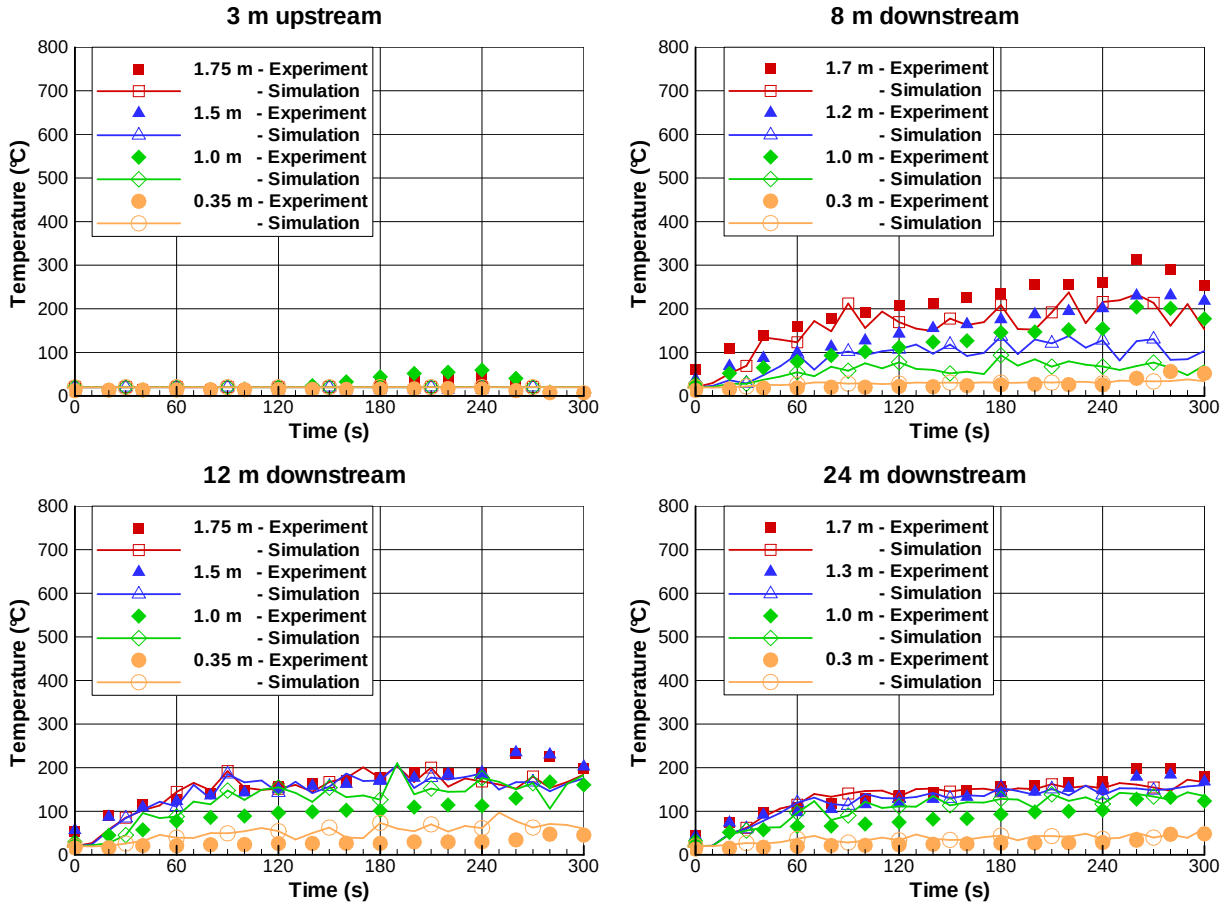

Fig. III.29 — Before mitigation system activation, predicted and measured temperature versus time on the vertical centerline of four measurement sections (point for experimental data and solid line for simulation)

In both experiment and simulation, while HRR increases from 1500 kW to 1750 kW at mist activation, air temperature is constant and even in few locations, it (weakly) decreases. However, unlike test 27, the environment remains stratified. For instance, air temperature measured at 360 s (i.e. 1 minute after mist activation) 12 m downstream is around 190 °C close to the roof, 150 °C at mid-height and 50 °C close to the floor. The simulations predicts at the same time and at the same distance from the fire, 180 °C close to the roof, 150 °C at mid-height and 60 °C close to the floor.

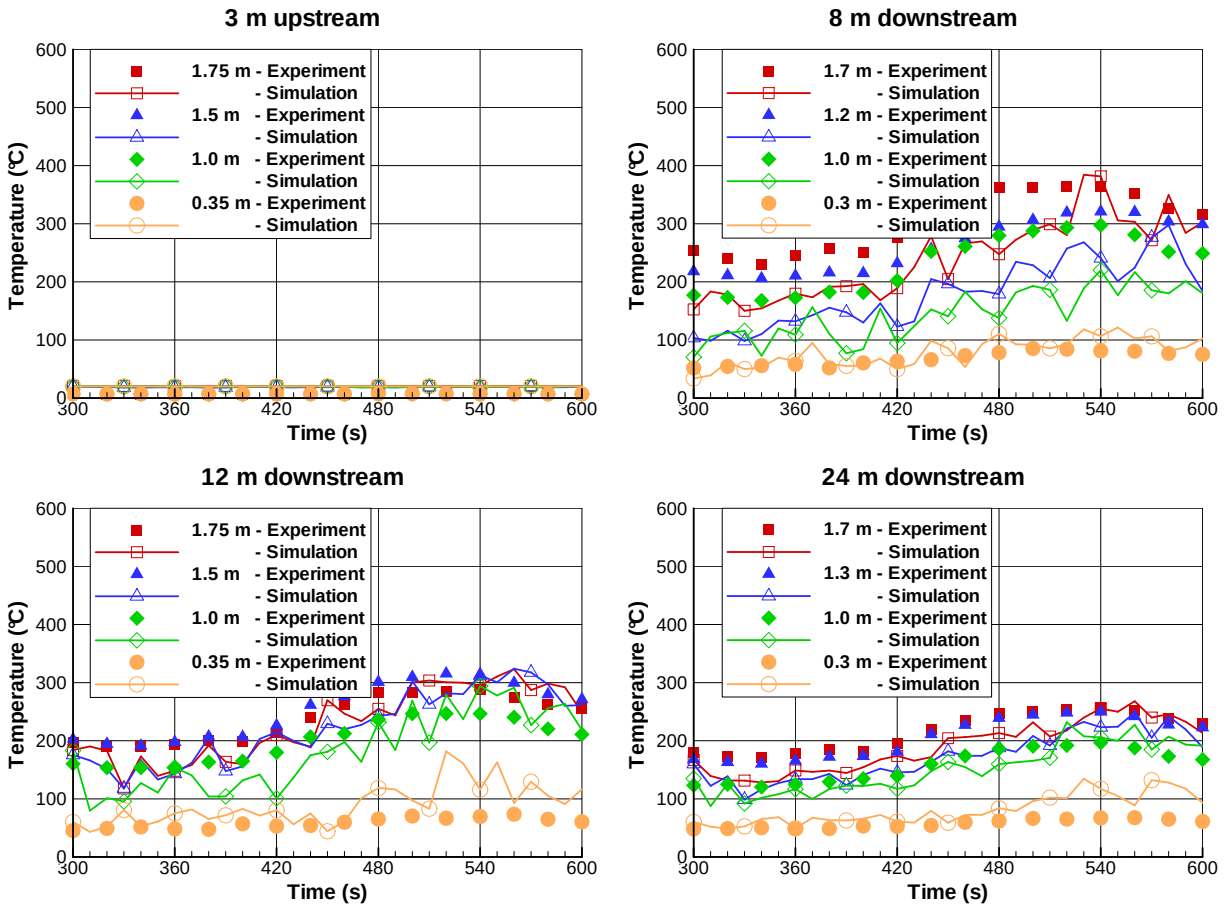

Fig. III.30 — After mitigation system activation, predicted and measured temperature versus time on the vertical centerline of four measurement sections (point for experimental data and solid line for simulation)

However, figure III.30 indicates that over [300 ; 600 s] the FDS code underestimates air temperatures at all measurement points located between mid-height and the roof 8 m downstream. Further, this figure shows a correct agreement between measured and predicted values in terms of slope and magnitude. In parallel, whereas heat fluxes are well predicted by the CFD code before mist activation, after this activation heat fluxes are greatly overpredicted. The highest discrepancy even reaches 2 kW/m^2 close to the floor and 3 kW/m^2 at mid-height at HRR peak around 540 s (cf. Figure III.31). The underestimation of air temperature at 8 m downstream associated to the overestimation of heat fluxes at 7 m downstream indicate that the CFD code overestimates the evaporation of water mist close to the fire location. It also under-predicts the water quantity transported in air flow and reduces the capability of water mist to act as a radiative shield.

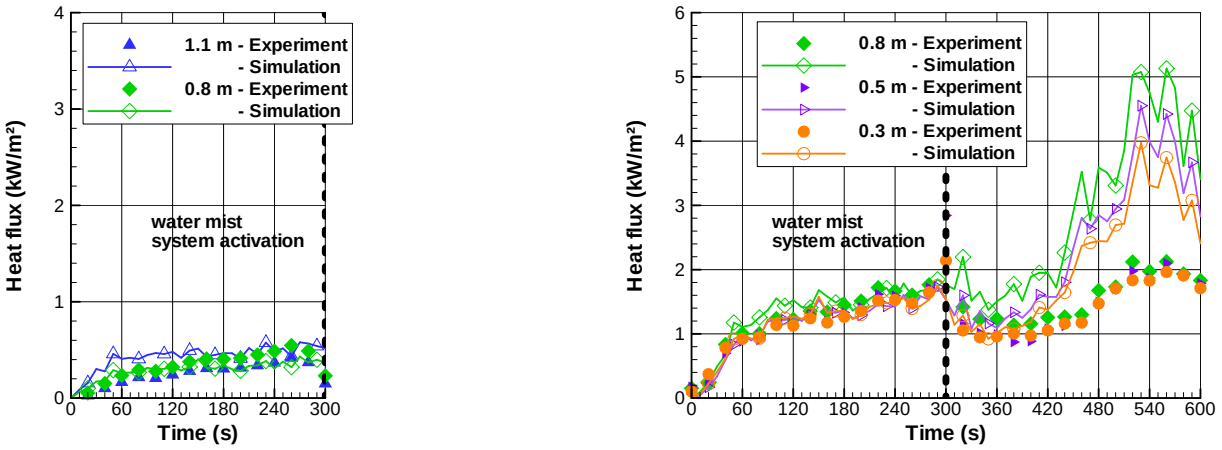

a- 7 m upstream

b- 7 m downstream

Fig. III.31 — Radiative fluxes versus time on the vertical centerline of two measurement sections (point for experimental data and solid line for simulation)

III.3.4 Interactions of water mist, tunnel longitudinal ventilation and fire

Once the validation is achieved, the computational tool is used intensively in order to improve the understanding of the interaction phenomena between water mist, tunnel longitudinal ventilation and fire in tests 27 and 28. In other words, we look into details the impact of water spray on tunnel air flow and thermal stratification. Vice versa, we study the impact of the fire environment on (liquid and vapor) water transportation and its evaporation.

Figure III.32 presents temporal evolution of gas flow rates at several distances from the fire. Before mist activation, at a given time, gas mass flow rate is constant along the longitudinal direction. Mass conservation is also verified [2]. Due to heat transfer to tunnel walls, volumetric gas flow rate simulated downstream is rather not constant. The further from the fire the measurement section is, the lower gas flow rate is.

Figure III.32 shows the large difference in volumetric rates between the upstream and the downstream tunnel parts. Rate is very low upstream in comparison with the downstream values. Moreover, rate has the inverse evolution of HRR (decrease followed by a level-off) upstream whereas downstream it is almost constant. These two differences are attributed to the way of setting a longitudinal air flow (a constant volumetric gas volume flux is extracted at the downstream extremity), gas displacement varies also upstream with HRR. The large difference in values is promoted by the supercritical ventilation regime, gas density being very higher upstream than downstream.

2. Mass created at the fire location is relatively low

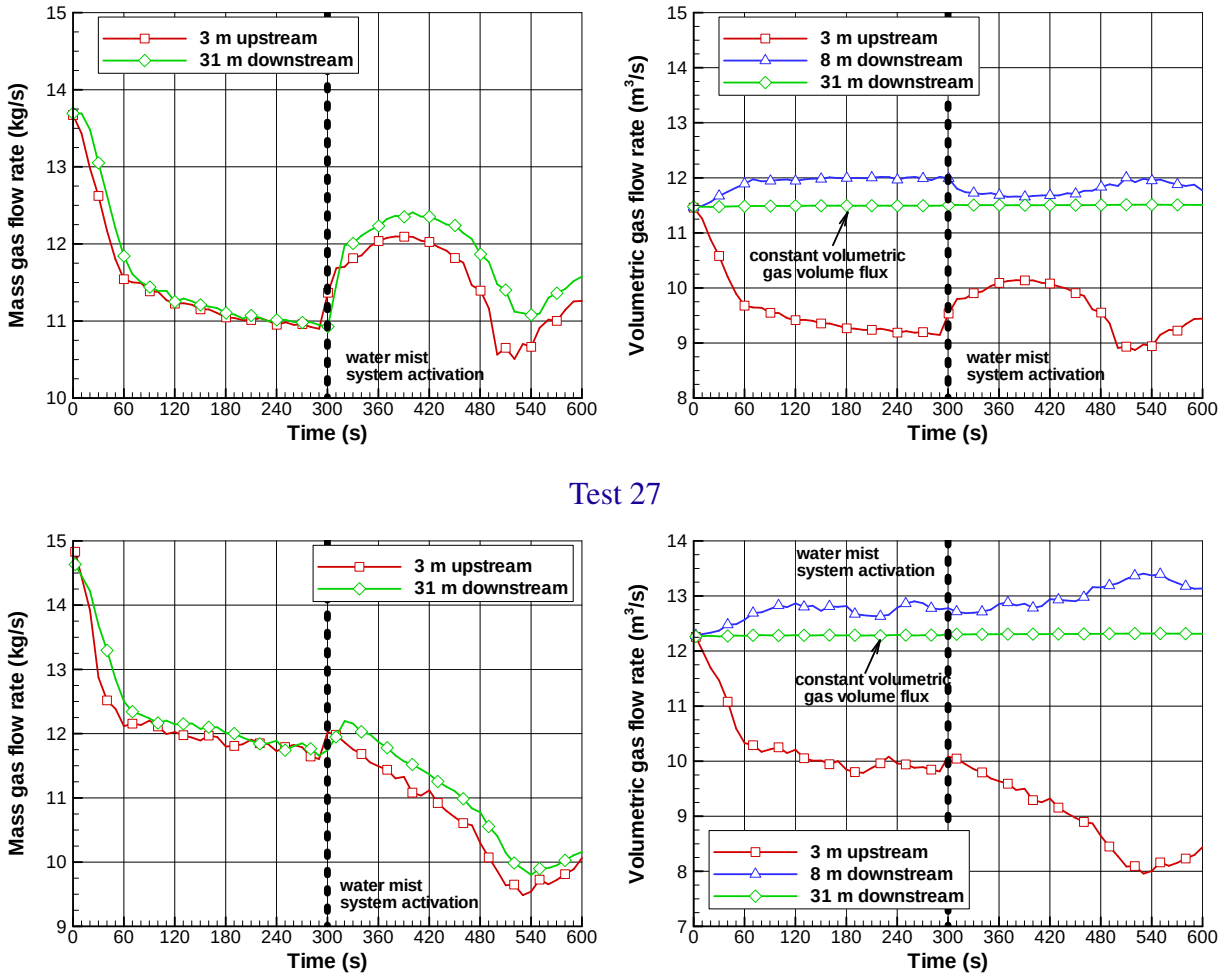

Fig. III.32 — Gas flow rates versus time in mass (left) and in volume (right) simulated at several distances from the fire

In test 27, mist activation induces a large increase in mass and volumetric flow rates upstream the fire due to the strong gas cooling in the downstream part. A large mass of air is thus transported from the upstream side to satisfy the boundary condition at the downstream extremity. This tendency is not as obvious in test 28 where gas cooling at mist activation is less important. Then, mass and volumetric flow rates simulated upstream follow as previously the inverse evolution of HRR whereas volumetric flow rate is almost constant downstream.

Note that after mist activation, gas mass flow rate is not constant along the longitudinal direction anymore, due to water mist evaporation.

Figure III.33 presents contours of liquid water concentration on mid-plane 420 s after ignition, i.e. 120 s after mist activation. This figure illustrates the transportation of the water droplets.

In test 27, whereas the activated nozzles operate from 4 m upstream to 3.5 m downstream the fire location, water droplets are transported up to 16 m downstream. The two-phase flow containing

water vapor and smoke also acts as a radiative shield. It explains the low heat fluxes measured and predicted downstream the fire during mist application when HRR is high (see Figures III.23-a and III.28).

In test 28, water droplets are transported to the fire location cooling the fire plume. Most of the sprayed water is also evaporated. Thus, liquid water concentration is very low downstream, even close to the fire, explaining the difference in predicted heat fluxes between tests 27 and 28 on figures III.28 and III.31 :

– in test 27, heat fluxes are comprised between 0.3 and 1.6 kW/m^2 after mist activation,

– in test 28, they are comprised between 0.9 and 5.1 kW/m^2.

Note that in test 28, the code over-predicts heat fluxes and underestimates air temperature downstream the fire (see Sub-section III.3.3). It means that water mist would not be as evaporated in reality and also water concentration would be higher downstream.

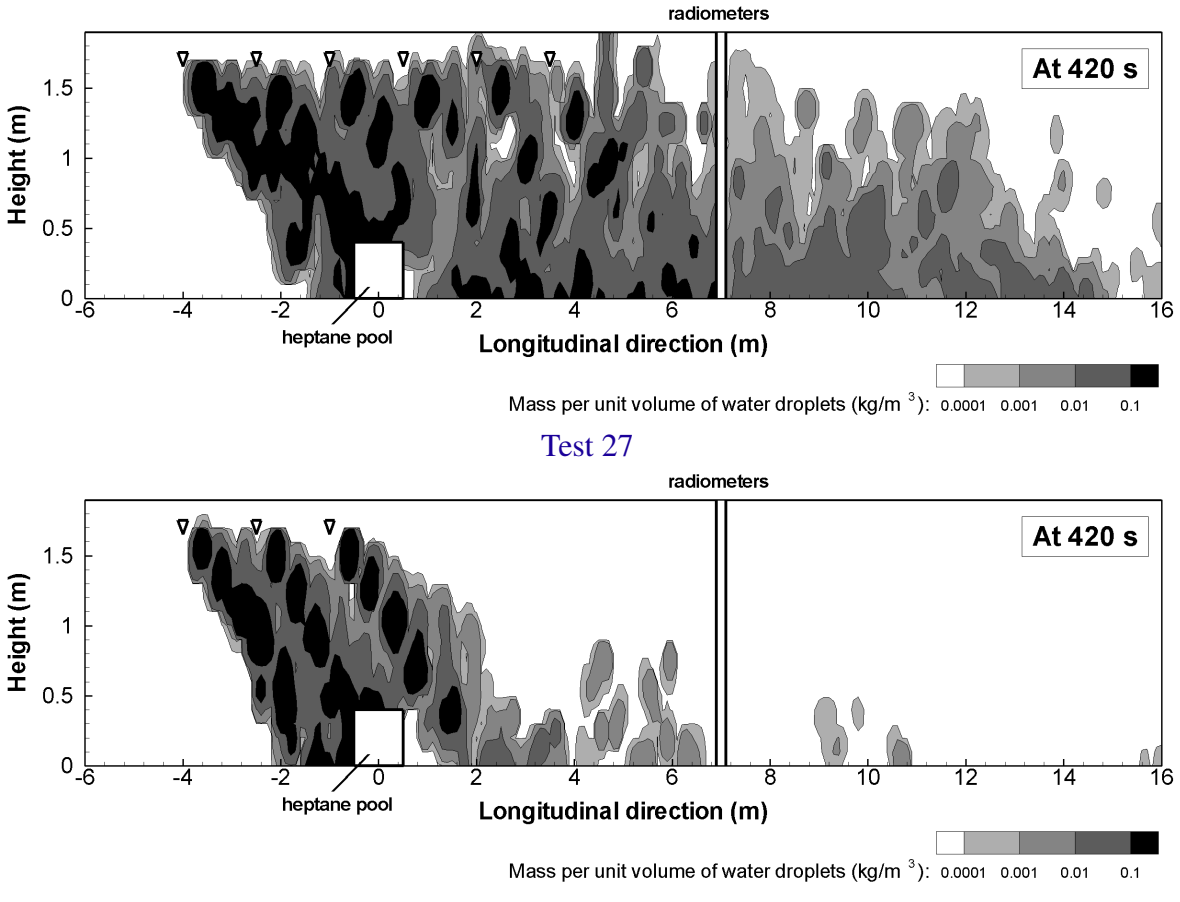

Fig. III.33 — Contours of liquid water concentration on mid-plane in the tunnel at 420 s. Triangles indicate nozzle positions

Water sprays act as a shield to air flow due to longitudinal ventilation and fire activity. Fire plume which was inclined at 24 ° in test 27 and at 31 ° in test 28 at mist activation is then more inclined (see Figures III.34 and III.35). At the same time, smoke is directly cooled down. Temperature close to the fire is consequently very low in comparison with HRR value. For instance, in test 27, when

HRR is around 1300 kW at 420 s, the simulated temperature is comprised between 30 and 135 °C at 4 m from the fire and between 30 and 90 °C at 8 m. At the same distance from the fire and at the same time, air temperature is comprised between 50 and 210 °C in test 28 when HRR reaches 2 MW.

Figures III.34, III.35 and III.36 confirm what we supposed before on the basis of local temperatures in both tests. In test 27, mist activation alters deeply thermal stratification, temperature gradient is also very low. Our previous observation is confirmed too : by the end of the simulation, when HRR is high despite the water injection, the environment tends to be thermally stratified. There is an obvious thermal gradient along the vertical axis, as shown by the vertical profiles on Figure III.36. Closer the measurement section from the fire is, clearer the vertical gradient is. It means that the hot gas in the upper part tends to get colder (upon contact with tunnel walls and due to the mist thermal contribution) and to mix with the fresher air in the lower part as it is flowing in the downstream direction. In test 28, the environment is rather still thermally stratified despite mist unlike test 27.

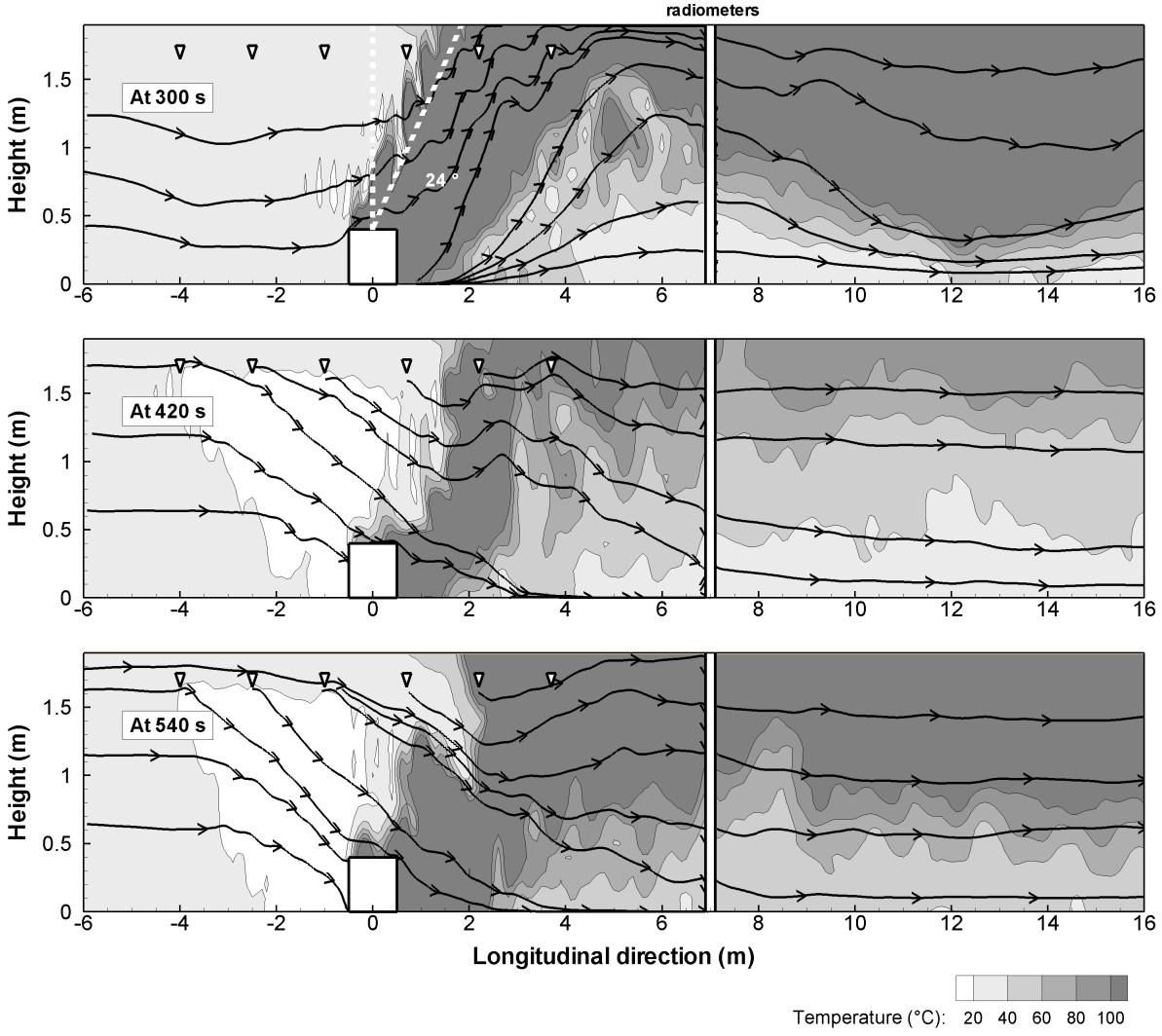

Fig. III.34 — Test 27 : Contours of air temperature on mid-plane in the tunnel at mist activation, two and four minutes after

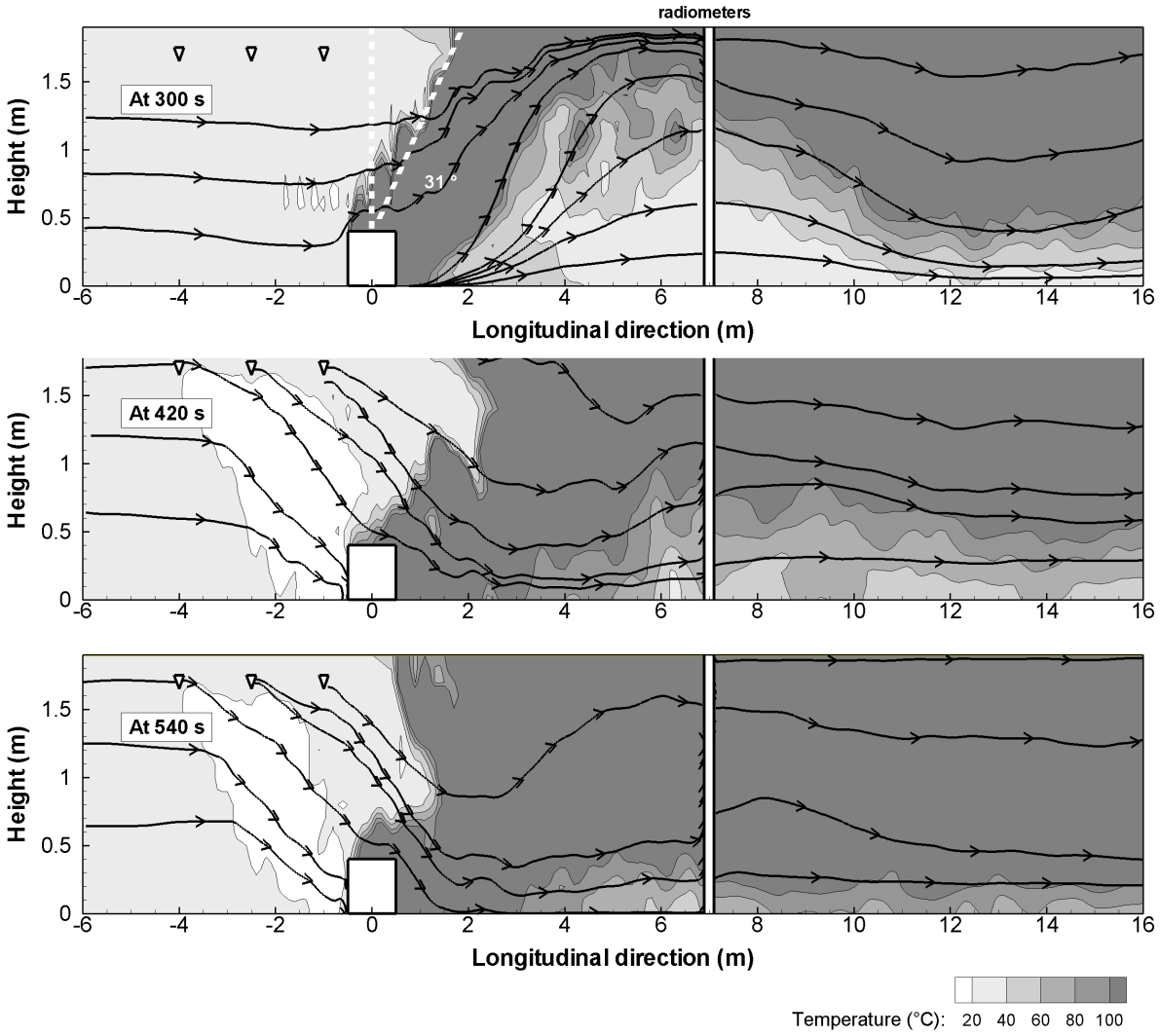

Fig. III.35 — Test 28 : Contours of air temperature on mid-plane in the tunnel at mist activation, two and four minutes after

These temperature contours allow to draw a cartography of the environment where smoke is expected in the hottest zone and fresh air in the coldest zone. However, in test 27, contours concerning gas composition draw a different cartography [3]. For instance, after 420 s, environment is thermally stratified whereas concentration in O_2, CO_2 and CO is almost constant over the vertical axis (see Figures III.38 and III.39). Difference can be attributed to :

- water mist. When water droplets are transported in the tunnel over a long distance, they are still absorbing heat by radiative attenuation and (gas and surface) cooling.
- water vapor. When it is produced or present somewhere, it decreases concentration of other species, it dilutes them. In that test, water vapor is transported over the whole tunnel height along about 10 m.
- fire plume. At the fire location, it is highly cooled down and pushed away toward the floor. A part of the fire plume transporting combustion products is also not visible on the temperature contour but it induces a decrease in O_2 and an increase in CO_2 and in CO.

3. This cartography cannot be qualified quantitatively since in reality, combustion reaction could be strongly influenced by water spray and it is defined here as input

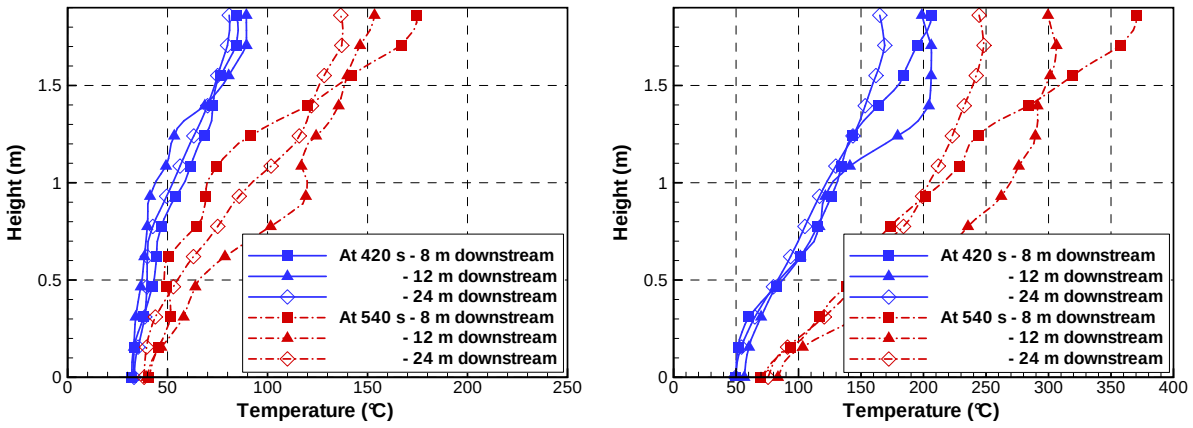

a- Test 27 b- Test 28

Fig. III.36 — Profiles of air temperature along the vertical centerline of three measurement sections two and four minutes after mist activation

In test 28, the situation is different in the way that there is an obvious gradient along the vertical axis in concentration of gas species (see Figure III.37). For instance, at 420 s, volumetric fraction in oxygen (respectively carbon dioxide or carbon monoxide) varies between 18.2 and 20.1 % (respectively 0.2 and 1.2 % or 13 and 65 ppm) along the vertical axis at 12 m downstream.

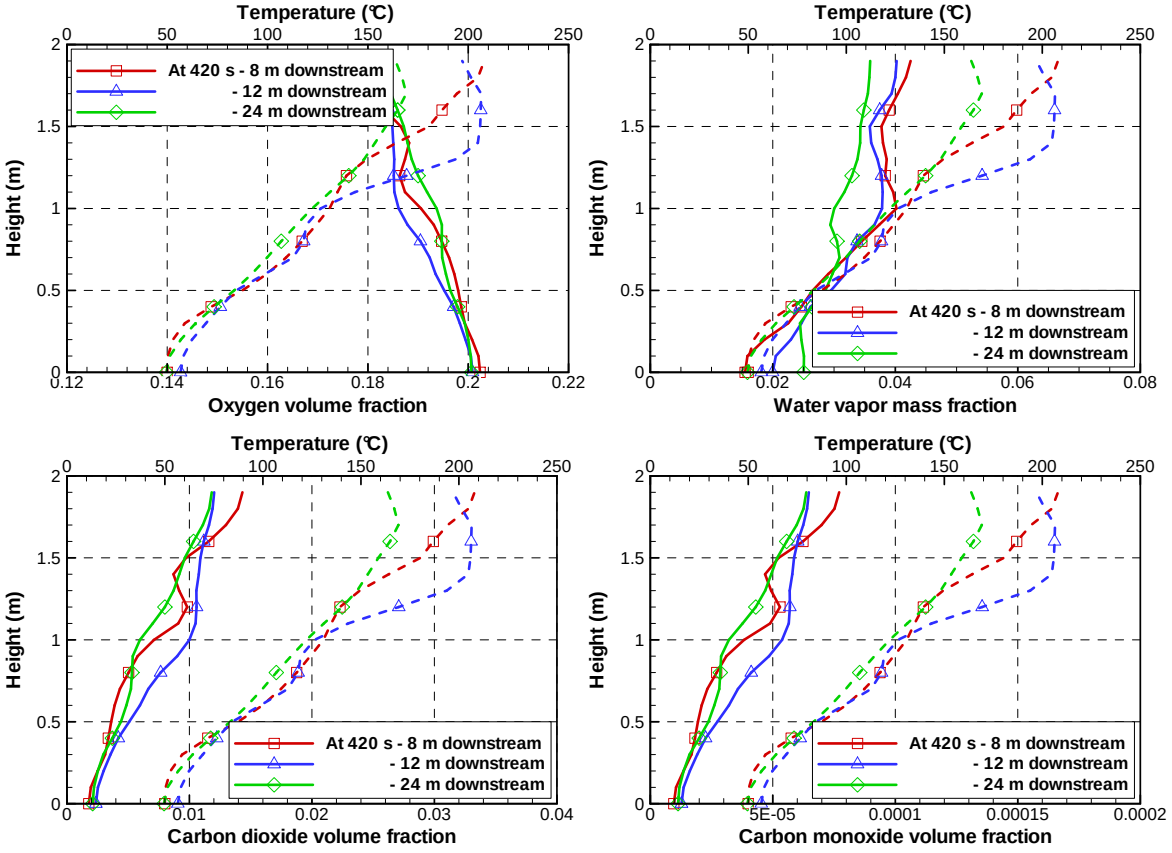

Fig. III.37 — Test 28 : Profiles of gas species (solid line) and air temperature (dash line) along the vertical centerline of three measurement sections two minutes after mist activation

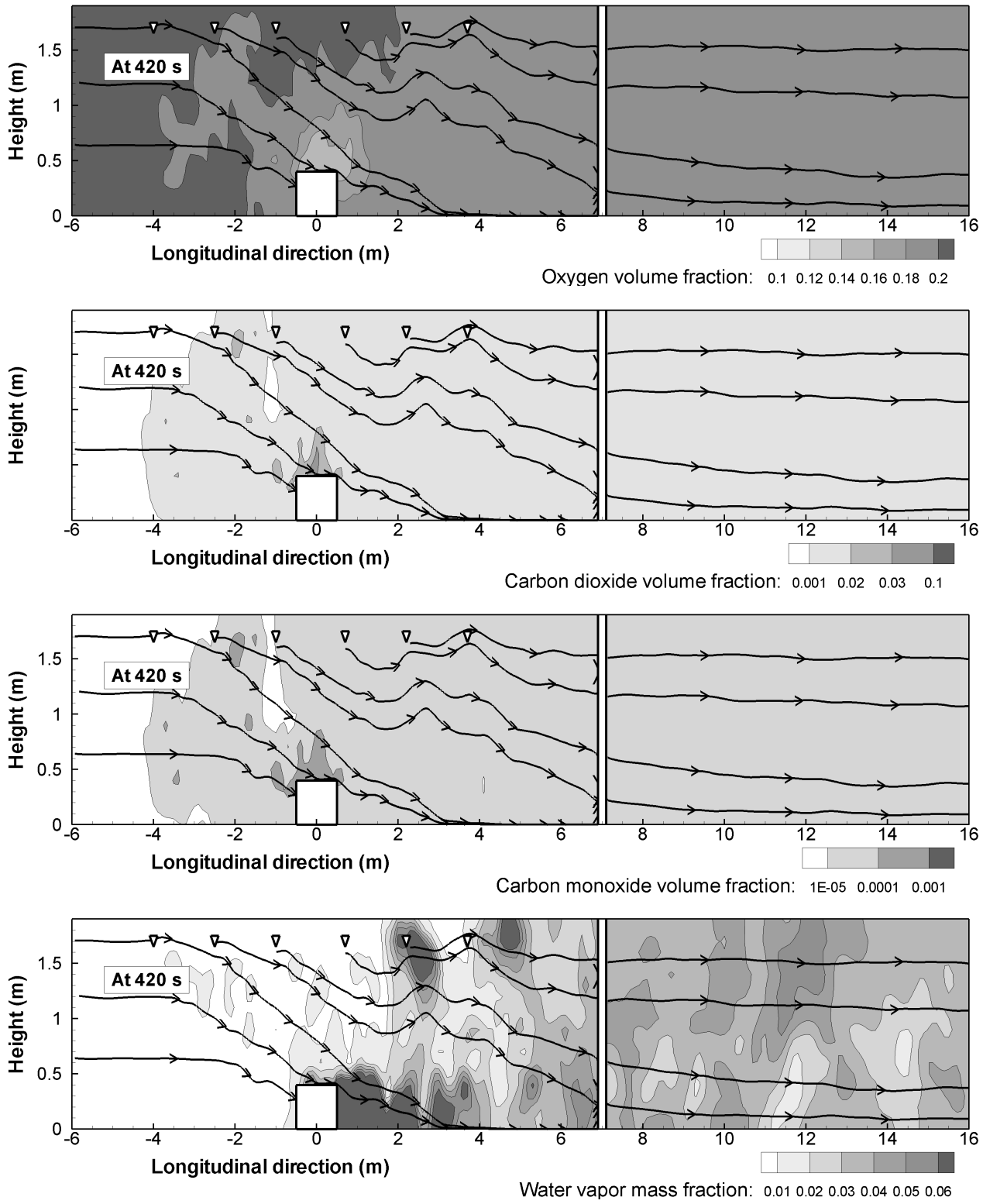

Fig. III.38 — Test 27 : Contours of chemical species on mid-plane in the tunnel two minutes after mist activation

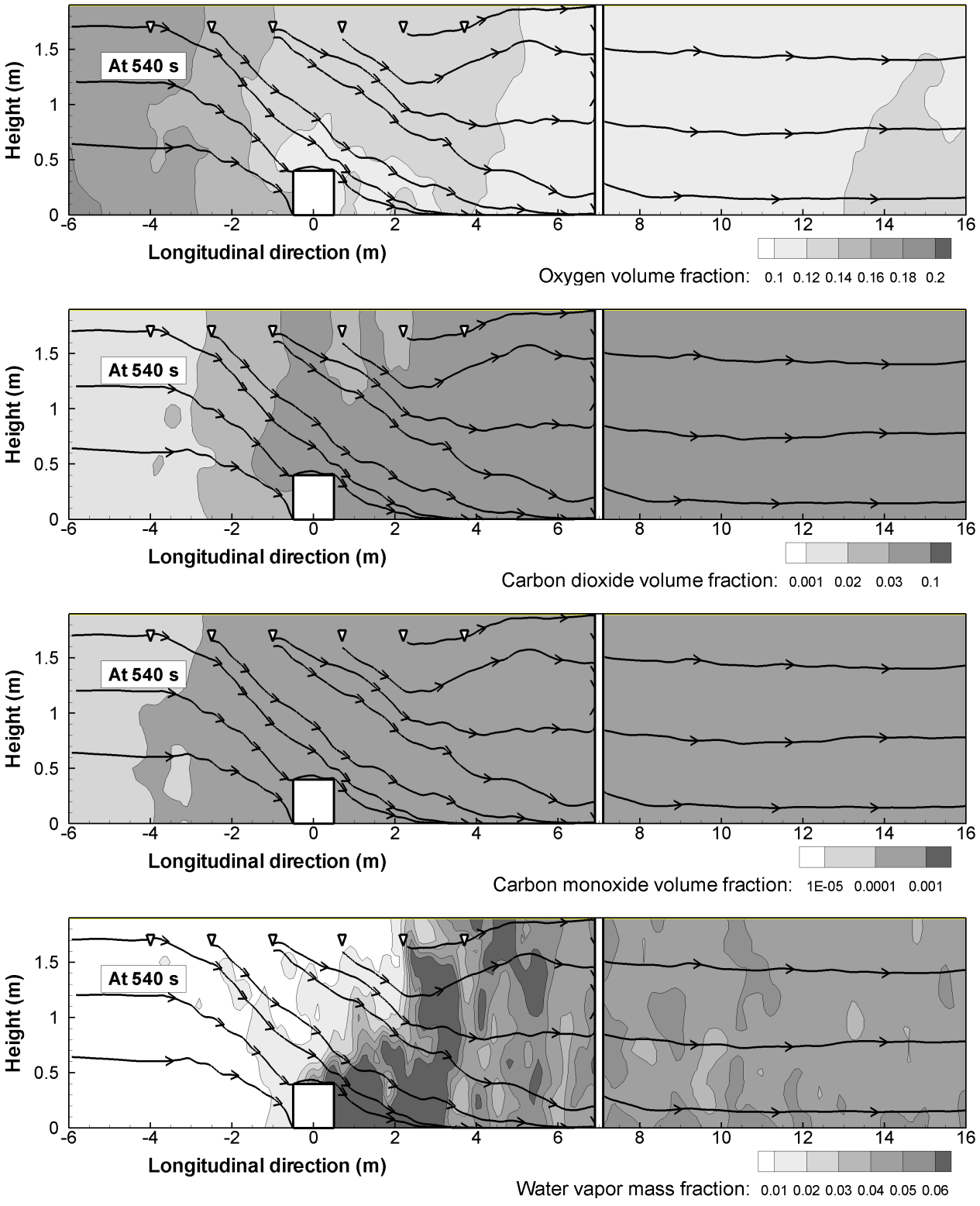

Fig. III.39 — Test 27 : Contours of chemical species on mid-plane in the tunnel four minutes after mist activation

III.3.5 Quantification of heat transfer

Sections III.3.2 and III.3.3 have shown a good capability of the FDS code to simulate the two tests 27 and 28. Measurements of air temperature and heat flux have highlighted the heat contribution of water mist. The following section aims at quantifying this contribution and understanding how this heat is absorbed. In a more general way, this section studies the energy distribution in the whole tunnel.

Conservation of energy holds that the fire heat release :
- goes to heat the gases within the domain,
- is transferred to boundaries by radiation and convection,
- is transported through the openings (minus heat injected through nozzles),
- is absorbed by the droplets.

Figure III.40 illustrates this energy distribution in tests 27 and 28 as a function of time before mist activation. For comparison, the heat release rate is also shown on this figure. Besides, energy can be considered as conserved in the control volume in both tests because the sum of wall loss, opening loss and energy is equal to fire heat. Figure III.40 highlights that nearly the half quantity of fire heat is lost toward tunnel walls (46 % in test 27 and 45 % in test 28) and the remaining heat is transported by the gases through the openings (52 % in both tests). This heat repartition which is similar to the one in test 2 (see Sub-section III.2.4) illustrates again the confined situation of tunnel fires.

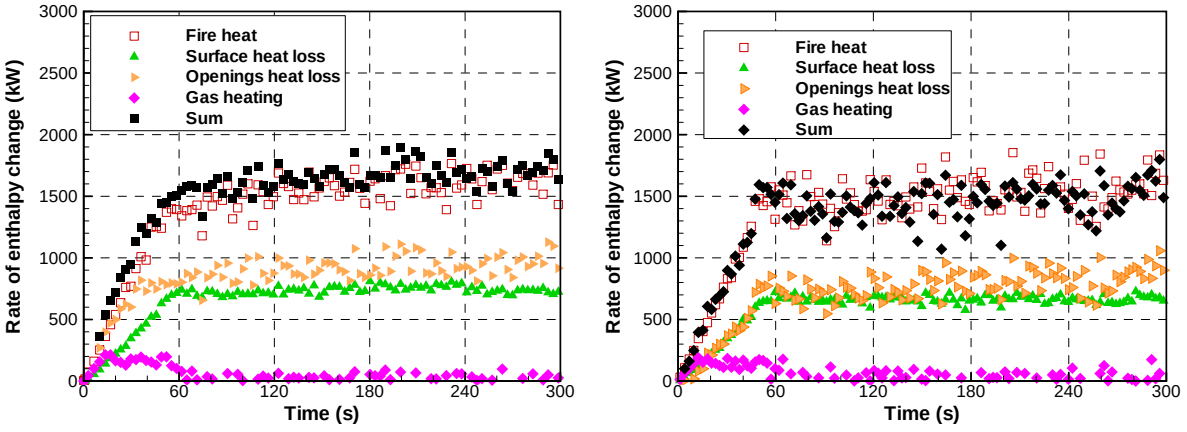

a- Test 27 b- Test 28

Fig. III.40 — Heat distribution in the test tunnel before mist activation

Figure III.41 illustrates the energy distribution in tests 27 and 28 as a function of time after mist activation. Heat heating gases in the control volume is not plotted since it is very low over this time duration in these tests. It represents -0.5 % of fire heat in test 27 traducing a global gas cooling and 0.25 % in test 28. Local data seemed to indicate that water mist plays a thermal role. Figure III.41 confirms that observation which appears indeed important :

– in test 27, roughly the half quantity of fire heat is absorbed by droplets. The remaining quantity goes to heat tunnel surface (24 %) or is conveyed by hot gases out of the tunnel (33 %).
– in test 28, roughly the quarter of fire heat is absorbed by droplets. The remaining quantity goes to heat tunnel surface (37 %) or is conveyed by hot gases out of the tunnel (37 %).

Note that in test 28 (with a lower quantity of water and a more powerful fire than in test 27), the decrease of heat loss to surface due to the effect of water mist is less important than in test 27.

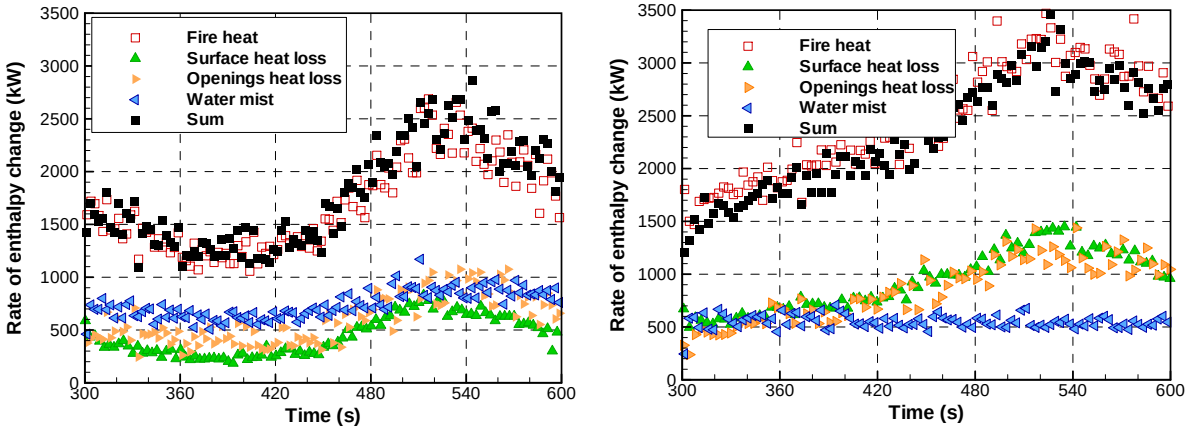

a- Test 27 b- Test 28

Fig. III.41 — Heat distribution in the test tunnel after mist activation

Here are detailed the heat transfer to surfaces and the absorption of heat by the water mist.

Heat transfer to surfaces

Figures III.42 and III.43 present the temporal evolution of heat loss to surface by convection and radiation in tests 27 and 28. Before mist activation, it confirms that heat transfer is mainly radiative in both tests as previously in tests 2 and 9 : it represents 38 % of HRR in the two tests 27 and 28 rather than the convective heat transfer to surfaces represents 8 % in test 27 and 7 % in test 28.

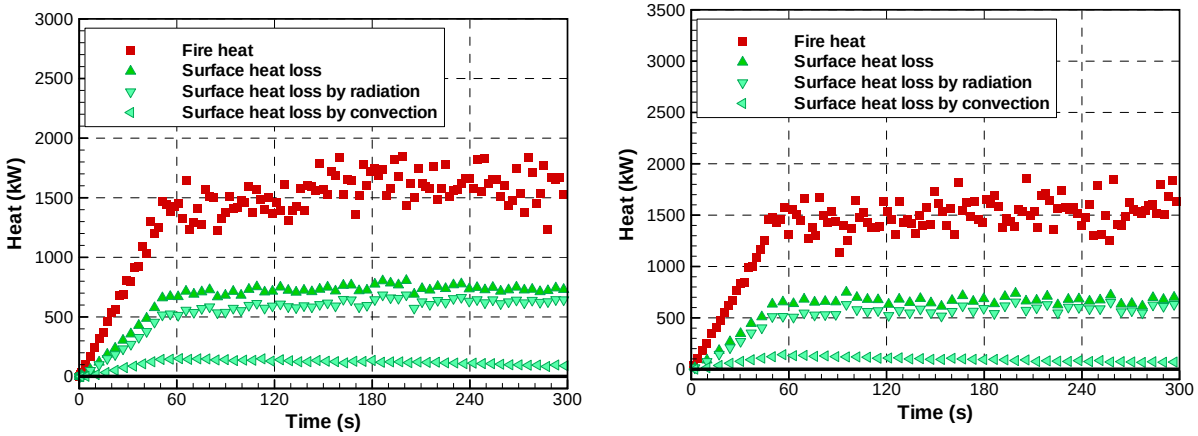

a- Test 27 b- Test 28

Fig. III.42 — Rate of heat loss to surfaces by radiation and convection in tests 27 and 9, before mist activation. For comparison, the global heat loss is also shown

After mist activation, heat transfer to surface remains mainly radiative. However, figure III.43 shows a difference between tests 27 and 28. This difference concerns the heat transfer to surfaces by convection and more precisely its sign :

– in test 27, its mean value is equal to -1.4 % over [300 ; 600 s]. Thus, heat is mainly transfered from tunnel walls to the gazeous phase.
– in test 28, its mean value is equal to 3.5 % over [300 ; 600 s]. Thus, heat continues to be transfered globally from the gazeous phase to tunnel walls.

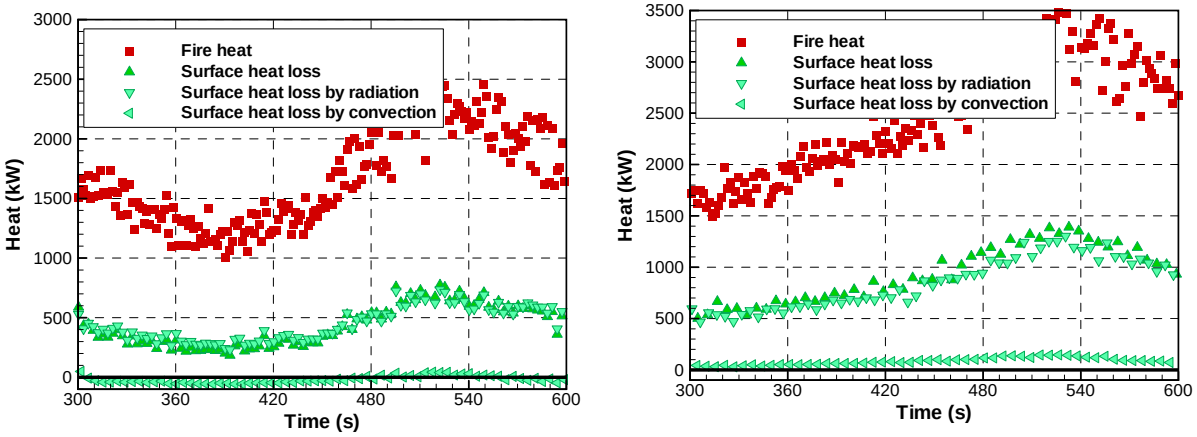

a- Test 27 b- Test 28

Fig. III.43 — Rate of heat loss to surfaces by radiation and convection in tests 27 and 9, after mist activation. For comparison, the global heat loss is also shown

In order to understand this particularity, the tunnel is divided into three zones in the longitudinal direction, the upstream and downstream parts separated by the fire region. The fire region is defined as previously as the zone where the released heat is higher than 0 kW. Rate of heat loss to surfaces in these three zones is plotted on figure III.44. Note that heat transfer in the upstream part is very low since the ventilation regime is supercritical. It appears that before mist activation, heat transfer by convection is mainly performed in the downstream zone where hot smoke is flowing along the tunnel roof toward the ventilation system. In the fire region, values are negative traducing that tunnel walls are hotter than the gaseous phase (see Figure III.45-a) since walls are still absorbing radiation emitted by the fire (see Figure III.44-b).

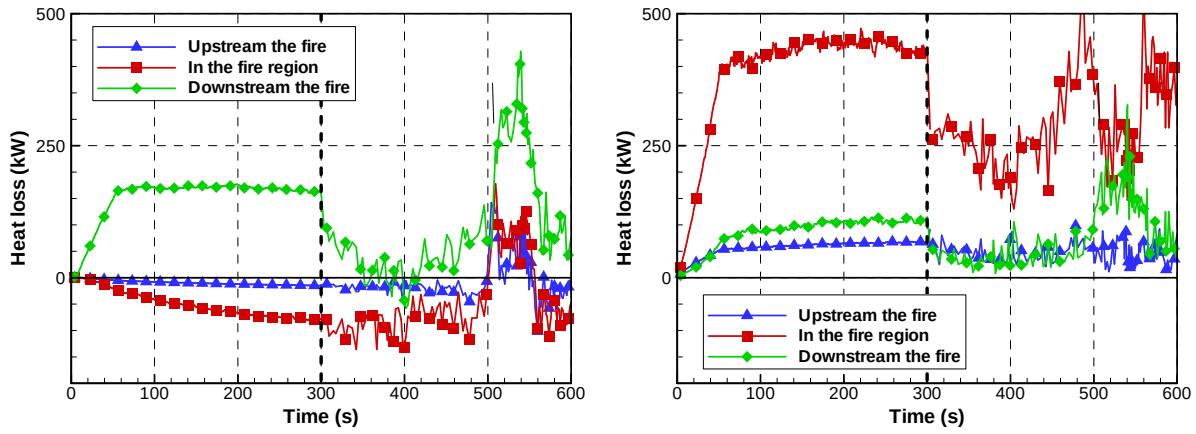

a- By convection b- By radiation

Fig. III.44 — Rate of heat loss to surfaces in the upstream zone, in the fire region and in the downstream zone predicted in test 27

In the particular test 27, a large quantity of water is sprayed in comparison with test 28 and the induced gas cooling is important from the fire location up to the downstream extremity and in particular the fire plume is greatly cooled down. Thus, heat transfer to walls drops in the downstream part, both by convection and radiation. However, despite the fire plume cooling, tunnel walls at the fire location remains hot and in particular hotter than gas till 500 s (see Figure III.45). Consequently, heat is still transfered from tunnel walls to the gaseous phase in the fire location. However, in addition to gas cooling at the fire location, water droplets act as radiative shield. Consequently, heat transfered to tunnel walls there by radiation decreases deeply and thus, tunnel walls are cooled down.

Then, after 500 s, HRR increases greatly inducing hotter fire plume and smoke downstream the fire (see Figure III.26). Consequently, the convective heat increases in the fire region and in the downstream part till becoming globally positive.

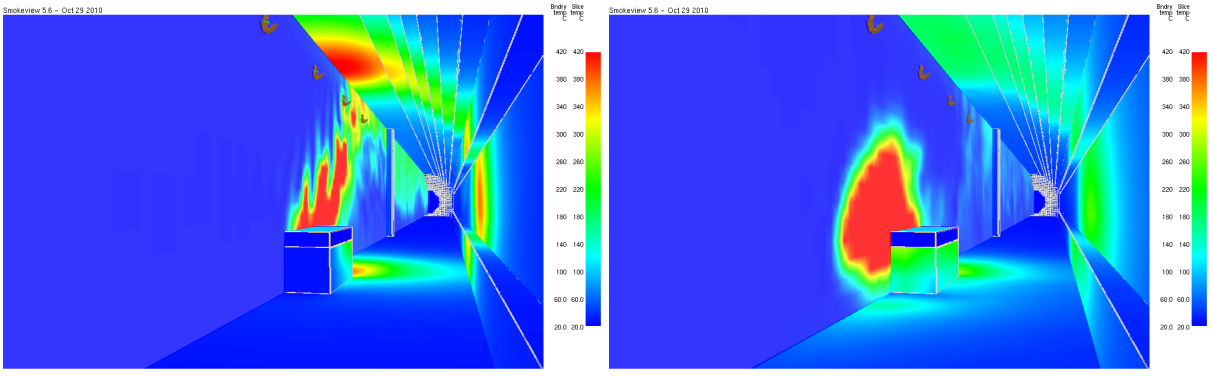

a- At 300 s b- At 420 s

Fig. III.45 — Test 27 : Temperature of surfaces and gases at the fire location on longitudinal mid-plane

Heat absorption by water mist

The use of the computational code has allowed to quantify the heat contribution of water mist in tests 27 and 28. It can allow to get a better understanding of how this heat is absorbed too. We also distinguish three phenomena, radiative attenuation and gas and surface cooling. Heat absorbed by each phenomenon is plotted III.46 and its ratio with the total heat absorbed by water is plotted on figure III.47.

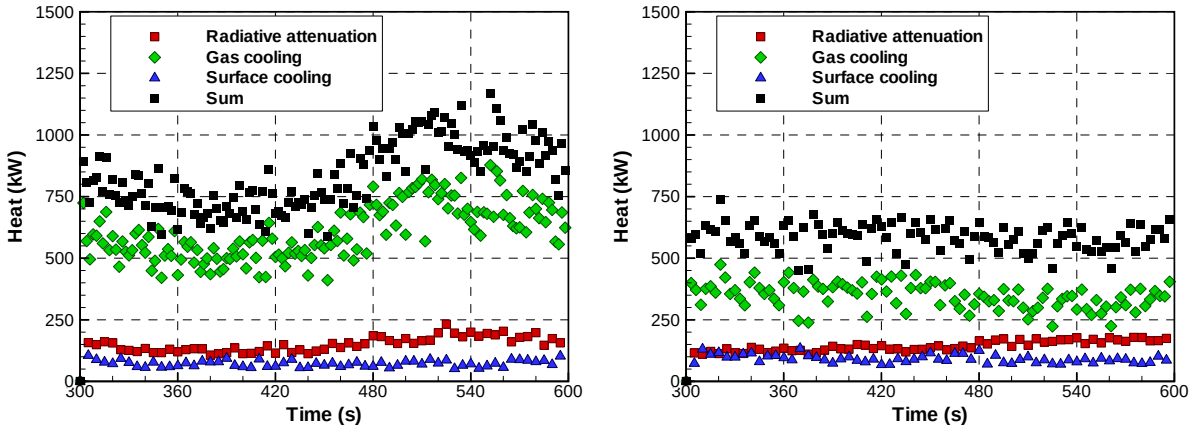

a- Test 27 b- Test 28

Fig. III.46 — Temporal evolution of the absorbed heat by water droplets

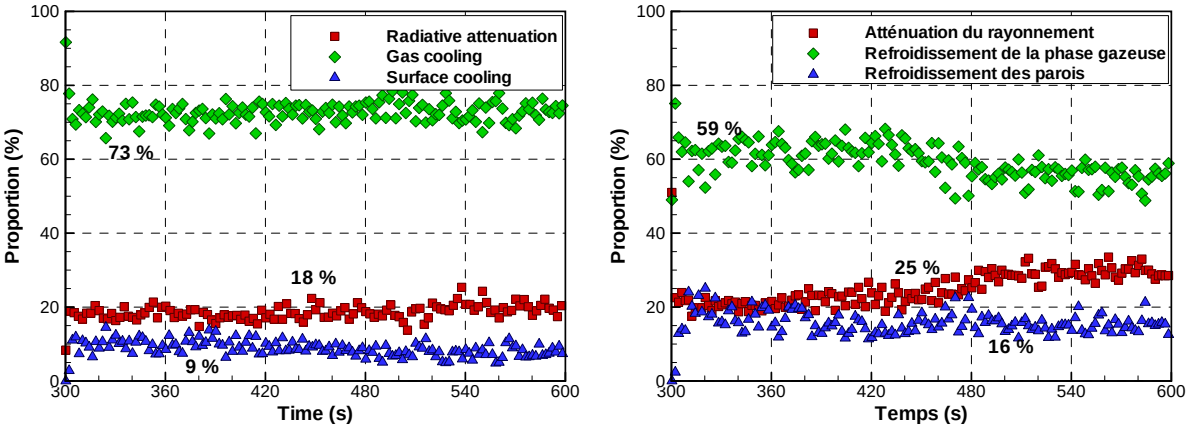

a- Test 27 b- Test 28

Fig. III.47 — Temporal evolution of the rate of absorbed heat by water droplets

In tests 27 and 28, the absorbed energy mainly comes from gaseous phase. It represents 73 % in test 27 and 59 % in test 28 over [300 ; 600 s]. In other words, main absorbed energy due to droplets induces a gaseous phase cooling. The remaining heat absorbed by droplets results from radiation attenuation (18 % in test 27 and 25 % in test 28) and wall surface cooling (9 % in test 27 and 16 % in test 28).

Efficiency of the water application

A part of the heat transferred to each water droplet serves to vaporize it. Energy balance could also be next exploited to determine the water mist system efficiency η defined as the absorbed heat by heating and evaporating the water droplets versus the maximum heat that would be absorbed if the whole injected water quantity was evaporated

$$\eta = \frac{Q_{\text{particule}}}{\left(L_v + C_{p,p}\left(T_{p,evap} - T_{p,inj}\right)\right) \cdot \dot{m}_{\text{p,inj}}} \tag{III.5}$$

where $\dot{m}_{\text{p,inj}}$ is the sprayed water mass flow rate, $T_{p,evap}$ the boiling temperature and $T_{p,inj}$ the initial water temperature at the injection point.

This definition of efficiency allows to assess the use in water and not the impact of the mist on surroundings or fire activity. The useful water quantity could also be present on the floor or transported by the air flow by acting as a gas/surface cooler and a radiative shield.

In test 27, efficiency follows the same evolution as HRR (see Figure III.48). It varies between 40 and 70 %, the time average value over [300 ; 600 s] being 53 %. In test 28, it is almost constant over the mist application ans is around 80 %. This stationary state whereas HRR changes deeply over the same duration, gives us to understand that a level is reached in test 28. More precisely, even by increasing HRR, it appears that the amount of energy absorbed by water mist can not be increased.

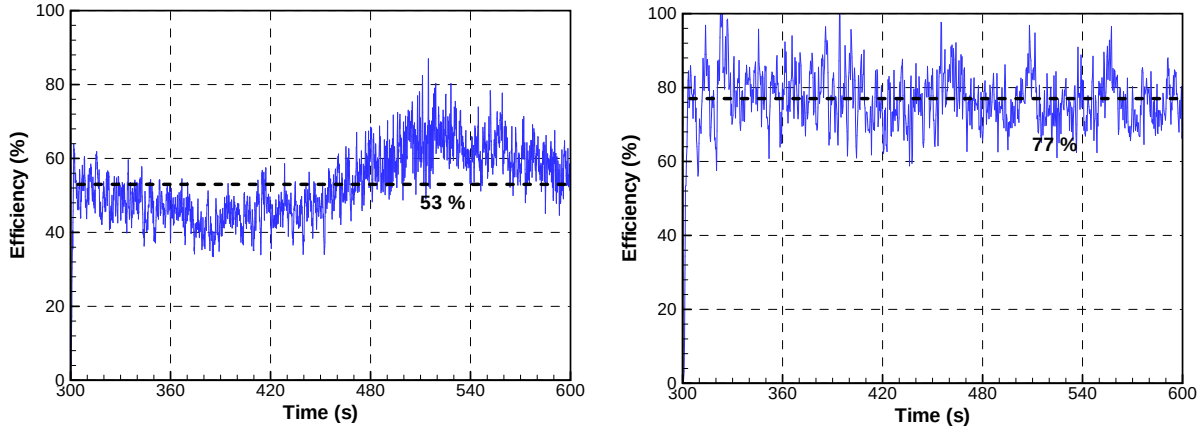

a- Test 27 b- Test 28

Fig. III.48 — Efficiency of the water application in tests 27 and 28

III.4 Conclusion

This chapter deals with the study of fire in tunnel ventilated longitudinally involving or not water mist. Four tests conducted in an intermediate (1/3) scale tunnel have been studied. Their main characteristics are listed in table III.4. Once the validation of the CFD code (version 5.4) is achieved, an extensive use of this code allows to improve the understanding and quantify the involved phenomena. Moreover, such use allows to highlight the key parameters influencing the surroundings.

Tab. III.4 — Summary table of simulated tests

Test	Ventilation regime	Nozzle locations
Tests without water mist		
n° 9	sub-critical	
n° 2	supercritical	
Tests with water mist		
n° 27	supercritical	3 nozzles upstream and 3 nozzles downstream
n° 28	supercritical	3 nozzles upstream

The simulations of **tests without water mist** have shown the good capability of the CFD code FDS for predicting the thermal environment and the air flow when HRR and the longitudinal ventilation are known. In fact, the discrepancy for air temperature is comprised between 15 and 26 % for test 9 conducted with a sub-critical regime and between 11 and 19 % for test 2 conducted with a supercritical regime. Moreover, the predictions of air velocity are within the overlapping uncertainty limits. Last, comparison between measured and predicted heat flux shows a correct agreement when air temperature at the radiometer location is not in the order of or higher than the measurement limits.

More precisely, the comparison between measured and predicted data have highlighted that the discrepancy is not distributed uniformly within the tunnel. Firstly, the CFD code tends to underestimate temperatures close to the fire location and further the measurement section from the fire is, better the agreement is. These two tendencies have been attributed to a bad representation of the tricky zone releasing heat due to the ventilation. Secondly, the CFD code underestimates the mixing of hot smoke layer in the upper part with fresher air in the lower part.

The computational results have allowed to draw the heat distribution within the tunnel. The energy balance appears to strongly depend on the ventilation regime (sub-critical or supercritical) and not to HRR. In fact, whereas the main part of the heat released (2/3) is dissipated through exchanges with the wall for the sub-critical regime, the fire heat is half-distributed through exchanges with the wall and in the gas phase for the supercritical regime.

The difference in energy balance between the two regimes has been attributed (in order of importance) to **the backlayering phenomenon** which increases the heat exchange surface between smoke and tunnel walls and to **the influence of ventilation velocity on air temperature downstream the**

fire location. Such cooling conducted to a decrease in heat transfer by radiation. Note that despite this difference in energy balance, in the two tests 2 and 9 conducted with two different ventilation regimes, a similar heat quantity is lost to tunnel walls in the fire region even if its length varies with longitudinal velocity.

Last, a sensitivity analysis has been conducted (a detailed presentation is available in the French version) for the two test 2 and 9. For instance, the longitudinal ventilation velocity influences the thermal stratification in terms of vertical temperature gradient. HRR variation within the overlapping uncertainty limits and combustion reaction (soot and CO yields) have appeared not influent on the thermal conditions (thickness and temperature of the smoke layer) and the air flow. Note that air composition is not studied. Last, the low influence of tunnel walls composition in the two tests 2 and 9 is to the short test durations (5 min for test 9 and 8 min for test 2).

In, the simulations of **tests with water mist**, the FDS code has shown a code capability for predicting the fire environment during mist application and in particular gas cooling and radiative attenuation.

In the particular test 27, during the three first minutes after mist activation, the FDS code has predicted the homogeneity of air temperature at each measurement section, traducing the thermal destratification. After this period, the vertical thermal gradient observed in test 27 has been predicted by the computational code. However, it seems important to mention that in test 27, the mist application induces very low air temperatures (even close to the fire location) in comparison with HRR.

This validation has also highlighted one weakness in test 28. Note that this test is very special in that it involves a small amount of water (16.5 l/min) whereas HRR is relatively high (between 1.5 and 3.5 MW). Thus, water mist activation does not induce a significant gas cooling and a drop in heat flux. The environment is even clearly stratified downstream the fire during the mist application. In that test, the FDS code has overestimated the evaporation of water droplets close to the fire. The main consequences concern air temperature at 8 m downstream which is under-estimated and heat flux at 7 m downstream which are over-estimated. However, further from the fire, the code has produced a good agreement.

Then, the FDS code has been used for studying the interaction between water mist, tunnel ventilation and smoke. In particular, this study has highlighted that it is difficult or even impossible to assess totally the impact of water mist (thermal and toxic) on the only basis of temperature measurements. In other words, it is necessary to measure gas composition in addition to the usual temperature measurements for addressing the question.

The FDS code has been next used for measuring the heat contribution of water mist in the two tests. The sprayed water droplets absorb the half of fire heat over the mist application [300 ; 600 s] in test 27. In test 28 where water flow rate is half as much, it represents roughly the quarter of fire heat and most of the sprayed water is evaporated. The following question we aimed at answering concerns the way of heat absorption. In both tests, heat is mainly absorbed by the droplets from the gaseous phase. Heat transfer to gas represents 73 % of the total heat absorbed by the droplets in test 27 and 50 % in test 28. Radiative attenuation and solid surface cooling are nevertheless important. They represent respectively 18 and 9 % of the total heat absorbed by the droplets in test 27 and respectively 31 % and 19 % in test 28. In practice way, this quantification has an other interest. It can help the developers to focus on one particular phenomenon.

Last, a sensitivity analysis has been conducted (it is only available in the French dissertation). In particular, it appears that the initial droplet velocity at the injection point is not an influent computational parameter. Droplet size and tunnel ventilation rather affect the dynamic of water mist and heat transfer, both with the gas phase and with the surfaces of the tunnel. This influence is mainly related to the droplet residence time in the gaseous phase. Concerning HRR, sensitivity of heat contribution of water mist to this parameter is different in tests 27 and 28. In test 27, this influence is weak rather than in test 28 involving a low water quantity, HRR influences the evaporated water quantity and the importance of each involved phenomenon. Concerning tunnel wall composition, the computational results appear not sensitive to this parameter over the test duration.

IV At the compartment scale

The following application in buildings is motivated by the current context in France. Building fire safety is based on the use of ventilation systems for preserving a free smoke area and promoting self-evacuation. Since mid-2000s, many discussions have dealt with the use of mitigation systems in buildings and more particularly in hotel corridors overlooking for rooms. The French Directorate for Civil Security has indeed gathered a working group (among them CSTB and LEMTA) whose mission consists in investigating the possibility of completing the actual regulations for considering water mist systems. This working group has recently proposed a modification of the building safety regulation and a new technical instruction (IT). These ones have been published in a public report of meeting December 2 2010, they will be likely effective quite soon. Before any installation, a test campaign must be conducted. On the only basis of this campaign, the effect of water mist on egress and operating conditions must be assessed.

In this context, CSTB is to conduct a test campaign in 2012 for understanding the interaction of water spray, smoke layer and ventilation in case of fire. The test set-up, already built, consists in a room connected to a corridor (see Figure IV.1).

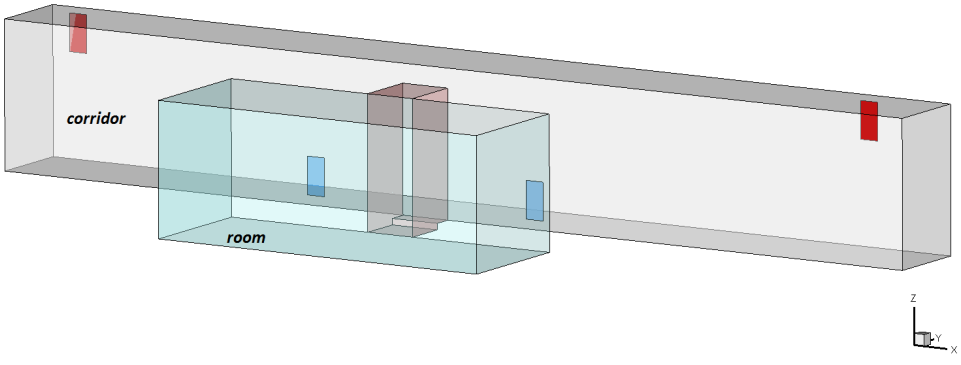

Fig. IV.1 — Schematics of the test set-up

In chapters II and III at different scales, the CFD code FDS (version 5) has shown a good capability for predicting the influence of water mist on environmental conditions : gas cooling, radiative attenuation and in the tunnel configuration : smoke destratification and tunnel air flow. Based on this assessment, the present chapter presents a computational preliminary study of the test campaign. It aims at understanding the interaction of water mist, smoke movement and ventilation.

The approach consists in first defining the fire load (position, HRR, type), the ventilation (natural, mechanical, number and positions of vents, gas flow rate through each vent) and a water mist system (position, spray shape, water flow rate, droplets size). Then, we use the computational code for studying the influence of water mist on (liquid and vapor) water transport, the thermal and toxic stratification for different droplets size distribution at the injection point.

IV.1 Presentation of the tests

IV.1.1 Set-up

The test set-up id drawn on figures IV.1 and IV.2. It is a room connected to a corridor via an opening. The room is 12 m^2 area and 2.15 m high. The corridor is 15 m long, 1.4 m wide and 2.40 m high. The opening is 80 cm wide and 1.90 m high. The internal walls are covered by 7 cm of a fire resistant mortar cement.

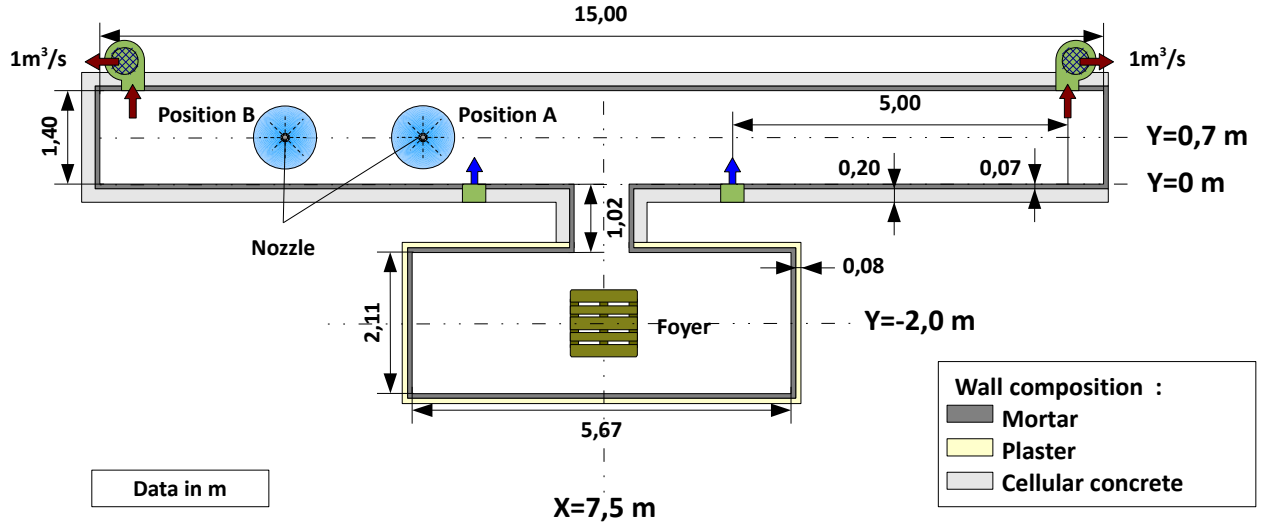

Fig. IV.2 — Schematics representation of the test set-up

IV.1.2 Corridor ventilation

To consider a realistic air flow, the ventilation system is defined for satisfying the French regulation (in that case, the reference is the technical instruction 246). The ventilation system is composed of four vents :

- two for natural gas supply. These vents are located close to the opening between the room and the corridor, they are represented by blue arrows on figure IV.2. They measure 30 cm wide and 60 cm high and their lower parts are 25 cm high from the floor.
- two for mechanic gas exhaust. These vents are located at the extremities of the corridor, they are represented by red arrows on figure IV.2. They measure 30 cm wide and 60 cm high and their lower parts are 1.75 m cm high from the floor. The exhausted volumetric rate is set at 1 m^3/s.

IV.1.3 Fire load

The purpose of this study being the interaction of water mist, smoke layer and ventilation, the fire load is placed inside the room. The fire load is a wood crib for four reasons :

- it is known to produce sufficiently opaque smoke,

– it is relatively well described in the scientific literature. In particular, Ref. [2] proposes an estimation of HRR relative to its geometrical arrangement,
– it is preferred to liquid fuel since wood is one the main material in buildings for furnitures.

The simulation of under-ventilated fires remaining tricky, fire is set to be controlled by its pyrolysis rate. In other words, gas quantity coming in the room and the corridor through the supply vents must be sufficient for ventilating the fire and for supplying the combustion reaction.

The exhaust system extracts 2 m^3 of gas per seconde. By assuming that its temperature is comprised between 20 and 500 °C, the extracted gas mass flow is at least higher than 0.9 kg/s. Mass conservation indicates that smoke production plus gas supply and sprayed water corresponds to the extracted gas quantity. By assuming that the first quantity is negligible in comparison with the others, gas quantity available for combustion is around 0.64 kg/s i.e. 0.15 kg of oxygen per seconde. These values correspond to a peak HRR higher than 1.9 MW. In the present study, the maximum HRR is set around 700 kW.

Concerning HRR evolution, HRR is supposed to increase linearly with time during the first 300 seconds, then to be constant till 900 s for decreasing at the end during 600 s (see Figure IV.3).

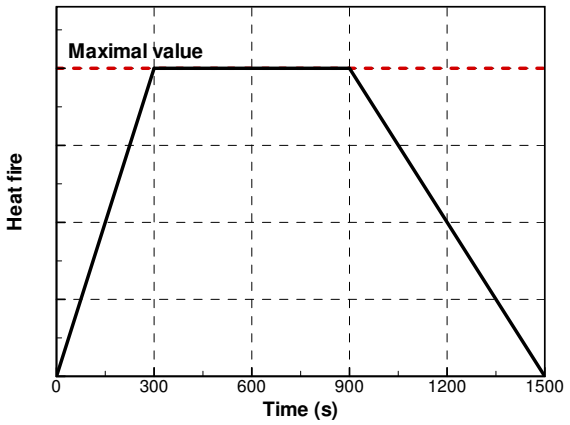

Fig. IV.3 — HRR versus time

IV.1.4 Water mist system

The water mist system is composed of one single nozzle for simplifying the involved phenomena and avoiding dynamic interactions between different sprays. Since the present study does not deal with fire activity, the nozzle is placed on mid-plane in the corridor (at Y=0,7 m) under the roof. Air flow within the corridor is induced by the ventilation system, the flowing smoke and the spray dynamics. Consequently, two positions were studied in the original work (see Figure IV.2).

– *position A*, the nozzle is located close to a gas supply vent,

– *position B*, the nozzle is located close to a gas exhaust vent

The influence of these two positions is studied in the French dissertation. Here is only presented the work for position A.

The water mist system is defined on the basis of characteristics of a system already used in a previous campaign at CSTB conducted in a compartment.

The operating pressure is set equal to 90 bars. Consequently, the corresponding flow rate is around 16 l/min, flow rate number being equal to 1.7 l/min/bar$^{1/2}$. The nozzle in manually activated in order to control this parameter and to be able to compare tests involving different fires. The activation time is chosen during the level-off period, when interaction of smoke and ventilation is stationary. Thus, mist system is activated at 400 s.

Th nozzle has a single central orifice. The produced spray is conic defined by en angle around 40 °. Since the manufacturer provided no particular data for droplet size, a sensitivity analysis is conducted to this parameter. The polydisperse spray is defined at the injection point with a hybrid law parametrized with a dispersion parameter equal to 2.85 and a mean diameter comprised between 100 and 1000 μm.

The following table summarizes the spray characteristics considered in the present study.

Tab. IV.1 — Spray characteristics

Spray shape	conic
Angles of injection	40 °
Operating pressure	90 bars
Water flow rate	16.2 l/min
Mean diameter at the injection point	between 100 and 1000 μm

IV.2 Simulations with water mist – Position A

In this configuration, the nozzle is located at 2/3 of the horizontal distance between the gas exhaust vent and the gas supply vent (see Figure IV.2). At mist activation, gas temperature is around 200 °C at the nozzle location.

IV.2.1 Thermal environment

The sprayed water interact with the environment, in particular thermally. Heat is also transfered between water droplets, corridor walls (by convection and radiation), gaseous phase (by convection and radiation) and fire (only by radiation in this configuration). Heat absorbed by water droplets is directly traduced in their heating and their vaporization. As it is described in the French dissertation with the bibliographic synthesis, the heat quantity depends deeply on droplets size. The following figure IV.4 shows gas temperature on mid-plane in the corridor at 600 s i.e. 200 s after mist activation, for two droplet sizes at the injection point 100 and 1000 µm. In these two simulations, the sprayed water flow rate is the same. This figure illustrates the relation between the absorbed heat quantity (traduced by gas cooling) and droplet size : for the smallest droplets, gas cooling is more important.

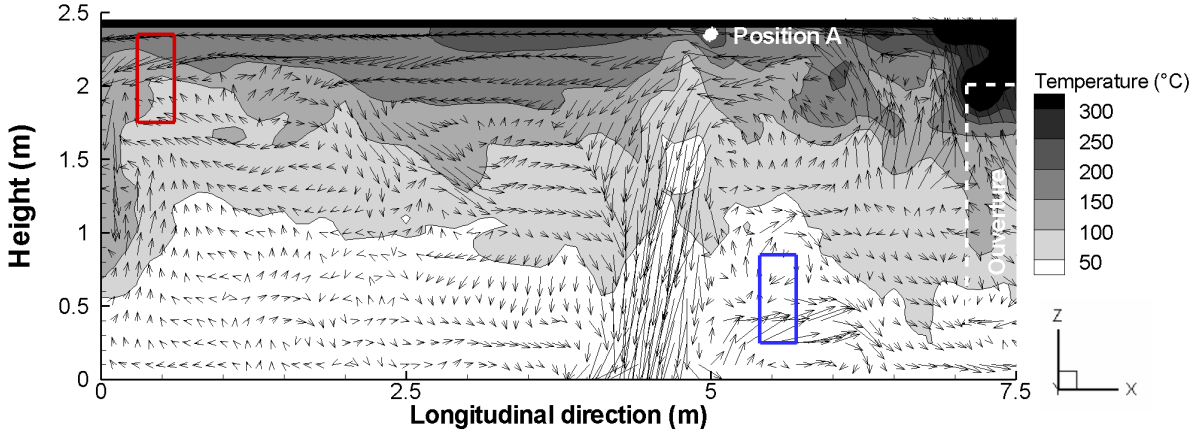

a- Droplet mean diameter : 100 µm

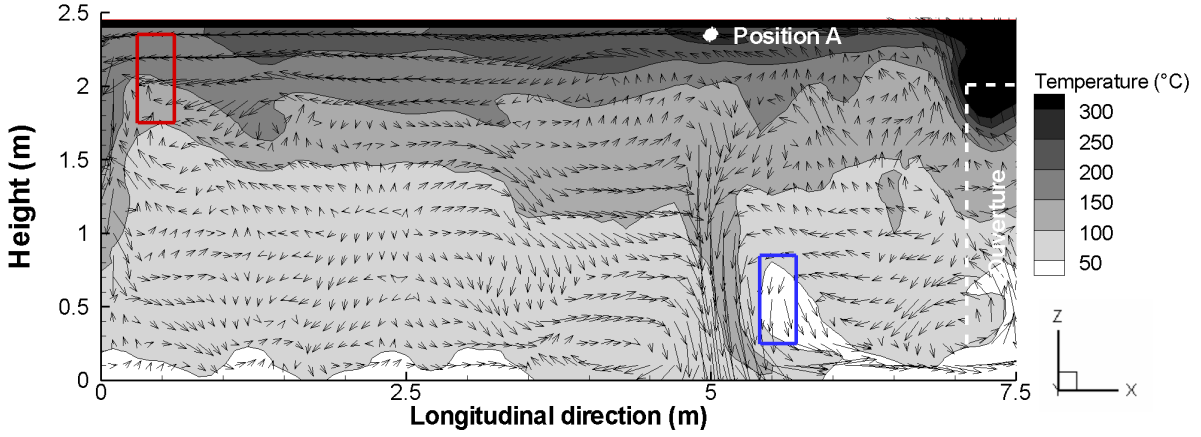

b- Droplet mean diameter : 1000 µm

Fig. IV.4 — Contours of air temperature on mid-plane in the corridor at 600 s for two mean diameters

Moreover, figure IV.4 illustrates the dynamic effect of water mist. It appears that water mist transports gas toward the floor and it is transported himself. This effect appears very sensitive to the droplet size : the smaller the droplets are, the more sensitive the spray to the air flow is and the weaker its influence on the thermal stratification at the mist location is. For instance, unlike the spray defined with a diameter equal to 100 µm, the two sprays defined with diameters equal to 500 and 1000 µm induce a gas heating in the lower part at the mist location traducing a thermal destratification. However, except at mist location, figure IV.4 indicates that the environment remains stratified despite the mist application especially for spray with smallest droplets. To confirm this observation, the vertical profiles of air temperature is first verified on figure IV.5 at three distances from the corridor extremity (at Y=0.7 m and X=2 m, X=4 m and X=6 m). Secondly, the height of thermal stratification defined like in Refs [13] and [25] is plotted on mid-plane of the corridor versus the distance from the extremity (see Figure IV.6).

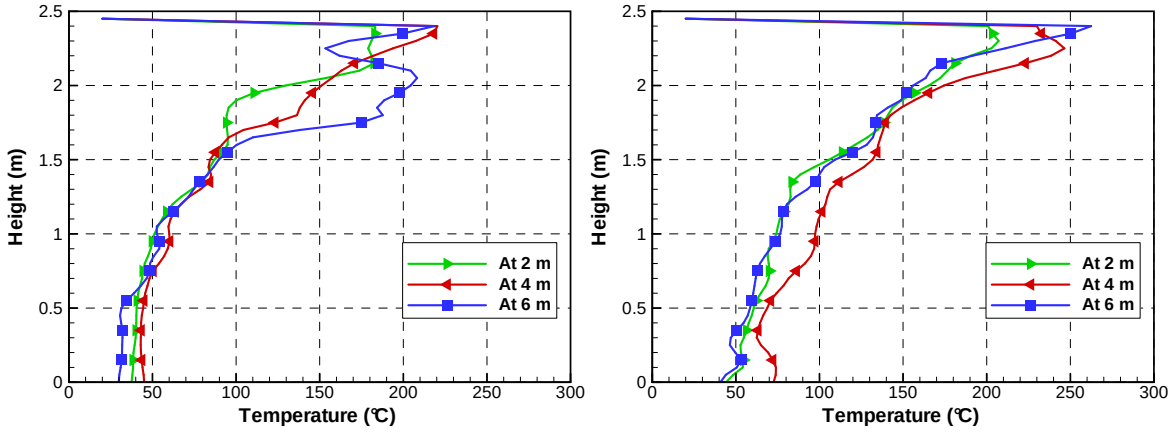

a- Droplet mean diameter : 100 µm b- Droplet mean diameter : 1000 µm

Fig. IV.5 — Vertical profiles of air temperature at three distances from the corridor extremity at 600 s

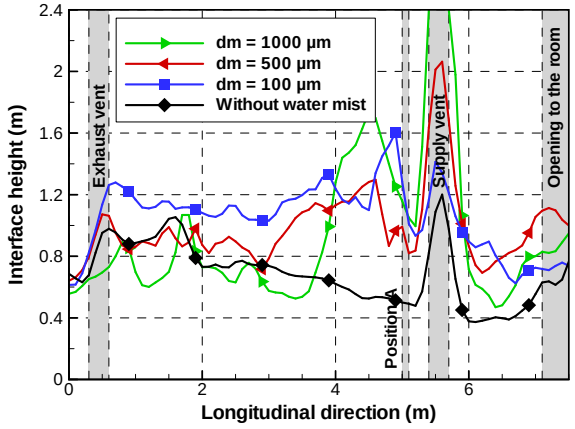

Fig. IV.6 — Height of thermal stratification on mid-plane of the corridor at 600 s, with and without water mist

IV.2.2 Transportation of liquid water and water vapor

Water mist system are characterized by the small sprayed droplet size. This parameter influences the transportation of liquid water and heat transfer to gaseous phase and also to corridor walls. For this reason, it is interesting to study the liquid water concentration within the corridor. This study allows furthermore to determine if a fraction of sprayed water reaches the lower part of the corridor.

The quantity of liquid water is plotted in two different ways on figure IV.7. It is first presented as the mass versus height i.e. each value at a given height z corresponds to the liquid mass integrated over the whole corridor between z and $z+5$ cm. It is next plotted by differing the liquid mass present in the upper layer and the one present in the lower layer. These two layers are delimited by the stratification height defined in Refs [13] and [25].

Figure IV.7 indicates that liquid water quantity varies with height. For the three sprays, it is maximal close to the floor, at less than 50 cm high. This tendency results from the droplets inertia. In other words, droplets are rapidly slowed down and (partly) evaporated, their residence time is thus longer in the lower part. This residence time can be also be promoted by the fact that at low speed, droplets are more sensitive to air flow and are more likely transported.

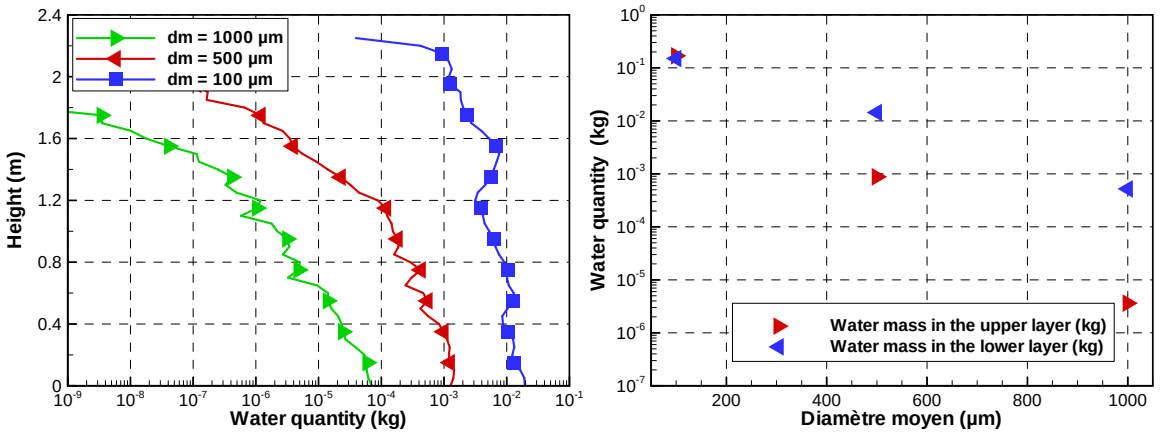

Fig. IV.7 — Liquid water quantity in the corridor versus its height (left) and integrated in the lower and upper layers (right), at 600 s

Moreover, figure IV.7 illustrates the strong influence of droplet size on the liquid water in suspension : the bigger the droplets in the spray are, the lower the water quantity within the corridor is, as in the lower layer and in the upper one (see Figure IV.7). For instance, the ratio of water quantity at a given height is higher than 100 between the sprays defined at the injection point by a mean diameter equal to 100 µm and the one defined by a mean diameter equal to 1000 µm. In other words, by multiplying the mean droplet diameter at the injection point by 10 and even if the water flow rate is conserved, the liquid water quantity present in the gaseous phase is divided by more than 100.

This tendency could result either by an evaporation more important for largest droplet spray or a shorter residence time for largest droplet spray. Note that the first hypothesis goes against theory. Indeed, for a given mass of water, decrease the droplet size leads to increase the exchange surface area with gaseous phase and the water concentration in suspension. It also accelerate the vaporization and promotes radiative attenuation. Consequently, a more important quantity of water is vaporised. To assess these two hypothesis, mass fraction of water vapor is plotted on figure IV.8 and concentration of liquid water is plotted in 3 dimensions on figure IV.9.

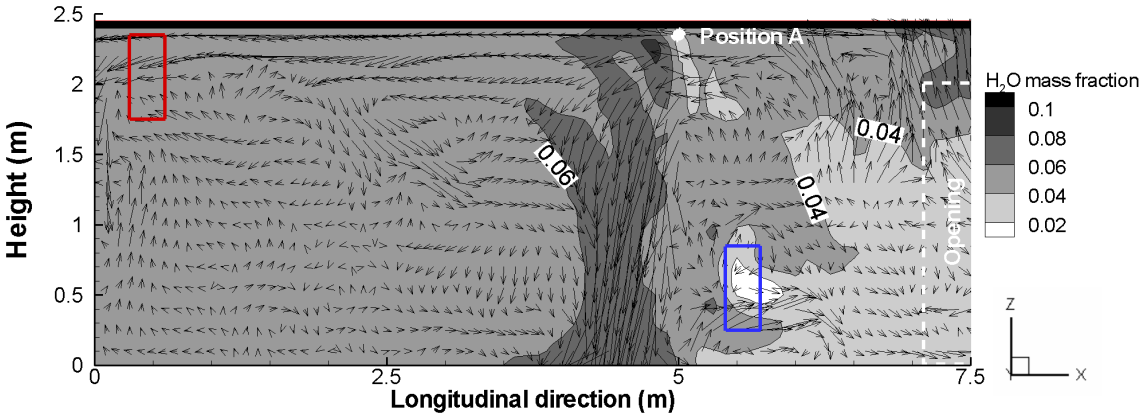

a- Droplet mean diameter : 100 µm

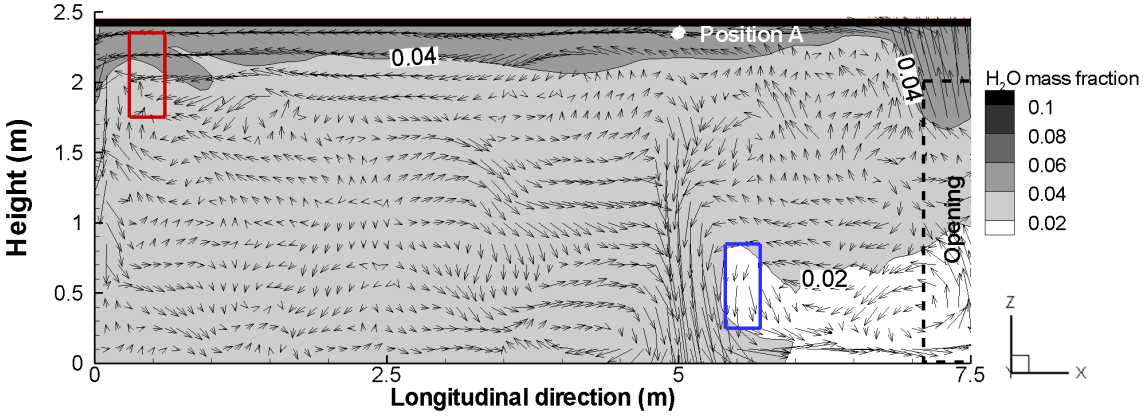

b- Droplet mean diameter : 1000 µm

Fig. IV.8 — Contours of water vapor mass fraction on mid-plane of the corridor at 600 s, for two mean diameters

Figures IV.8 and IV.9 illustrate that the smaller the droplets are, the higher the concentrations of water vapor and liquid water are. In other words, the smaller the droplets are, the more evaporated the water droplets are and also the more the spray is transported within the whole corridor. These observations are along the lines of the theory. The residence time of water droplets in suspension is also considerably loner for the small droplet spray.

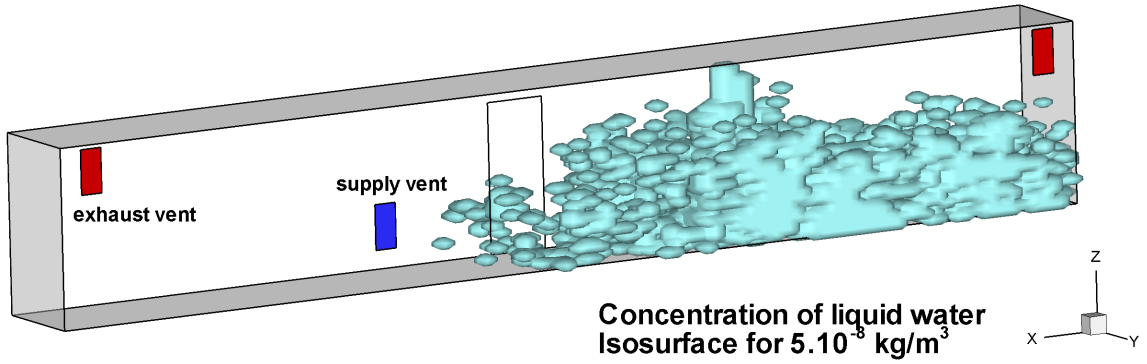

a- Droplet mean diameter : 100 µm

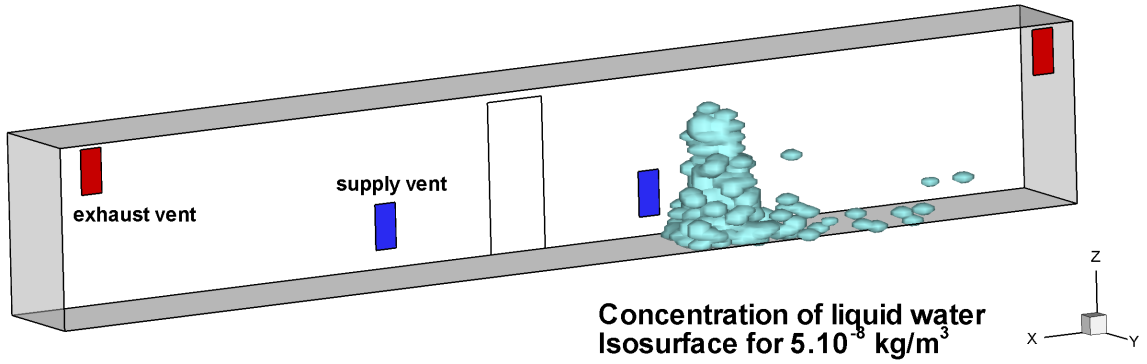

b- Droplet mean diameter : 1000 µm

Fig. IV.9 — Concentration of liquid water (kg/m^3) within the corridor at 600 s, for two mean diameters

IV.2.3 Heat transfered and transported by water droplets

Figure IV.10 presents the temporal evolution of heat absorbed and transported through the vents by the water droplets in the three simulations. We distinguish three phenomena in the absorbed heat, radiative attenuation, gas and surface cooling. Heat corresponding to radiative attenuation is not plotted since it is lower than 2 kW over mist application time period for the three diameters.

Unlike the tunnel application in chapter III, figure IV.10 shows that heat is not mainly absorbed from the gaseous phase in all cases. It depends indeed of the droplet size

- for the smallest droplet spray, heat is mainly absorbed from the gaseous phase, it represents 60 % of the total heat absorbed and transported over [400 ; 900 s]. Note that surface cooling represents a quarter of the total heat and heat transported 16 % over the time period,
- for the two other sprays involving bigger droplets, heat distribution is different. First of all, heat transported through the vent is around zero (<1 kW). Secondly, heat extracted from the gaseous phase is less important in absolute values than in the previous case for the smallest droplet spray. In relative proportions, it represents roughly 2/3 of the total heat for the spray defined with a mean diameter equal to 500 µm at the injection point and roughly the half for the other defined with a diameter equal to 1000 µm.

Thus, figure IV.10 illustrates once again the importance of the water droplet transportation and their residence time in the gas phase on heat transfer. It also confirms the observations on the basis of figure IV.4 because gas temperature is really higher for the spray involving the biggest droplet.

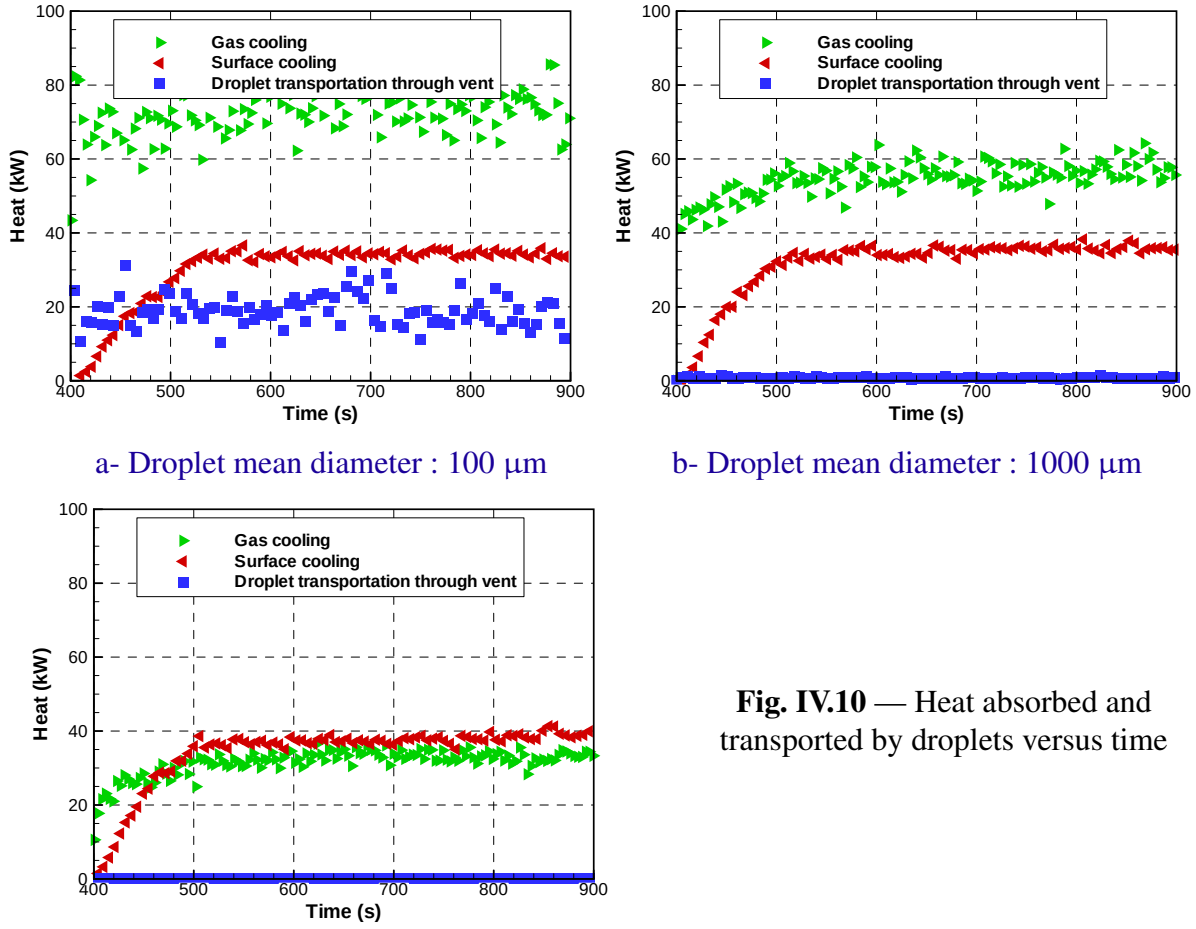

a- Droplet mean diameter : 100 µm

b- Droplet mean diameter : 1000 µm

c- Droplet mean diameter : 1000 µm

Fig. IV.10 — Heat absorbed and transported by droplets versus time

IV.2.4 Toxic environnement

Figures IV.4 and IV.6 highlighted that the gas environment remains thermally stratified during mist application. Moreover, they also indicated that the interface is higher with mist than without mist. A cartography of the environment is also drawn where smoke would be expected in the hottest zone and fresh air in the coldest zone. We want to know now if this cartography is consistent with the one drawn by gas composition. For this reason, contours of concentrations of two gas species (oxygen and carbon monoxide) are plotted on figures IV.11 and IV.12.

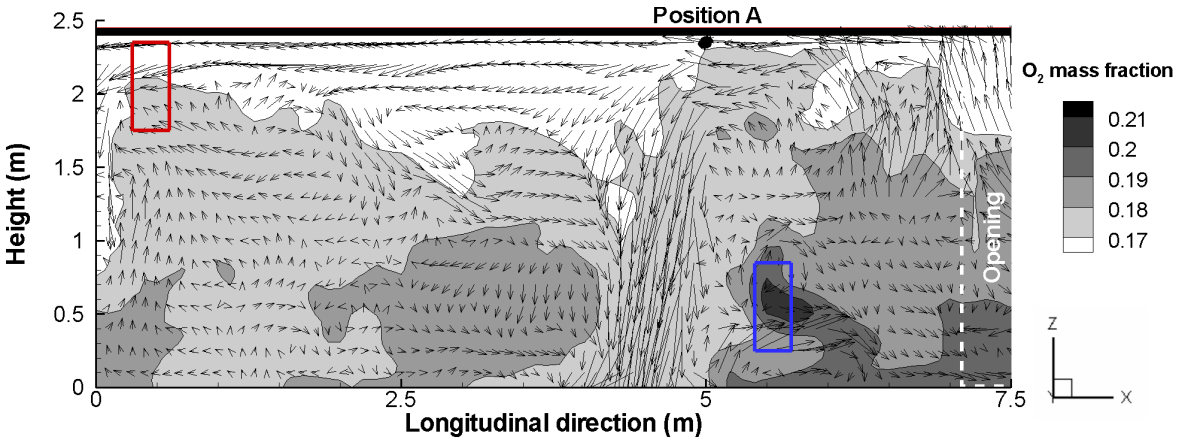

a- Droplet mean diameter : 100 µm

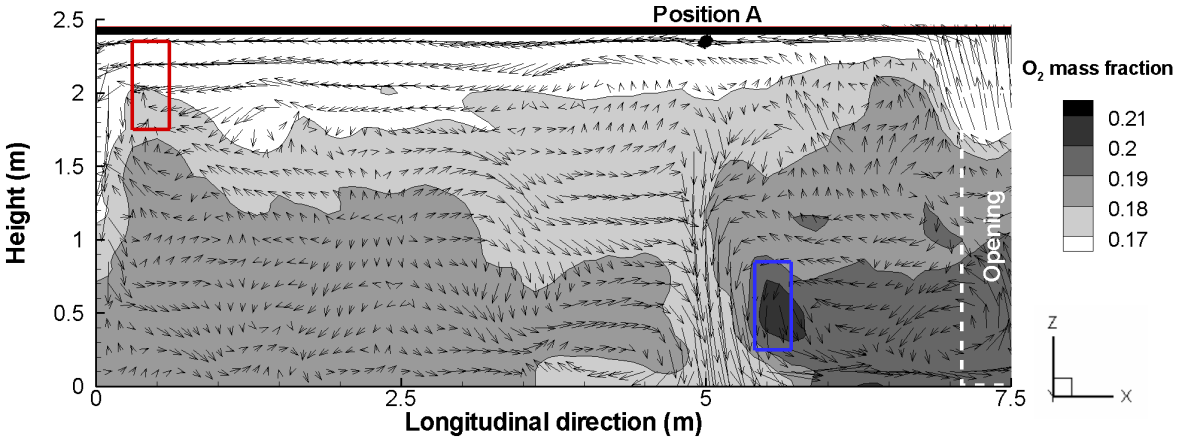

b- Droplet mean diameter : 1000 µm

Fig. IV.11 — Contours of oxygen volume fraction on mid-plane in the corridor at 600 s for two mean diameters

Figures IV.11 and IV.12 show that contours of gas species are globally along the lines of contours of air temperature on figure IV.4. Indeed, there seems to be a vertical gradient in air composition with less oxygen and more combustion products in the upper part and the opposite in the lower part. However, figures IV.11 and IV.12 highlight also that few differences between the two cartographies, especially where mist is sprayed and for the smallest droplet spray between the mist location and the exhaust vent. These few differences can be attributed like in the tunnel configuration to

- water droplets. When they are transported in the corridor, they are still absorbing heat and also evaporating. Water vapor is also created,
- water vapor. When it is produced or present somewhere, it decreases concentration of other species, it dilutes them. For instance, for the spray involving the smallest droplets, water vapor is transported toward the exhaust vent over the whole corridor height (see Figure IV.8),
- smoke cooling. At the mist location, smoke is partly cooled down and pushed away toward the floor. A part of smoke transporting combustion products is also not visible on the temperature contour but it induces there a decrease in O_2 and an increase in CO_2 and in CO.

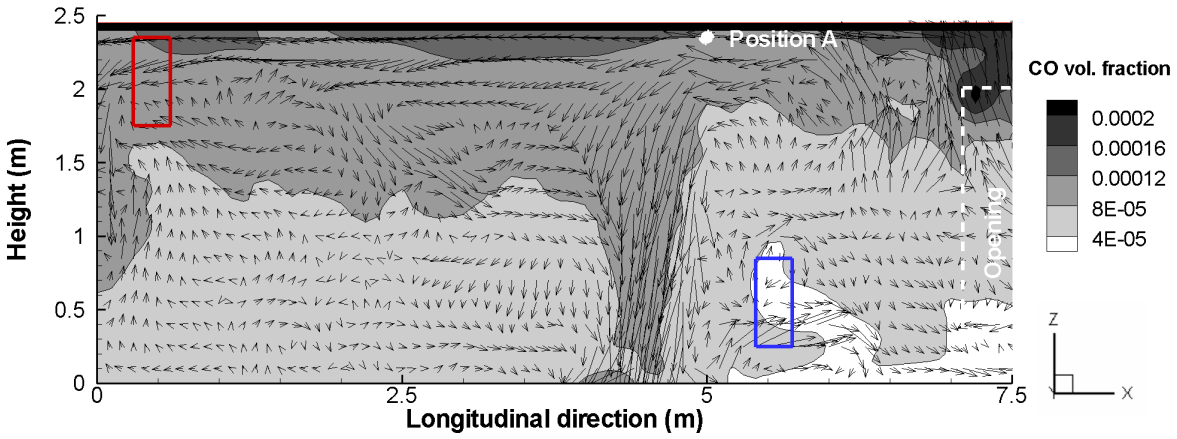

a- Droplet mean diameter : 100 µm

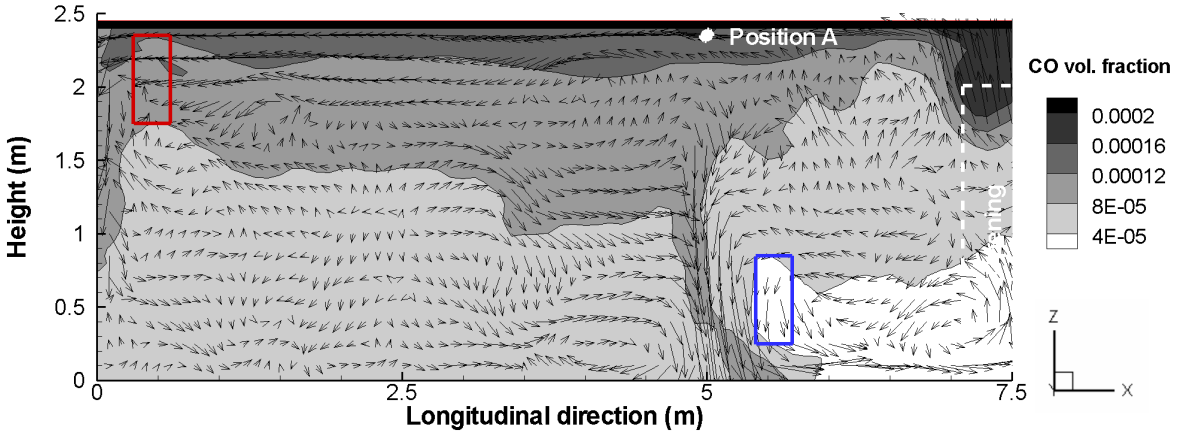

b- Droplet mean diameter : 1000 µm

Fig. IV.12 — Contours of carbon monoxide volume fraction on mid-plane in the corridor at 600 s for two mean diameters

IV.3 Conclusion

The present chapter has allowed to study interaction of water mist, mechanical ventilation of a corridor and smoke layer.

The configuration consists in a room connected to a corridor. The studied scenario involves a wood crib placed in the room and the produced smoke is flowing into the corridor. The water mist system with one nozzle is in the corridor, close to the roof, to avoid interaction with fire activity. The water mist system is defined on the basis of characteristics of a system already used in a previous campaign at CSTB. In particular, for a given operating pressure, we associate a water flow rate. Since no particular data for droplet size has been provided by the manufacturer, a sensitivity analysis has been conducted.

The computational study has highlighted the important influence of water droplet size on interaction phenomena in terms of both dynamics and heat transfer. In particular, heat transfer differs with droplet sizes. For a spray involving the smallest droplets, heat is mainly transfered with gaseous phase rather than for the same sprayed water quantity, when bigger droplets are involved, heat is mainly transfered to solid surface. Concerning the dynamic interaction, the spray with the biggest droplets are less transported by the corridor air flow and also alter more the thermal stratification. Moreover, such spray with the biggest droplets has a strongest surface wetting effect. This fact could be interesting in real condition when the burning objects are located close to the spray, it can thus limit fire propagation. *A contrario*, the smaller the water droplets in the spray are, the more gaseous phase is cooled down over long distances and the thermal stratification is preserved.

The computational study has highlighted the duality of thermal aspects and toxic aspects, especially when a water mist system is activated. In other words, the computational study has confirmed our observations in the tunnel configuration, that is to say it is difficult or even impossible to assess totally the impact of water mist (thermal and toxic) on the only basis of temperature measurements. When a water mist system is activated, oxygen depletion is indeed induced by the transport of combustion products, the evaporation of (transported) water droplets and the transport of produced water vapor. To characterize an environment, it is necessary to measure gas composition and even the water quantity falling on the floor in addition to the usual temperature measurements for addressing the question.

The computational study has dealt with a configuration characterized by a fire load (position, HRR, type), a water mist system (number of nozzle, spray shape, water flow rate, droplets size in particular) and a corridor ventilation (natural gas supply, mechanical exhaust, gas flow rate through each vent). For further work, it would be interesting to pursue this computational study and next to conduct a test campaign for evaluating the influence of each characteristic on the gas air flow,

heat transfer, gas composition and gas opacity. For instance, several fire could be tested : low HRR, moderate HRR and high HRR. The fire load could be placed in the room for avoiding interaction between spray and fire activity or on the contrary in the corridor. The whole test campaign could help to understand, or even determine, the interest of mist in case of fire relative to its position, its time activation, droplet size distribution, etc.

Conclusion and perspectives

The present PhD study is devoted to the interaction of water mist and fire. The integration of such mitigation system in road tunnel fire safety management is more and more considered as a way to improve the fire safety level As the bibliographic synthesis shows (see French dissertation), phenomena involved in tunnel fire, and moreover involving water mist, are very complex and still difficult to predict. For those reasons, design and assessment of a water mist system for a real tunnel are now only based on real sale tunnel test campaign. Even if such campaigns are very expensive and difficult to conduct, design and assessment remain complex in particular due to the limited number of sensors. In this context, we decided for the present work to assess and then to use intensively the capability of an existing CFD code for studying the interaction of water mist, ventilation and fire and for determining the potential contribution of computational codes in a real situation.

The present PhD study uses the code Fire Dynamics Simulator (FDS) developed by the American institute NIST in cooperation with the Finnish research center VTT. First of all, the spray model in its version 5 has been comprehended for understanding its main hypothesis, this work has also led to some propositions of change for the next version. Next, the code has undergone testing. It has been verified and validated based on comparison with analytical solutions and experimental cases of increasing complexity : from the laboratory scale for assessing one particular part of the water spray model up to the tunnel scale. This evaluation has allowed to identify the capability of the code to simulate a water spray, tunnel fires with or without water mist. Once the validation is achieved, the computational tool has been used intensively in order to improve the understanding of the interaction phenomena between water mist, tunnel longitudinal ventilation and fire. In particular, the water mist influence on the tunnel air flow has been studied, the water mist heat contribution has been quantified and the heat transfered to the droplets has been identified. Furthermore, the CFD code has been used to assess the impact of several parameters such as the longitudinal air velocity, the heat release rate and the water droplet size on the water mist efficiency. The last stage has consisted in a preliminary study before a test campaign which will be conducted in 2013. This work has allowed to illustrate how a CFD code can be used on a given situation, here a compartment fire test campaign, in order to foresee the interaction between the water mist, the smoke layer and the smoke extraction.

The two applications in tunnel and compartment have highlighted the complexity and the interdependence of the involved phenomena when water is sprayed during a fire. In that way, the use

of computational tools appears as an interesting complement to experimentation, as much as it has been firstly evaluated. In this PhD study, water spray model in FDS version 5 has shown a good capability to predict the impact of water mist on environmental conditions during a fire, as much as water spray (shape, flow rate, droplet size in particular) and its operations conditions (tunnel air flow, fire activity) are known and reproduced conveniently by the code. In particular, if the use of the computational code aims at dealing with the influence of water mist not only from the thermal point of view (gas temperature, surface temperature and thermal heat) but only from the toxic point of view, the strong influence of spray on fire activity requires to know the temporal evolution of HRR and also the combustion reaction during mist application. This requirement is motivated by the current difficulty of computational codes to predict these two variables.

Regarding the toxic aspects, the present PhD study has highlighted the necessity of measuring gas composition in addition to the usual temperature measurements for addressing completely the impact of water mist on the environment. Unlike a fire without water mist, when water is sprayed, it is difficult or even impossible to study the smoke movement (defined as the combustion products) on the only basis of temperature measurements.

Perspectives

In the present PhD study, the two applications in tunnel and compartment have highlighted that the installation of water system can be of interest in case of fire. Indeed, in these applications, it has induced a fast and important gas cooling, it has cooled the surfaces and it has also acted as a radiative shield due to the small droplet size and their relatively long residence time in gas. Furthermore, this work has shown that water mist influences the stratification of the environment. During mist application, the environment can be unstratified or even it can be stratified thermally but not toxically. However, a destratification (thermal and/or toxic) does not ensure safe egress conditions. This indicates that to take advantage of the installation of a water mist system, it is necessary to think about its operating conditions : deluge system, automatic system, activation temperature, etc. In buildings and more particularly in hotel corridors, it is necessary to consider the nozzle locations relative to gas supply vents, exhaust vents, room doors. All these considerations must be conducted by defining clearly the objective of such installation (improve the egress conditions, the operating conditions, limit the structure damages).

To conduct such consideration by taking into account all the aspects, it would be necessary to take interest in and/or to improve the modeling of three phenomena.

First of all, we can mention the interaction phenomena between water droplets, gaseous phase and solid surface. In particular, the evaluation of evaporation model and begun during the present work should be pursued. Experimentations could also be used involving other liquids and even li-

quid fuel such as heptane or decane, even if these configurations question the hypothesis of infinite conductivity for droplets. Furthermore, model of heat transfer to surface (cold or hot) should be validated on relatively simple cases, the same for model of droplet impact.

Then, it would be interesting to work on visibility both with and without water mist. We should study the influence of water droplets and the increase of soot concentration on the gas opacity or even visibility. This study would allow to define criteria for "optical stratification" for characterizing an environment, such as what is done for thermal and toxic hazards. Moreover, this study would improve the current models on this aspect. By coupling them with egress models, this computational work would help at the end at considering computationally new ways to alleviate a bad visibility such as color, intensity, surface area, locations of luminous egress way.

Last, it seems important to study the interaction of water mist and fire load, it means the influence on fire activity and combustion reaction in case for instance of oxygen depletion. This study would contribute to the improvement of modeling for being able for instance to assess the impact of mist activation time.

References

[1] B. ABRAMZON, W. A. SIRIGNANO. Droplet vaporization model for spray combustion calculations. *International Journal of Heat and Mass Transfer*, 32 : 1605–1618, 1989.

[2] V. BABRAUSKAS. *SFPE Handbook of Fire Protection Engineering*. National Fire Protection Association, Quincy, Third edition, pages 3–1–3–37, 2002.

[3] E. BLANCHARD, P. BOULET, S. DESANGHERE, E. CESMAT, R. MEYRAND, J. GARO, J. VANTELON. Experimental and numerical study of fire in a midscale test tunnel. *Fire Safety Journal*, 47, 2012.

[4] E. BLANCHARD, S. DESANGHERE, G. GIOVANNELLI, X. PONTICQ. Utilisation de brouillard d'eau en tunnel - Bilan de la campagne d'essais menée au CSTB -. Rapport technique, CSTB, CETU, AGEFLUID, Août 2010.

[5] S. COCHARD. Validation of Fire Dynamics Simulator (version 2.0) freeware. *Tunnel Management International Journal*, 6(4), Décembre 2003.

[6] A. COLLIN. *Transferts de chaleur couplés rayonnement-conduction-convection. Application à des rideaux d'eau soumis à une intense source radiative*. PhD thesis, Université Henri Poincaré, Nancy, France, 2006.

[7] A. COLLIN, P. BOULET, G. PARENT, D. LACROIX. Numerical simulation of a water spray - radiation attenuation related to spray dynamics. *International Journal of Thermal Sciences*, 46 : 856–868, 2007.

[8] N. H. DANZIGER, W. D. KENNEDY. Longitudinal ventilation analysis for the Glenwood Canyon tunnels. In *Proceedings of the Fourth International Symposium on Aerodynamics and Ventilation of Vehicle Tunnels*, pages 169–186. BHRA Fluid Engineering, 1982.

[9] F. DEMOUGE. Incendie en tunnel : Approche combinée expérimentation/modélisation. Rapport de recherche CSTB ER DSSF 08, Centre Scientifique et Technologique du Bâtiment, Marne-la-Vallée, France, Mai 2006.

[10] S. DESANGHERE. *Détermination des conditions d'échauffement de structure extérieure à un bâtiment en situation d'incendie*. PhD thesis, Institut National des Sciences Appliquées, Rouen, France, 2006.

[11] P. B. HUSTED. *Experimental measurements of water mist systems and implications for modelling in CFD*. PhD thesis, Lund University, Lund, Suède, 2007.

[12] C. C. HWANG, J. C. EDWARDS. The critical velocity in tunnel fires - a computer simulation. *Fire Safety Journal*, 40 : 213–244, 2005.

[13] M. JANSSENS, H. C. TRAN. Data reduction of room tests for zone model validation. *Journal of Fire Science*, 10, 1992.

[14] D. C. KINCAID. Volumetric water droplet evaporation measurement. *Transactions of the American Society of Agricultural Engineers (ASAE)*, 32(3) : 925–927, 1989.

[15] D. C. KINCAID, T. S. LONGLEY. A water droplet evaporation and temperature model. *Transactions of the American Society of Agricultural Engineers (ASAE)*, 32(2) : 457–463, 1989.

[16] J. P. KUNSCH. Simple model for control of fire gases in a ventilated tunnel. *Fire Safety Journal*, 37(1) : 67–81, Février 2002.

[17] S. LECHÊNE. *Étude expérimentale et numérique des rideaux d'eau pour la protection contre le rayonnement thermique*. PhD thesis, Université Henri Poincaré, Nancy, France, 2010.

[18] S. LECHÊNE, G. PARENT, Z. ACEM, E. BLANCHARD, S. DESANGHERE, P. BOULET. Experimental study of radiation attenuation by a water curtain at laboratory scale. *Experimental Thermal and Fluid Science*, in progress.

[19] S. MARUYAMAA, H. NAKAIB, A. SAKURAIB, A. KOMIYA. Evaluation method for radiative heat transfer in polydisperse water droplets. *Journal of Quantitative Spectroscopy and Radiative Transfer*, 109, 2008.

[20] J. R. MAWHINNEY. Fixed fire protection systems in tunnels : Issues and directions. *Fire Technology*, 47 : 1–32, 2011.

[21] R. MCDERMOTT. A formulation and numerical method for treating droplet evaporation. Nist technical note, National Institute of Standards and Technology, Gaithersburg MD, États-Unis, Août 2007.

[22] R. MCDERMOTT, K. MCGRATTAN, S. HOSTIKKA, J. FLOYD. Fire Dynamics Simulator, Technical Reference Guide, Volume 2 : Verification. NIST Special Publication 1018-5, National Institute of Standards and Technology, Gaithersburg, Maryland, October 2010.

[23] K. MCGRATTAN, A. HAMINS. Numerical simulation of the Howard Street tunnel fire (Baltimore, Maryland). Rapport technique 6902, National Institute of Standards and Technology, Gaithersburg MD, États-Unis, Juin 2001.

[24] K. MCGRATTAN, S. HOSTIKKA, J. FLOYD, R. MCDERMOTT. Fire Dynamics Simulator, Technical Reference Guide, Volume 3 : Validation. NIST Special Publication 1018-5, National Institute of Standards and Technology, Gaithersburg, Maryland, October 2010.

[25] K. MCGRATTAN, R. MCDERMOTT, S. HOSTIKKA, J. FLOYD. Fire Dynamics Simulator, User's Guide. NIST Special Publication 1019-5, National Institute of Standards and Technology, Gaithersburg, Maryland, Octobre 2010.

[26] K. B. MCGRATTAN, S. HOSTIKKA, J. E. FLOYD, H. BAUM, R. REHM, W. E. MELL, R. MCDERMOTT. Fire Dynamics Simulator, Technical Reference Guide, Volume 1 : Mathematical Model. NIST Special Publication 1018-5, National Institute of Standards and Technology, Gaithersburg MD, États-Unis, Janvier 2011.

[27] R. MEYRAND. *Étude sur l'usage de brouillards d'eau en milieu tunnel - Travail en réduction d'échelle*. PhD thesis, École Nationale Supérieure de Mécanique et d'Aérotechnique, Poitiers, France, 2009.

[28] O. MÉGRET. *Étude expérimentale de la propagation des fumées d'incendie en tunnel pour différents systèmes de ventilation*. PhD thesis, Université de Valenciennes et du Hainaut-Cambresis, Valenciennes, France, 1999.

[29] M. F. MODEST. *Radiative heat transfer*. Mechanical Engineering Series. Mc Graw-Hill International Editions, Second edition, 1978.

[30] Y. OKA, G. T. ATKINSON. Control of smoke flow in tunnel fires. *Fire Safety Journal*, 25(4) : 305–322, Novembre 1995.

[31] X. PONTICQ. *Études sur les systèmes fixes d'aspersion d'eau en tunnel*. PhD thesis, Université Claude Bernard, Lyon, France, 2008.

[32] W. E. RANZ, W. R. MARSHALL. Evaporation from drops - part II. *Chemical Engineering Progress*, 48(4) : 173–180, 1952.

[33] R. TAYLOR, R. KRISHNA. *Multicomponent mass transfer*. Wiley Series in Chemical Engineering, pages 152–219, 1993.

[34] A. TEWARSON. *SFPE Handbook of Fire Protection Engineering*. National Fire Protection Association, Quincy, Third edition, pages 3–83–3–161, 2002.

[35] J. TRELLES, J. R. MAWHINNEY. CFD investigation of large scale pallet stack fires in tunnels protected by water mist systems. *Journal of Fire Protection Engineering*, 20 : 149–198, 2010.

[36] F. VINCENT, X. PONTICQ, B. BROUSSE, D. LACROIX, M. TESSON. Les brouillards d'eau dans les tunnels routiers. Document d'information, Centre d'études des tunnels, Lyon, France, Juin 2010.

[37] Y. WU, M. Z. A. BAKAR. Control of smoke flow in tunnel fires using longitudinal ventilation systems - A study of the critical velocity. *Fire Safety Journal*, 35(4) : 363–390, Novembre 2000.

Modélisation de l'interaction entre un brouillard d'eau et un feu en tunnel

Résumé

Ce travail de thèse est consacré à l'étude de l'interaction entre une aspersion par brouillard d'eau et un feu. Il s'appuie sur une modélisation existante figurant dans le code à champs *Fire Dynamics Simulator*. L'approche consiste en premier lieu à appréhender, par le biais d'une synthèse bibliographique, les phénomènes physiques mis en jeu lors d'un feu en tunnel et lors d'une aspersion par brouillard d'eau. Ensuite, un travail d'évaluation est mené. L'évaluation se veut évolutive, en commençant par des cas simples à l'échelle du laboratoire afin de travailler le plus indépendamment possible sur certaines parties du modèle d'aspersion, pour ensuite s'intéresser à la configuration tunnel. Ce travail d'évaluation permet de mieux cerner les aptitudes du code à simuler les phénomènes physiques mis en jeu lors d'un feu en tunnel soumis ou non à une aspersion. Des comparaisons sont effectuées avec plusieurs essais réalisés entre 2005 et 2008 sur une maquette de tunnel à échelle 1/3. Une fois cette évaluation accomplie, l'outil est exploité pour améliorer notre compréhension des phénomènes d'interaction entre le brouillard d'eau, la ventilation du tunnel et le feu. En particulier, l'influence de l'aspersion sur l'écoulement longitudinal est analysée, le rôle énergétique du brouillard d'eau est mesuré et les modes de transfert de chaleur associés aux gouttes sont quantifiés. Cette exploitation permet également d'évaluer numériquement l'influence de quelques paramètres sur l'efficacité de l'aspersion telles que la vitesse de ventilation longitudinale, la puissance du feu et la taille des gouttes pulvérisées. En dernier lieu, le code à champs est exploité dans le cadre d'une étude numérique exploratoire en vue d'une campagne d'essais en bâtiment pour appréhender l'interaction entre l'aspersion, la nappe de fumée et le désenfumage mécanique.

Mots-clés : Sécurité contre l'incendie, feu en tunnel, brouillard d'eau, simulation numérique, CFD

~

Computational study of water mist for a tunnel fire application

Abstract

This work deals with the study of the phenomena involved when a water mist is sprayed in a tunnel fire environment. It relies on an extensive use of numerical simulations using the CFD code *Fire Dynamics Simulator*. The first chapter of this thesis provides an overview of the tunnel fire characteristics and the phenomena involved when the water mist is sprayed. A bibliographical review on the research on tunnel fires with or without any mitigation system is conducted, allowing to outline the reason and the context for this research. In the second and third chapters, the computational tool undergoes testing. It is verified and validated based on comparison with analytical solutions and experimental cases of increasing complexity : from the laboratory scale for assessing one particular part of the water spray model (chapter 2) up to the tunnel scale (chapter 3). For the last case, the code validation makes use of the results of a reduced scale ($1/3^{rd}$) tunnel fire test campaign conducted between 2005 and 2008. Once the validation is achieved, the computational tool is used intensively in the third chapter in order to improve the understanding of the interaction phenomena between water mist, tunnel longitudinal ventilation and fire. In particular, the water mist influence on the tunnel air flow is studied, the water mist heat contribution is quantified and the heat transfered to the droplets is identified. Furthermore, the CFD code is used to assess the impact of the longitudinal air velocity, the heat release rate and the water droplet size on the water mist efficiency. The last chapter illustrates how a CFD code can be used on a given situation, here a compartment fire test campaign, in order to foresee the interaction between the water mist, the smoke layer and the smoke extraction.

Keywords : Fire safety, tunnel fire, water mist, fire numerical simulation, CFD